

**Centro de Investigación Científica y de Educación
Superior de Ensenada, Baja California**



**Doctorado en Ciencias
en Ciencias de la Vida
con orientación en Biología Ambiental**

**Biophysical controls of ecosystem fluxes of carbon in a
semiarid Mediterranean shrubland**

Tesis
para cubrir parcialmente los requisitos necesarios para obtener el grado de
Doctor en Ciencias

Presenta:
M. C. Alejandro Hiram Cueva Rodríguez

Ensenada, Baja California, México
2017

Tesis defendida por
Alejandro Hiram Cueva Rodríguez

y aprobada por el siguiente Comité

Dr. Stephen Holmes Bullock Runquist
Co-Director de tesis

Dr. Rodrigo Vargas Ramos
Co-Director de tesis

Miembros del comité

Dra. Rufina Hernández Martínez

Dr. Rodrigo Méndez Alonzo

Dr. David Lipson



Dra. Clara Elizabeth Galindo Sánchez
Coordinador del Posgrado en Ciencias de la Vida

Dra. Rufina Hernández Martínez
Directora de Estudios de Posgrado

Resumen de la tesis que presenta **Alejandro Hiram Cueva Rodríguez** como requisito parcial para la obtención del grado de Doctor en Ciencias en Ciencias de la Vida con orientación en Biología Ambiental.

Biophysical controls of ecosystem fluxes of carbon in a semiarid Mediterranean shrubland

Resumen aprobado por:

Dr. Stephen Holmes Bullock Runquist
Co-Director de tesis

Dr. Rodrigo Vargas Ramos
Co-Director de tesis

Se sabe que los ecosistemas áridos y semiáridos podrían desempeñar un papel fundamental en el ciclo global del carbono; sin embargo, todavía existen desafíos en la comprensión de la variabilidad temporal y espacial de los flujos de carbono a escala de ecosistemas, que van desde procedimientos estándar para realizar mediciones a nivel parcela, hasta la parametrización de modelos y procesos empíricos. El incremento en el conocimiento de las respuestas de los ecosistemas áridos y semiáridos respecto a los factores ambientales, mejorará la comprensión de la retroalimentación de este tipo de ecosistemas sobre el sistema terrestre. El objetivo principal de esta tesis fue comprender la variabilidad temporal y espacial de los principales flujos de carbono del ecosistema en un matorral semiárido con clima mediterráneo. Para abordar el objetivo general de esta investigación se emplearon técnicas micro-meteorológicas, edafológicas, y de percepción remota cercana a la superficie. Se exploró el efecto contrastante de dos años anormales en precipitación, uno excesivamente húmedo y otro seco en extremo, sobre los controles físicos del intercambio neto del ecosistema (NEE), así como sobre la magnitud y duración del sumidero de carbono. Los resultados sugieren que los controles físicos de NEE cambian cuando el agua no es un factor limitante y que un exceso de disponibilidad de agua en el ecosistema puede extender y hacer más fuerte el sumidero de carbono del ecosistema. Además, se desarrolló un modelo empírico para estimar la producción primaria bruta diaria (GPP), que utiliza como datos de entrada variables meteorológicas y un índice de vegetación derivado de cámaras digitales. Las estimaciones diarias de este modelo fueron comparables con la estimación de GPP derivada de la técnica de covarianza de vórtices. Al incluir un parámetro de senescencia de follaje las estimaciones de GPP mejoraron, especialmente a finales del verano y otoño. Además, se analizó la variabilidad espacial y temporal de la respiración del suelo (R_s) en una parcela de 50x100 m. Estos resultados sugieren que los valores promedio de R_s no cambian en relación con la secuencia espacial entre sitios de medición a nivel parcela; sin embargo, sus factores biofísicos (i.e., temperatura y humedad de suelo, índice de área foliar) cambiaron dependiendo de la secuencia de mediciones. Finalmente, se estimaron sesgos potenciales debidos al muestreo temporal en ciclos de 24 horas en la R_s . Se encontró que las horas de la mañana podrían sobrestimar R_s , mientras que durante la noche podrían ocurrir subestimaciones; por lo tanto, se propuso un factor de corrección simple para tener en cuenta estos posibles sesgos. Como conclusión, se sugiere generar protocolos estándar y reproducibles que minimicen las compensaciones entre las mediciones espaciales y temporales, con el fin de generar bases de datos robustas que servirán como insumos en modelos basados en procesos. Por otra parte, es necesario comprender cómo los ecosistemas responderán a eventos extremos para tener mejores predicciones del cambio climático global, por lo que se necesitan esfuerzos a largo plazo para incorporar nueva información en modelos basados en procesos para actualizar y validar observaciones y parámetros usados actualmente, así como incorporar nuevos procesos que no fueron considerados.

Palabras clave: Covarianza de vórtices, cámaras fenológicas, eventos extremos, respiración de suelo.

Abstract of the thesis presented by **Alejandro Hiram Cueva Rodríguez** as a partial requirement to obtain the Doctor of Science degree in Life Sciences with orientation Environmental Biology

Biophysical controls of ecosystem fluxes of carbon in a semiarid Mediterranean shrubland

Abstract approved by:

Dr. Stephen Holmes Bullock Runquist
Thesis Co-Director

Dr. Rodrigo Vargas Ramos
Thesis Co-Director

It has been recognized that arid and semiarid ecosystems might play a pivotal role in the global carbon cycle. Nonetheless, there are still challenges to the understanding of the temporal and spatial variability of ecosystem scale carbon fluxes, that goes from standard procedures to perform plot-scale measurements, to the parameterization of empirical- and process-based models. Thus, enhancing the knowledge of the response of arid and semiarid ecosystems to environmental forces will improve our understanding on how these ecosystems could feedback the Earth system. Thus, the main aim of this thesis was to understand the temporal and spatial variability of the principal ecosystem carbon fluxes in a semiarid shrubland with a Mediterranean climate. To address the overarching objective of this research, a set of micro-meteorological, edaphological, and near-surface remote sensing techniques was employed. I explored how two abnormal years in terms of precipitation, one that was excessively humid, and another extremely dry, influenced the physical controls of the net ecosystem exchange of CO₂ (NEE) and the strength and duration of the ecosystem carbon sink. My results suggest that the physical controls of NEE changed when water is not a limiting factor, as an excess of water availability within the ecosystem can extend and enhance the ecosystem carbon sink. In addition, I developed a semi-empirical model to estimate daily gross primary production (GPP) that uses meteorological data and a vegetation index derived from consumer-grade digital cameras as inputs. Daily estimates of this model were comparable with the estimation of GPP derived from the eddy covariance technique, and these estimations improved when including a senescence parameter of foliage, especially in late-summer and autumn. Furthermore, I tested for the effect of temporal discrepancies in spatial surveys of soil respiration (Rs), in a 50x 100 m plot. These results showed that Rs does not change spatially, providing support for temporal representation of Rs based on plot-scale measurements; however, its biophysical controlling factors changed depending on the sequence of measurements. Finally, the potential biases due to temporal sampling in 24 hours cycles in soil respiration were tested. It was found that customary and convenient morning hours could overestimate Rs, while during nighttime underestimations could occur; thus, it was proposed a simple correction factor to take into account this potential biases. As a conclusion, it is suggested to generate standard and reproducible procedures that minimize the tradeoffs between spatial and temporal surveys, in order to generate robust databases that could serve as inputs in empirical- and process based models. Moreover, it is necessary to understand how ecosystems will respond to extreme events in order to have better predictions of global climate change, thus long-term efforts are needed to bring new information into process-based models to update and validate previous observations and parameters, as well as to incorporate new processes that were not taken into account.

Keywords: Eddy covariance, phenocams, extreme events, soil respiration.

Dedicatoria

Para

*Lluvia,
Araceli,
José,
Gaby,
Christian,
mi familia.*

Agradecimientos

Al CICESE, en especial a su programa de Posgrado en Ciencias de la Vida, por haber provisto mis estudios de posgrado, tanto a su personal académico, técnico, y administrativo. Al CONACyT, por haberme asignado una beca para manutención y estudios de doctorado, así como una beca mixta para realizar una estancia en el extranjero. Así mismo, se agradece el financiamiento a los proyectos: SEP-CONACYT SEP-2003-C02-43422, CONACYT (INFR-2014-01 227615), SEP- CONACYT (CB-2010-152671-F), y CICESE (681115).

A mis Co-Directores de tesis, Dr. Rodrigo Vargas y Dr. Stephen Bullock, fue una larga jornada, pero lo hicimos, y aún queda mucho por hacer. Rodrigo, gracias por las enseñanzas académicas, profesionales y personales, que empezaron en San Carlos, y que actualmente están dando resultados. Steve, gracias por tener la puerta de tu oficina siempre abierta, la paciencia y aliento constante, así como tus historias en las salidas de campo.

A mi comité de tesis, Dra. Rufina Hernández, Dr. Rodrigo Méndez, y Dr. David Lipson, por sus valiosos comentarios y discusión durante mi investigación de tesis doctoral.

Al personal del Departamento de Biología de la Conservación, en especial al Técnico Eulogio López Reyes, por su apoyo logístico, así como su ayuda constante en el trabajo de campo, así como a la Secretaria del Departamento, Eva Robles, por su apoyo indispensable en los trámites administrativos. Así mismo, se agradece a la Secretaria del Posgrado, Adriana Mejía, por su apoyo en relación a los tramites del posgrado.

A mi familia, Lupita y José, mis padres, Gaby y Christian, mis hermanos, por su apoyo incondicional durante estos años de mi formación académica. Sin duda su apoyo ha sido invaluable para poder seguir en este camino, que todavía no se acaba.

A Lluvia, el pilar más importante para haber llegado hasta la meta, y el motivo para despertarme todos los días y ser una mejor persona, por su cariño y amor incondicional que me ha brindado durante estos años, por cuidarme, escucharme, y enseñarme la ciencia de esto que llamamos vida. En especial por haber decidido compartir su vida conmigo, formando una nueva familia. Lluvia, ¡Gracias! Por ser mi amiga, por haber sido mi novia, y ser ahora mi esposa. ¡Este es y seguirá siendo el claro ejemplo del que persevera alcanza!

A Moisés Rodríguez, que se nos adelantó en el camino, pero que, sin su apoyo y cariño incondicional, esto no hubiera sido posible.

A los amigos y compañeros que se traslaparon en este camino durante este tiempo, con los que compartí risas, frustraciones, discusiones, y una que otra cerveza. Son muchos para mencionarlos aquí, pero si tu nombre empieza con A, B, C, D, E, F, G, H, I, J, K, L, M, N, Ñ, O, P, Q, R, S, T, U, V, W, X, Y, o Z, ¡Gracias por lo que creas que sea bueno! En especial a los amigos y compañeros del Departamento de Biología de la Conservación, Departamento de Microbiología, y anexos. A Falkor, el mejor compañero.

Finalmente, te agradezco a ti, lector, que sostienes esta tesis en tus manos, o en su defecto, las estás leyendo en formato electrónico. Si consideras que debieras estar en esta sección de agradecimientos la omisión de tu nombre se debe exclusivamente a mi mala memoria.

Tabla de contenido

	Página
Resumen en español.....	ii
Resumen en inglés.....	iii
Dedicatorias.....	iv
Agradecimientos.....	v
Lista de figuras.....	ix
Lista de tablas.....	xii
Chapter 1. General Introduction	
1.1 Introduction.....	1
1.2 General Objective.....	4
1.3 Specific objectives.....	4
Chapter 2. Contrasting effects of extreme wet and dry years in net ecosystem exchange in a Mediterranean shrubland	
2.1 Introduction.....	5
2.2 Methodology.....	6
2.2.1. Study site.....	6
2.2.2 Eddy covariance and meteorological measurements.....	8
2.2.3 Data analysis.....	8
2.3 Results.....	10
2.3.1 Meteorology.....	10
2.3.2 Carbon Exchange.....	11
2.3.3 Physical controls of NEE.....	14
2.4 Discussion.....	17
2.5 Conclusion.....	19
Chapter 3. Gross primary productivity in a dryland ecosystem: models with greenness, meteorological factors and a proxy of foliage senescence	
3.1 Introduction.....	20
3.2 Methodology.....	22

3.2.1 Study site.....	22
3.2.2 Time-lapse repeated photography.....	22
3.2.3 Image analysis.....	23
3.2.4 Eddy covariance and meteorological data.....	23
3.2.5 Growing season index.....	24
3.2.6 GPP derived from a light use efficiency model and GSI.....	25
3.2.7 Evaluation of model performance.....	26
3.3 Results.....	27
3.3.1 Meteorology.....	27
3.3.2 Repeated photography and greenness index.....	28
3.3.3 Gross primary production from flux measurements.....	29
3.3.4 Comparison between GPP_{EC} and GPP_{mod}	30
3.4 Discussion.....	32
3.4.1 Digital repeated photography.....	33
3.4.2 Modeled gross primary productivity.....	34
3.4.3 Foliage senescence.....	35
3.5 Conclusion.....	36
Chapter 4. On the spatial variability of soil respiration: does timing of measurements matter?	
4.1 Introduction.....	38
4.2 Methodology.....	40
4.2.1 Study site.....	40
4.2.2 Measurements and experimental design.....	41
4.2.3 Ecosystem respiration.....	42
4.2.4 Spatial analysis.....	43
4.2.5 Statistical analysis.....	44
4.3 Results.....	45
4.3.1 Temporal variability.....	45
4.3.2 Spatial variability.....	45
4.3.3. Comparison between measurement sequences.....	52
4.4 Discussion.....	53
4.5 Conclusion.....	56

Chapter 5. Potential bias of daily soil CO₂ efflux estimates due to sampling time

5.1 Introduction.....	57
5.2 Methodology.....	59
5.2.1 Estimation of the most representative time interval.....	59
5.2.2 Study site.....	61
5.2.3 Sampling design and measurements.....	61
5.2.4 Statistical analysis.....	62
5.3 Results and discussion.....	62
5.4 Conclusion.....	67
Chapter 6. General Conclusions	
6.1. Conclusion.....	69
Literatura citada.....	72

Lista de figuras

Figura	Página	
1	Monthly averages of air temperature ($^{\circ}\text{C}$, black line) and monthly sums of precipitation (mm, grey bars) for a) 1954-2012 period from a meteorological station located ~ 755 m from our study site, b) hydrological year of 2009-2010, and c) hydrological year 2013-2014. The precipitation axis was limited to a maximum of 120 mm for comparison, but the month of January in panel b) accumulated 240 mm.	7
2	Five-day average (black line) and half-hourly values (grey dots) of air temperature ($^{\circ}\text{C}$), global radiation (W m^{-2}), vapor pressure deficit (kPa), and daily mean values of soil water content ($\text{m}^3 \text{m}^{-3}$) at 10 cm (grey line in bottom panel) and precipitation (mm; bars in bottom panel) over our study period at El Mogor	11
3	Five-day average (black line) and half-hourly values (grey dots) of net ecosystem exchange over our study period at El Mogor	12
4	Flux duration curves of daily averages of net ecosystem exchange in a) all year, b) wet season, and c) dry season. By convention, negative values of NEE represent carbon uptake by the ecosystem, and positive values represent carbon losses to the atmosphere	13
5	Regression trees for daily means of net ecosystem exchange (NEE) for: (a, b, c) all year, (d, e, f) wet season, and (g, h, i) dry season, for the control year (a, d, g), wet year (b, e, h), and dry year (c, f, i). The variable controlling each branching is noted with its critical value; lesser values define the left side branch, greater value the right side. At terminal points, the mean NEE value for the cluster is indicated. Abbreviations are as follows: PAR: Photosynthetic Active Radiation ($\mu\text{mol Photon m}^{-2} \text{s}^{-1}$), SWC: Soil Water Content ($\text{m}^3 \text{m}^{-3}$), VPD: Vapor Pressure Deficit (kPa)	15
6	Relationship of daytime net ecosystem exchange and global radiation for: (a, b, c) all year, (d, e, f) wet season, and (g, h, i) dry season, for the control year (a, d, g), wet year (b, e, h), and dry year (c, f, i). Filled circles (\bullet) represent data where soil water content $> 0.1 \text{ m}^3 \text{m}^{-3}$; open circles (\circ) represent data where soil water content $< 0.1 \text{ m}^3 \text{m}^{-3}$. Dashed lines represent $\text{NEE} = 0$	16
7	Daily averages of air temperature, vapor pressure deficit, global radiation, soil water content, and daily sum of precipitation, in our study sites during 2016	28
8	Time series of (A) daily averaged gross primary production derived from eddy covariance measurements (GPP_{EC}), (B) the average of the greenness index (lg) derived from our three phenocams located in our study site, and (C) the linear relationship of GPPEC and lg	29
9	(A) Time series of daily averaged gross primary production derived from eddy covariance measurements (black dots; GPP_{EC}) and daily estimations of gross primary production (white dots; GPP_{mod}), from the $\text{GSI}_{\text{T+V+P+W}}$ formulation including the	

	senescence parameter. The red line represents the linear regression for the entire study year, while the dashed black line is for the growing season, and the dashed grey line is for the non-growing season. DOY= Day of the year	32
10	Schematic representation of the role of excluding the senescence parameter in models to predict gross primary productivity. In the upper panel, a “normal” year is exemplified for a Mediterranean-type ecosystem, where the physiological activity (i.e., GPP) increases during winter, have a plateau in early spring, level off in late spring and early summer, and decrease into late summer and fall. In bottom panel, the grey area represents the “ideal” model that predicts timely the phenological stages of vegetation, and the gradient area represents the potential overestimation of gross primary productivity due to the absence of limiting vegetation senescence. The omission of incorporating vegetation senescence will lead to an extended carbon uptake period, as well as a wider amplitude of the magnitude of physiological activity, with an apparent increase in gross primary productivity magnitude. This draw is based in those of Richardson et al. (2010)	36
11	Mean monthly precipitation (bars, mm) and mean monthly temperature (dots, °C) during the period of 1954-2012 (A) and during the study period (July 2015-June 2016; B) at El Mogor, Baja California, Mexico	40
12	Schematic representation of the study plot and how was measured. The eddy covariance tower is located at the center (star). The plot extent is ~0.5 ha (approximately 50x100 m). Forward measurements (blue line) starts in the sampling point 1 in ascending order and finish in the sampling point 25, and backward measurements starts in the sampling point 25 in descendent order and finish in the sampling point 1 (yellow line)	42
13	Temporal variability of ecosystem respiration (Reco; open circles) and soil respiration (Rs; filled circles) during the study period. For Rs each point represents the average value of 25 sampling points measured on a monthly basis across the study period. For Reco each point represents the monthly average value from half hourly estimations. Errors bars represents the standard deviation	45
14	Spatial patterns of soil respiration (Rs) derived from ordinary kriging. Left column (A, D, G, and J) represents forward measurements, middle column (B, E, H, and K) represents backwards measurements. Right column (C, F, I, and L) represents the difference between forward minus backwards measurements. Panels A, B and C are the measurements made in August; panels D, E, and F are the measurements made in November; panels G, H, and I are the measurements made in January; panels J, K, and L are the measurements made in April	48
15	Spatial patterns of soil moisture (SWC) derived from ordinary kriging. Left column (A, D, G, and J) represents forward measurements, middle column (B, E, H, and K) represents backwards measurements. Right column (C, F, I, and L) represents the difference between forward minus backwards measurements. Panels A, B and C are the measurements made in August; panels D, E, and F are the measurements made in November; panels G, H, and I are the measurements made in January; panels J, K, and L are the measurements made in April	49

16	Spatial patterns of soil temperature (Ts) derived from ordinary kriging. Left column (A, D, G, and J) represents forward measurements, middle column (B, E, H, and K) represents backwards measurements. Right column (C, F, I, and L) represents the difference between forward minus backwards measurements. Panels A, B and C are the measurements made in August; panels D, E, and F are the measurements made in November; panels G, H, and I are the measurements made in January; panels J, K, and L are the measurements made in April	50
17	General spatial patterns of leaf area index (LAI) derived from ordinary kriging. LAI data represents the average value of each measurement point from September 2011 until June 2016	51
18	Bean plots of soil respiration (left), soil temperature (middle), and soil moisture (right) showing the distribution of forward (white) and backward (grey) measurements. The black line within the distributions represents the average value for the measurement direction	53
19	Histogram of number of entries sorted by sampling interval reported in the Soil Respiration Database (SRDB V3.0). Note that the most common sampling interval is from 28-45 days (e.g., monthly, n=1236), followed by 14-18 (e.g., biweekly, n= 542). Also note that, despite the sampling interval, the annual coverage could be less than 365 days. The total number of entries in the SRDB V3.0 is 5174, but only 3332 reported a sampling interval. The SRDB V3.0 has data from 1961 to 2011	58
20	Mean relative difference (MRD) values \pm standard deviation for all the 24hr campaigns for the treatments (A) Trenched and (B) Shrub, and separated in (C) dry season and (D) wet season	63
21	Corrected (A) and uncorrected (B) annual series of soil respiration. Note that we use a hydrological year (from November to October) instead of a calendar year (January to December)	65

Lista de tablas

Tabla		Página
1	Annual values of precipitation (PPT, mm), air temperature (T_a , °C), vapor pressure deficit (VPD, kPa), volumetric soil water content at 10cm (SWC, $m^3 m^{-3}$), and net ecosystem exchange (NEE, $\mu mol CO_2 m^{-2} s^{-1}$). The wet (W) and dry (D) years are indicated	10
2	Values of the parameters of the relationship of daytime net ecosystem exchange with global radiation under different seasons and soil moisture conditions. Bold text represent significant ($P < 0.05$) relationship	17
3	Representation of the different formulations used to test the growing season index (GSI), as described in Sections 2.5 and 2.6. Shaded areas represents the parameters used	27
4	Fitting statistics of linear regressions for the gross primary production (GPP_{mod}) estimated with the different formulations for the Growing Season Index described in Table 3, during all the study period, compared to the gross primary production from eddy covariance estimations (GPP_{EC})	30
5	Fitting statistics of linear regressions for the different formulations for the Growing Season Index described in Table 3, during the growing season, compared to the gross primary production from eddy covariance estimations (GPP_{EC})	31
6	Fitting statistics of linear regressions for the different formulations for the Growing Season Index described in Table 3, during the non-growing season, compared to the gross primary production from eddy covariance estimations (GPP_{EC})	31
7	Semivariogram estimated parameters and models for soil respiration (R_s) during the campaigns of simultaneous measurements	46
8	Semivariogram estimated parameters and models for soil temperature in the sampling months	46
9	Semivariogram estimated parameters and models for soil moisture in the sampling months	47
10	Semivariogram estimated parameters and models for leaf area index (LAI) in the sampling months	47

11	Model parameters from the stepwise multiple regression and variation partitioning for the campaigns of simultaneous measurements	51
12	Descriptive statistics for soil respiration (Rs), soil temperature (Ts), and soil moisture (SWC) (mean values \pm standard deviation) during the campaigns of simultaneous measurements	52
13	Correlation analysis between forward and backward measurements for soil respiration measurements	52
14	Summary table of the main results of this study	54
15	Summary statistics for mean relative difference (MRD) values	62
16	Bayesian paired samples Student's T-test of the time series of soil respiration data ...	65
17	Annual and seasonal average (μ) \pm standard deviation (σ) of soil respiration from monthly mid-day measurements in trench and shrub treatments, corrected and uncorrected for temporal bias.	66
18	Bayesian linear relationships of soil respiration with soil temperature (Temp) and soil moisture (SWC)	67

Chapter 1. General Introduction

1.1 Introduction

The study of the components of the global carbon cycle as well as its biophysical drivers, in special those factors that control if an ecosystem is a source or a sink of CO₂, has increased greatly in the last decades (Chapin et al., 2006). In particular, three functions have become foci of ecosystems research at all spatial scales: net ecosystem exchange (NEE) of carbon dioxide (CO₂) with the atmosphere, and its underlying functions, namely, gross primary production (GPP), which consists of the carbon fixed through photosynthesis in vegetation, and ecosystem respiration (R_{eco}), mainly derived from heterotrophic metabolism, root respiration within the soil, as well as leaf respiration. One of the most critical gaps in the knowledge about carbon fluxes is how arid and semiarid ecosystems may feedback to global climate, affecting the observed and projected in trends of precipitation and temperature globally. This is so because it has recently been suggested that most of the global terrestrial carbon uptake (i.e., GPP) occurs in arid and semiarid ecosystems (Ahlström et al., 2015; Poulter et al., 2014).

Arid and semiarid ecosystems cover ca. 40% of the terrestrial surface (Reynolds et al., 2007). These ecosystems are limited in NEE, GPP, and R_{eco} by water availability (Austin et al., 2004; Huxman et al., 2004; Schwinning and Sala, 2004). Currently, the dynamics of these systems are changing due to altered rainfall patterns (Diffenbaugh et al., 2008; Dore, 2005), and to changes in temperature and CO₂ concentrations in the atmosphere (Cox et al., 2000; Friedlingstein et al., 2006), together causing an intensification of the water cycle at global scale (Jung et al., 2010). Moreover, there are clear indications that water-limited ecosystems are expanding (Reynolds et al., 2007), while soil water deficits are increasing (Jung et al., 2010). Thus, even a small change in the balance of the terrestrial carbon cycle, especially in arid and semiarid ecosystems, could intensify or mitigate the trend of increasing atmospheric CO₂, with potential impacts on global climate (Heimann and Reichstein, 2008). Hence, to predict the impacts of climate change on arid and semiarid ecosystem and feedbacks to the Earth system, it is important to evaluate how these ecosystems are going to respond to a changing climate.

Due to technological advances in the last decades, the biophysical factors that control NEE, GPP, and R_{eco} have been studied across different temporal (e.g., from seconds to years) and spatial (e.g., from plot to

continental) scales around the world. It has become possible to make detailed studies of the consequences of ecosystem perturbations, due to extreme events (e.g., hurricanes, floods, fire, drought) or land use changes (e.g., agriculture) (Baldocchi, 2003). For example, it was possible to study the consequences on GPP of a continental-scale drought across Europe (Ciais et al., 2005), or how soil respiration is influenced by a hurricane in a tropical forest (Vargas, 2012; Vargas and Allen, 2008a). Furthermore, this technological improvement has contributed to the differentiation of biophysical factors that control ecosystem metabolism. For example, in temperate ecosystems with no pronounced dry season, R_{eco} is mainly controlled by seasonal temperature changes (Valentini et al., 2000), while in arid and semiarid ecosystems GPP and R_{eco} are triggered and limited by rainfall (Huxman et al., 2004; Yopez et al., 2007).

Precipitation pulses usually exert the main control on carbon fluxes in arid and semiarid ecosystems, influencing the temporal variability of soil moisture and vapor pressure deficit (Huxman et al., 2004), such that these ecosystems 'pivot' between being carbon sinks or sources (Scott et al., 2015). Longer dry spells and more intermittent precipitation are expected in these ecosystems. But while drought is relatively a well-studied phenomenon (Ciais et al., 2005b; Reichstein et al., 2013; Scott et al., 2009; Schwalm et al., 2010; Wolf et al., 2016; Zhao and Running, 2010), the responses of these ecosystems to unusual excess of water availability has been less studied. Understanding the consequences and how ecosystems response to both water excess and deficit, will provide new information to create more realistic models that represent extreme events, and to improve projections of global climate change.

Despite the technological advances in monitoring the exchange of carbon between ecosystems and the atmosphere, there are still different challenges, methodological difficulties, as well as uncertainties related to measurements. One of them is the spatial restriction inherent to the technique applied. For ecosystem-scale measurements of carbon fluxes, using the eddy covariance (EC) technique, the spatial restriction consists of 1) the representativeness and uniformity of the area sampled (called the flux footprint which varies with the wind between 100 to 1000 m in length), 2) ideally, the flux footprint and a much larger area around it must be on flat terrain, and 3) restrictions for security of the instruments (Baldocchi, 2003). On the other hand, soil respiration measurements are mainly restricted by the area of sampling of the instruments (much less than 1 m²), as well as by the area where the instruments can be applied, which force decisions on the balance between sampling the spatial or the temporal variations of soil respiration (Savage and Davidson, 2003). The restrictions in both techniques lead to potential discrepancies when comparing R_{eco} estimates from the EC technique with soil respiration measurements (Phillips et al., 2016).

Thus, to assess the local spatial variability of carbon fluxes, it is important to improve upscaling approaches in order to have more-representative estimates.

To extrapolate terrestrial-atmosphere carbon fluxes to regional, continental, or global scales, both empirical (i.e., those based in statistical relationships) and process (i.e., those simulating a process numerically) -based models have been developed, but these are limited by our understanding of the processes involved, as well as by their parameterization, by data availability (Jägermeyr et al., 2014; Phillips et al., 2016; Scheiter et al., 2013), and by uncertainties inherent to the measurements and models (Hagen et al., 2006; Hollinger and Richardson, 2005; Richardson and Hollinger, 2005). It is known that empirical and process-based models for estimating carbon fluxes have pitfalls when drought occurs (Vargas et al., 2013a), potentially leading to biases in their estimates in arid and semiarid ecosystems. Furthermore, it is acknowledged that empirical and process-based models do not have a good representation of vegetation phenology (Richardson et al., 2013; Schaefer et al., 2012). Thus, the study of phenology across arid and semiarid ecosystems could provide valuable information to improve empirical and process-based models for predicting global scale carbon fluxes.

Among the challenges to improve estimates of local ecosystem carbon fluxes, there is an increasing interest to include soil respiration in Earth System Models (ESMs), because soil processes are currently poorly represented. Nonetheless, measuring soil respiration involves the trade-off between studying its temporal or spatial variability: when measurements at one point are frequent, the number or dispersion of points must be less, whereas when spatial surveys are made, the frequency usually must usually be lowered. This represents a challenge when upscaling soil respiration. Moreover, in order to improve ESMs, it is necessary to include the influence and feedbacks of extreme events in terrestrial ecosystems. For example, the consequences of drought are not comprehensively understood, causing higher uncertainties in the estimates of global carbon budgets in process-based models. Moreover, the counterpart of an unusual excess of available water has rarely been studied. An excess of available water could promote higher photosynthesis rates, as well as faster decomposition of organic matter in the soil. It is also recognized that ESMs do not have a proper representation of vegetation phenology, which could also cause biases in carbon flux estimates. This problem is not limited to the estimation of the beginning and end of the growing season, but also to quantifying and explaining progressive senescence of the foliage. Thus, incorporating proper information about soil respiration rates and vegetation phenology can improve ESM estimations of carbon flux and contribute to the improvement of global climate-change projections.

To address the challenges mentioned above, this PhD Dissertation is organized as follows. Chapter 2 contrasts years with average precipitation against years with abnormally high and low precipitation, showing the alterations of net ecosystem exchange and its responses to other physical drivers. Chapter 3 describes a semi-empirical model to estimate daily gross primary productivity (GPP), using meteorological data and a vegetation index derived from digital photographs, and emphasizes the utility of a proxy for leaf senescence in improving the estimation of GPP. Chapter 4 shows how differences of hours to months in the timing of measurements of soil respiration influence its spatial representation and the evaluation of its biophysical drivers. Chapter 5 describes a simple method to determine the optimal time for sampling soil respiration and to correct for potential biases due to sampling time. Finally, Chapter 6 gathers together the main conclusions from this research.

1.2 General objective

To model the biophysical regulation of vertical carbon fluxes, including net ecosystem exchange of CO₂, soil respiration, and gross primary production, in a semiarid shrubland located in the Guadalupe Valley, Baja California, México, through micrometeorological, near-surface remote sensing, and edaphological techniques *in situ*.

1.3 Specific objectives

- To examine and compare the biophysical controls of net ecosystem exchange of CO₂ in a semiarid shrubland with Mediterranean climate between years of contrasting extremes in precipitation.
- To develop a semi-empirical model to estimate daily gross primary productivity using consumer-grade digital cameras and meteorological data and adjusted to estimates from eddy covariance techniques.
- To evaluate the effects of the timing of measurements on potential discrepancies of estimated soil respiration, its spatial representation and the weighting of controlling factors.
- To evaluate systematic bias of soil respiration estimates due to sampling time and develop a method of correction.

Chapter 2. Contrasting effects of extreme wet and dry years in net ecosystem exchange in a Mediterranean shrubland

2.1 Introduction

Drought is the most common factor influencing the carbon balance across terrestrial ecosystems (Reichstein et al., 2013). In particular, arid and semiarid ecosystems represent ~40% of the terrestrial surface and their area is increasing (Andela et al., 2013; Reynolds et al., 2007). Recently, they have been considered as "... natural models for a future world that is drier and warmer..." (Baldocchi et al., In Press). These ecosystems contribute significantly to the inter-annual variability of the terrestrial carbon cycle, as they have the largest variability in yearly precipitation across terrestrial ecosystems (Ahlström et al., 2015; Fatichi et al., 2012; Poulter et al., 2014), and this variability is expected to increase due to the ongoing climate change. Thus, understanding the response of arid and semiarid ecosystems to varying precipitation would improve projections of global-scale carbon budgets.

Global climate change is expected to modify the timing and amount of precipitation events, generating stronger, but highly infrequent, events of precipitation (Reichstein et al., 2013). The effects of drought have received some attention across terrestrial ecosystems, but the responses to unusual excess of water availability are less well known. Attention to extreme precipitation events has often been related to hurricanes, which may cause massive defoliation (Li et al., 2007), vegetation mortality (Zeng et al., 2009), and sudden large increases of decomposition of fresh organic matter (Vargas, 2012; Vargas and Allen, 2008a). However, the influences on ecosystem carbon fluxes of a higher than expected seasonal precipitation, without being an "extreme" event, need greater attention in arid and semiarid environments. There is evidence to suggest that the principal effect of higher water variability in arid and semiarid ecosystems is a shift from being a sink to a source of carbon (Scott et al., 2015). On the other hand, it has been seen that as the amount of precipitation increases, the magnitude of the carbon sink also increases in arid and semiarid ecosystems (Biederman et al., 2016). Changes in the amount of precipitation will influence the environmental factors that control the carbon sink/source magnitude, so it is of special interest to quantify how the biophysical mechanisms that regulate ecosystem carbon fluxes differ between abnormal wet and dry conditions. For instance, it is known that process-based models do not predict accurately ecosystem-scale carbon fluxes during drought conditions (Vargas et al., 2013a), but it is unknown how they respond to abnormal wet conditions. Thus, research over a broad range of conditions remains important to modeling, notably including global models because of the extent of drylands.

The eddy covariance (EC) technique has provided unique information about the exchange of carbon, in form of CO₂, between terrestrial ecosystems and the atmosphere. Using regional networks of EC, it has been possible to note the effects of drought on ecosystem scale carbon fluxes across Europe (Ciais et al., 2005) and the United States (Wolf et al., 2016). Nonetheless, regional-to-global networks of EC are mostly situated in mesic to temperate climates, where vegetation is highly sensitive to water stress, under-representing arid and semiarid ecosystems (Biederman et al., 2016), where vegetation is well-adapted to dry spells though poorly monitored.

In this study, we focus on the different responses of net ecosystem exchange (NEE) to physical controlling factors during extreme wet and dry years, compared to normal conditions. We use a 7-year long dataset of NEE derived from EC measurements in a semiarid shrubland in northern Baja California, México. Our dataset includes an abnormally wet year, with precipitation of 226% over the historical mean, and an abnormally dry year with precipitation 16% lower than normal. Research questions were as follows: Q1) How much is the carbon sink/source magnitude influenced by the extreme differences in precipitation? and Q2) How does the influence of other physical factors on NEE change in relation to precipitation? We hypothesized that: H1) During the dry season, as soil moisture becomes a limiting factor, the carbon sink/source strength becomes similar between wet and dry years; and H2) During the wet season, while soil moisture is not a limiting factor, NEE responds similarly to environmental drivers of NEE in the wet and dry years. Understanding these responses will improve our ability to predict potential feedbacks from terrestrial ecosystems to the Earth climate system, because climatic scenarios more frequent extremes are projected to be the new normal in coming decades (Berg and Hall, 2015).

2.2 Methodology

2.2.1 Study site

El Mogor is a MexFlux site (MX-EMg; Vargas et al., 2013b) located in the Valle de Guadalupe, Baja California, México (32.030 N, 116.604 W, 406 m above sea level). The climate is Mediterranean, with warm and dry summers and cool and wet winters. Mean annual temperature is 17 °C and mean annual precipitation is 281 mm (Figure 1A; data from 1954-2012, meteorological station 2036 - Olivares Mexicanos, located ~755 m from our study site; data acquired from the National Meteorological System (SMN), available at <http://clicom-mex.cicese.mx/>). Soils at the study site are shallow (~30 cm depth), and

developed from granitic parent material. Soil texture is sandy loam (75% sand, 14% silt, and 11% clay) with a bulk density of 0.93 g cm^3 and pH between 6.6 and 7.0, with 5% of carbon, 0.9% of nitrogen, and a fine root biomass of 0.5 kg m^2 (Franco-Vizcaíno and Sosa-Ramírez, 1997; León et al., 2014). The vegetation is a mixture of chaparral and sclerophyllous species. The species with the greatest ground cover at our study site (footprint) were *Ornithostaphylos oppositifolia*, *Eriogonum fasciculatum*, *Adenostoma fasciculatum*, *Xylococcus bicolor* and *Malosma laurina* (Díaz de León-Guerrero, Unpublished Data). The site was burned in 1988 but this type of perturbation is expected in this kind of ecosystems.

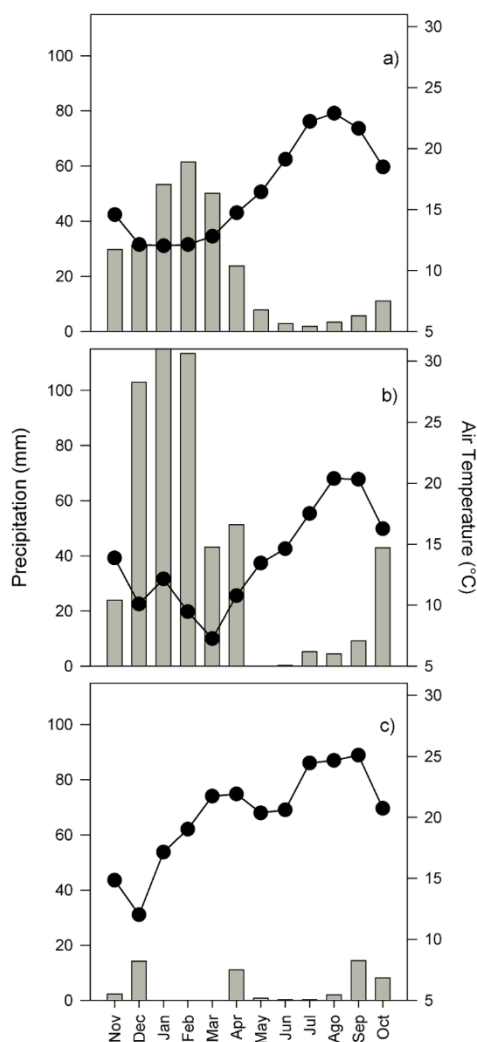


Figure 1. Monthly averages of air temperature (°C, black line) and monthly sums of precipitation (mm, grey bars) for a) 1954-2012 period from a meteorological station located ~755 m from our study site, b) hydrological year of 2009-2010, and c) hydrological year 2013-2014. The precipitation axis was limited to a maximum of 120 mm for comparison, but the month of January in panel b) accumulated 240 mm.

2.2.2 Eddy covariance and meteorological measurements

In 2007 an Eddy Covariance tower and an array of meteorological sensors were installed at El Mogor. The flux measurement system consisted of an open-path infrared gas analyzer (LI-7500, LI-COR, Lincoln, NE, USA), and a three-dimensional sonic anemometer (81000V, Young, Traverse City, MI, USA), located 3.54 m aboveground level. From January 2008 to April 2009 flux measurements were recorded at 10 Hz and after April 2009 at 20 Hz. Data acquisition was performed by a box computer WaySmall 200ax (Gumstix, Redwood City, CA, USA), running a Linux operating system and in-house software for data acquisition. Meteorological measurements included air temperature and relative humidity (HMP-45A, Vaisala, Helsinki, Finland), net radiation (NR Lite2, Kipp and Zonen, Delft, The Netherlands), photosynthetic photon flux density (PAR Lite, Kipp and Zonen, Delft, The Netherlands), precipitation (TR-52USW, Texas Electronics, Dallas, TX, USA), barometric pressure (PTB101B, Vaisala, Helsinki, Finland), soil heat flux plates at 8 cm depth in three separate locations (HFP01, Hukseflux, Delft, The Netherlands), soil volumetric water content using time domain reflectometers at 5, 10, 20 and 40 cm depth buried horizontally into the soil (10HS, Decagon Devices, Pullman, WA, USA), and soil temperature at 2 and 6 cm depth. All meteorological variables were recorded at 1/60 Hz. The LI-7500 calibration was checked monthly as part of the quality assurance and control protocols. For further information about the instrumentation and data acquisition system see Castro et al. (2017) and Villarreal et al. (2016).

Raw data of CO₂, H₂O and meteorological variables were processed to 30 min averages, using EddyPro (V6.0.0, LI-COR, Lincoln, Nebraska, USA; available at <https://www.licor.com/>). Half-hourly averages were not included in the time series if $\geq 10\%$ of the 30-min record was missing due to missing records or out of range values. Flux measurement corrections included the planar fit correction (Wilczak et al., 2001), Webb-Pearman-Leuning (WPL) correction (Webb et al., 1980), discard of fluxes measured under low turbulence ($u^* < 0.1 \text{ m s}^{-1}$ for all study years, similar to Villarreal et al. (2016)), and removal of values outside the average ± 3 standard deviations, using first year-round datasets and then 5-day running windows (Papale et al., 2006). Storage fluxes were not estimated since the study site has a short canopy with a well-mixed atmosphere, such that we assumed the storage flux was negligible.

2.2.3 Data analysis

For the analysis hydrological years rather than calendar years were used, as in Mediterranean climate ecosystems, the hydrological year, i.e. the year since the beginning of the rainy season, is a better reflection of climate variability than the calendar year, which regularly coincides with the peak of rainy

season (Biederman et al., 2016). It was designated the beginning of the hydrological year as November 1st and the end as October 31st. The data years were divided in two seasons: the wet season, beginning November 1st and ending April 30th, and the dry season, starting May 1st and ending October 31st. This study focused on two extreme years in terms of precipitation. During the hydrological year of November 2009-October 2010 (hereinafter *wet year*), the annual accumulated precipitation was 636.9 mm, which was 226% of the recent historical mean annual precipitation (Figure 1B). This climate anomaly was preceded by a combination of La Niña conditions in 2008-2009 and a slight El Niño in 2009-2010 (Waliser et al., 2012). In the hydrological year of November 2013-October 2014 (hereinafter *dry year*), annual precipitation reached only 45.25 mm, or 16% of the historical mean (Figure 1C). This water deficit was part of the unusual mega-drought that affected the California Floristic Province (Griffin and Anchukaitis, 2014), and their causes are arguable, from simple natural variability (Seager et al., 2015) to anthropogenic warming (Diffenbaugh et al., 2015). To compare the NEE responses of both the wet and dry years, a *control year* was estimated, which was based on the average of the measurements of NEE and meteorological data of the remaining 5 years of data which were not considered extreme in terms of weather conditions. Thus the wet season accounted for ~80% of the annual precipitation in the control year.

To test the Q1 and H1, we analyzed the sensitivity of the carbon sink/source strength using flux duration curves, analogous to flow duration curves in hydrology (Huxman et al., 2004; Potts et al., 2006; Potts et al., 2008). In brief, daily averages of 30-min NEE for a certain period (i.e., all year, wet or dry season) were ranked from most negative to most positive, regardless of date, and the rank number was adjusted to a scale of 1 to 100.

To test our Q2 and H2, regression trees were used in order to identify which environmental variables influence NEE across the study years. For this analysis, daily averages of 30-min NEE were used, as the dependent variable, and the independent variables were daily means of 30-min global radiation, vapor pressure deficit, and soil volumetric water content. Regression trees use an iterative and hierarchical process to split the data into groups, based on the explanatory variable that explains the maximum amount of deviance in the response variable in a previously remaining group. Thus, the regression trees show the meteorological variables that best divide NEE into clusters using a process known as binary recursive partitioning.

Finally, we analyzed variations in the relationship of daytime NEE (NEE_{Day}) to global radiation (R_g) using:

$$NEE_{Day} = Rg(AQY) + R_d \quad \text{Equation 1}$$

where AQY is the Apparent Quantum Yield ($\mu\text{mol CO}_2 \text{ m}^{-2} \text{ s}^{-1} / \text{W m}^{-2}$), and R_d represents the daytime ecosystem respiration ($\mu\text{mol CO}_2 \text{ m}^{-2} \text{ s}^{-1}$). Daytime was defined by global radiation $>20 \text{ W m}^{-2}$. We bin-averaged NEE_{Day} estimates, using intervals of 50 W m^{-2} in R_g , except for the first interval which was from 20 to $<50 \text{ W m}^{-2}$. Furthermore, for this analysis, data was separated for each year and period into two groups based on soil water content (dry vs wet, split at $SWC = 0.1$).

2.3 Results

2.3.1 Meteorology

The seasonal patterns of air temperature (T_a), global radiation (R_g), and vapor pressure deficit (VPD) followed a similar pattern across the period of measurements (Figure 2). Daily mean annual T_a for the wet year was $14.2 \pm 5.2 \text{ }^\circ\text{C}$, ranging from 1.1 to $23.3 \text{ }^\circ\text{C}$ during the wet season, and from 9.2 to $29.9 \text{ }^\circ\text{C}$ in the dry season; while for the dry year the daily mean annual T_a was $20.7 \pm 8.2 \text{ }^\circ\text{C}$, ranging from 6.2 to $26.3 \text{ }^\circ\text{C}$ in the wet season, and from 14.3 to $32.6 \text{ }^\circ\text{C}$ in the dry season. Annual daily mean of VPD in the wet year was $0.79 \pm 0.53 \text{ kPa}$, and $1.2 \pm 0.78 \text{ kPa}$ during the dry year. During the wet year, there was an annual accumulated precipitation of 636.9 mm, distributed in 65 precipitation events across the year, while 90.3% of the annual total occurred in the wet season. In the dry year, there was an annual total of 45.25 mm, distributed in 29 precipitation events across the year, with 60.8% occurring in the wet season. Table 1 presents the annual variation of meteorological data across the years.

Table 1. Annual values of precipitation (PPT, mm), air temperature (T_a , $^\circ\text{C}$), vapor pressure deficit (VPD, kPa), volumetric soil water content at 10cm (SWC , $\text{m}^3 \text{ m}^{-3}$), and net ecosystem exchange (NEE, $\mu\text{mol CO}_2 \text{ m}^{-2} \text{ s}^{-1}$). The wet (W) and dry (D) years are indicated.

Hydrological Year	PPT ¹	T_a ²	VPD ²	SWC ²	NEE ²
2007-2008	217.4	17.3 ± 5.7	1.09 ± 0.62	0.06 ± 0.05	-0.88 ± 1.49
2008-2009	345.5	15.9 ± 5.7	1.01 ± 0.63	0.07 ± 0.06	-0.61 ± 1.43
2009-2010 (W)	636.9	14.2 ± 5.2	0.88 ± 0.47	0.07 ± 0.06	-0.60 ± 1.38
2010-2011	352.1	15.3 ± 5.1	0.79 ± 0.53	0.05 ± 0.05	-0.66 ± 1.05
2011-2012	293.7	16.1 ± 5.5	1.01 ± 0.53	0.06 ± 0.04	-0.37 ± 1.19
2012-2013	246.3	16.4 ± 5.5	1.16 ± 0.47	0.05 ± 0.04	-0.23 ± 1.40
2013-2014 (D)	45.3	20.7 ± 8.2	1.17 ± 0.78	0.05 ± 0.06	-0.05 ± 0.69

¹Annual sum; ²daily average \pm standard deviation.

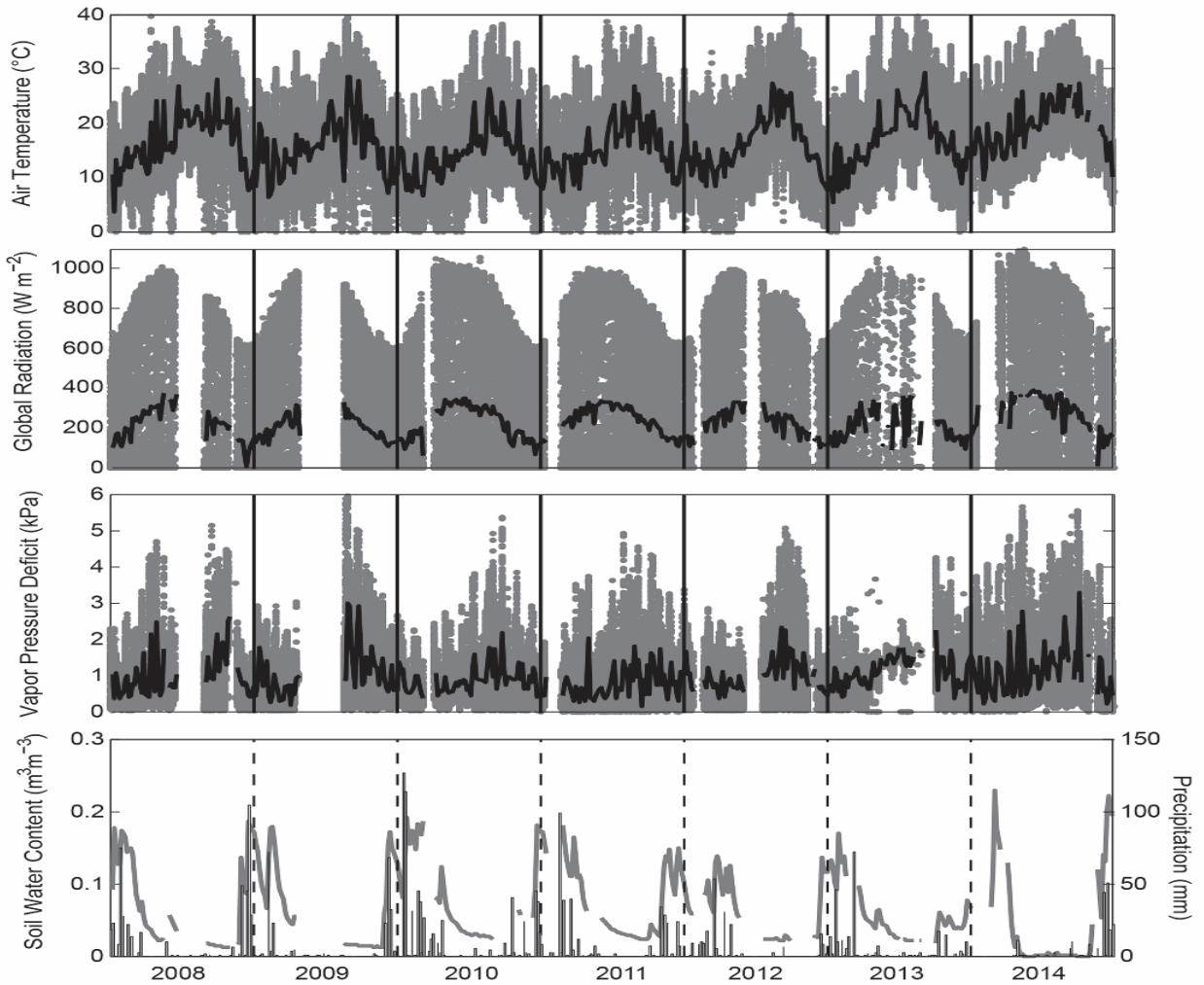


Figure 2. Five-day average (black line) and half-hourly values (grey dots) of air temperature ($^{\circ}\text{C}$), global radiation (W m^{-2}), vapor pressure deficit (kPa), and daily mean values of soil water content ($\text{m}^3 \text{m}^{-3}$) at 10 cm (grey line in bottom panel) and precipitation (mm ; bars in bottom panel) over our study period at El Mogor.

2.3.2 Carbon exchange

NEE was higher during the wet year in absolute terms (both negatively and positively) than during the dry year. During the wet year, daily NEE varied between -4.63 and $6.77 \mu\text{mol CO}_2 \text{m}^{-2} \text{s}^{-1}$; both the minimum and maximum values occurred during the wet season. During the dry season NEE varied between -4.06 and $2.67 \mu\text{mol CO}_2 \text{m}^{-2} \text{s}^{-1}$. In the dry year, daily NEE varied in the range of -3.29 to $3.76 \mu\text{mol CO}_2 \text{m}^{-2} \text{s}^{-1}$; both minimum and maximum values during the dry season. In the wet season NEE varied between -2.73 and $2.81 \mu\text{mol CO}_2 \text{m}^{-2} \text{s}^{-1}$. Mean annual daily NEE for the years in our study are presented in Table 1 and in Figure 3 is presented the time series of the 7 years that encompass this study.

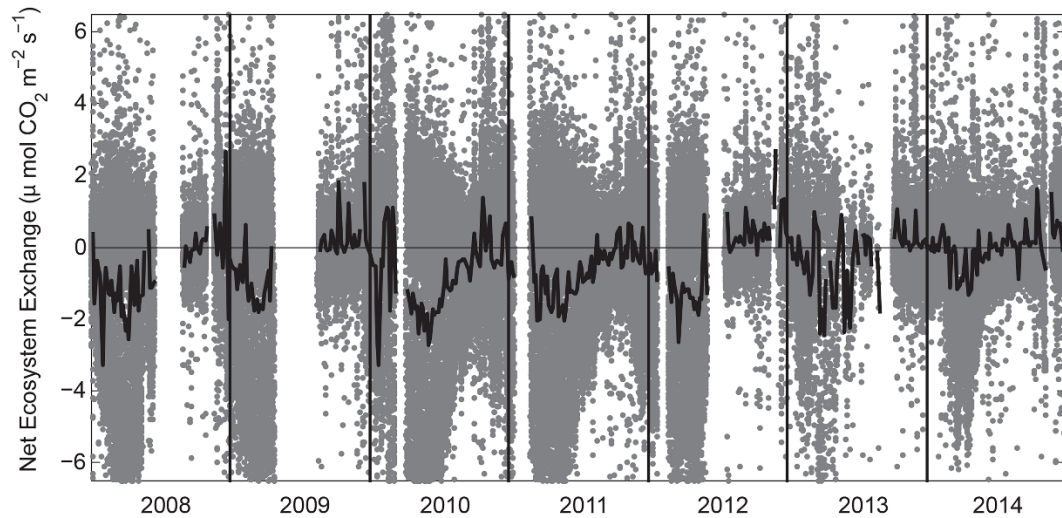


Figure 3. Five-day average (black line) and half-hourly values (grey dots) of net ecosystem exchange over our study period at El Mogor.

The flux duration curves (Figure 4) revealed that at the annual level, the ecosystem was a carbon sink during 69% of the control year, 73% of the wet year and only 48% of the dry year (Figure 4A). The ecosystem acted as a carbon sink 77% of wet season during the control year, and 57% and 54% of the wet season in the wet and dry years, respectively (Figure 4B). Finally, in the dry season, the ecosystem was a carbon sink 60% of the time in the control year, compared to 85% and 42% of the dry season in the wet and dry years, respectively (Figure 4C).

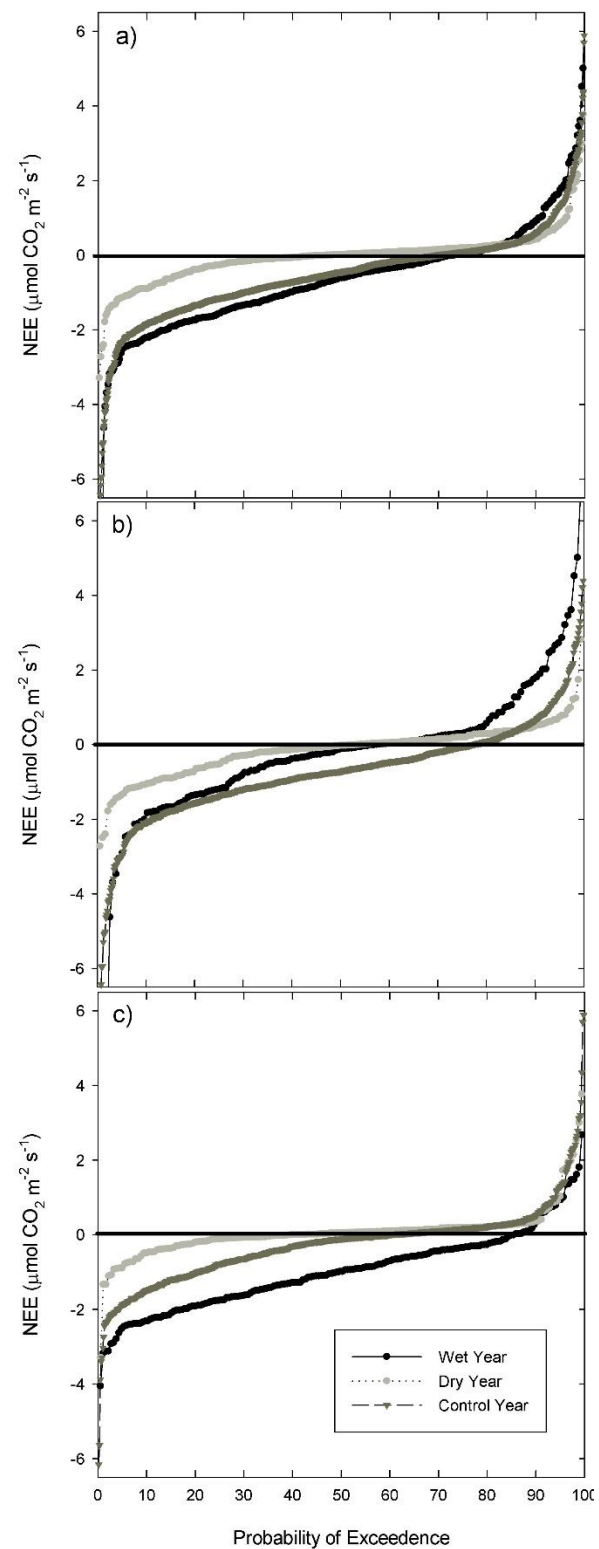


Figure 4. Flux duration curves of daily averages of net ecosystem exchange in a) all year, b) wet season, and c) dry season. By convention, negative values of NEE represent carbon uptake by the ecosystem, and positive values represent carbon losses to the atmosphere.

2.3.3 Physical controls of NEE

Using the regression tree analyses (Figure 5), we found that for the entire control year, soil water content (SWC) was the variable with the highest proportion of deviance explained, and photosynthetically active radiation (PAR) explained additional variation in the higher SWC group; however, only 16% of the total variance was accounted for. During the wet year, the first explanatory variable was PAR followed, in both low and high PAR groups, by vapor pressure deficit (VPD); in contrast to the control year, this simple model explained 47% of the variation. In the dry year SWC was the first explanatory variable, followed by VPD and PAR, and a total of 20% of the variation was explained (Figure 5G). Analyzing the wet season data, we found that PAR was the most important predictor for the control, wet and dry years (Figure 5). The control year's wet season had secondary effects by SWC under low PAR, but again the model was rather weak though significant. In the wet season of wet and dry years, VPD was a secondary factor, but at low PAR in the wet year and high PAR in the dry year; in both cases model power was higher than in the control year, though only moderate. Analyzing the dry season data, the power of the models for control and wet years was greater than in the wet season or all year, but the dry year model was weaker (Figure 5). VPD controlled the first branching, whereas PAR, SWC and VPD entered secondarily, with the most structure under high VPD values in control and dry years.

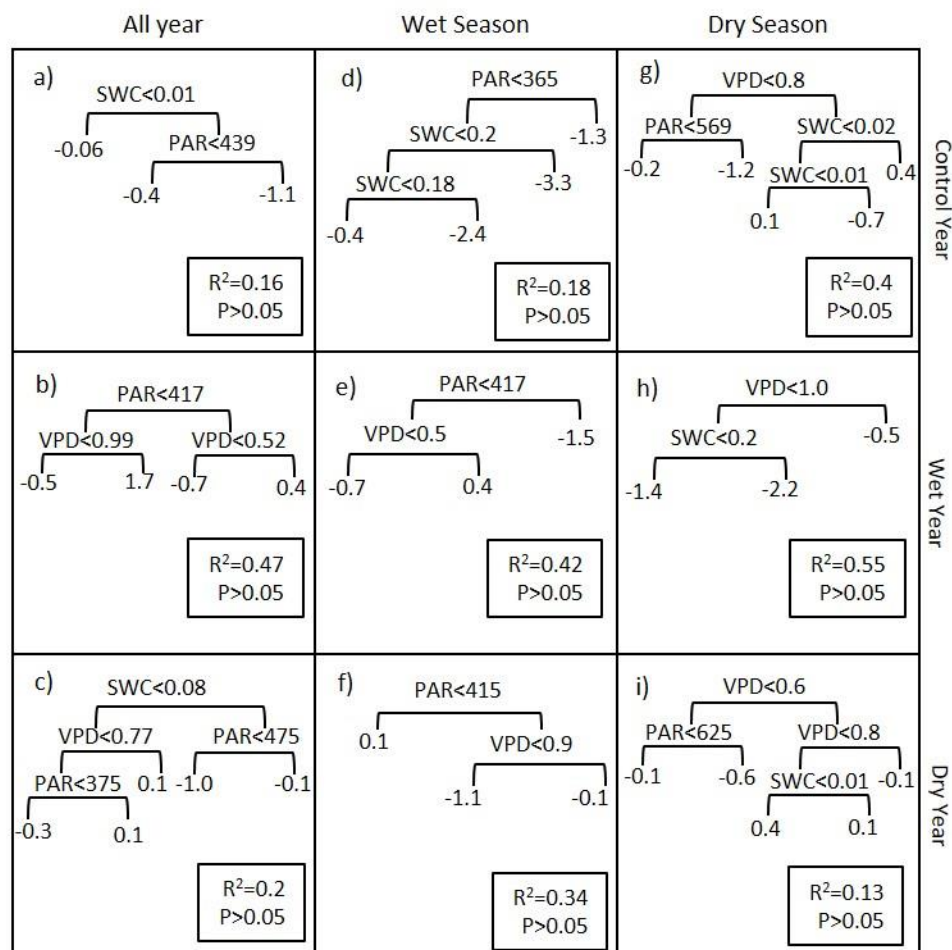


Figure 5. Regression trees for daily means of net ecosystem exchange (NEE) for: (a, b, c) all year, (d, e, f) wet season, and (g, h, i) dry season, for the control year (a, d, g), wet year (b, e, h), and dry year (c, f, i). The variable controlling each branching is noted with its critical value; lesser values define the left side branch, greater value the right side. At terminal points, the mean NEE value for the cluster is indicated. Abbreviations are as follows: PAR: Photosynthetic Active Radiation ($\mu\text{mol Photon m}^{-2} \text{s}^{-1}$), SWC: Soil Water Content ($\text{m}^3 \text{m}^{-3}$), VPD: Vapor Pressure Deficit (kPa).

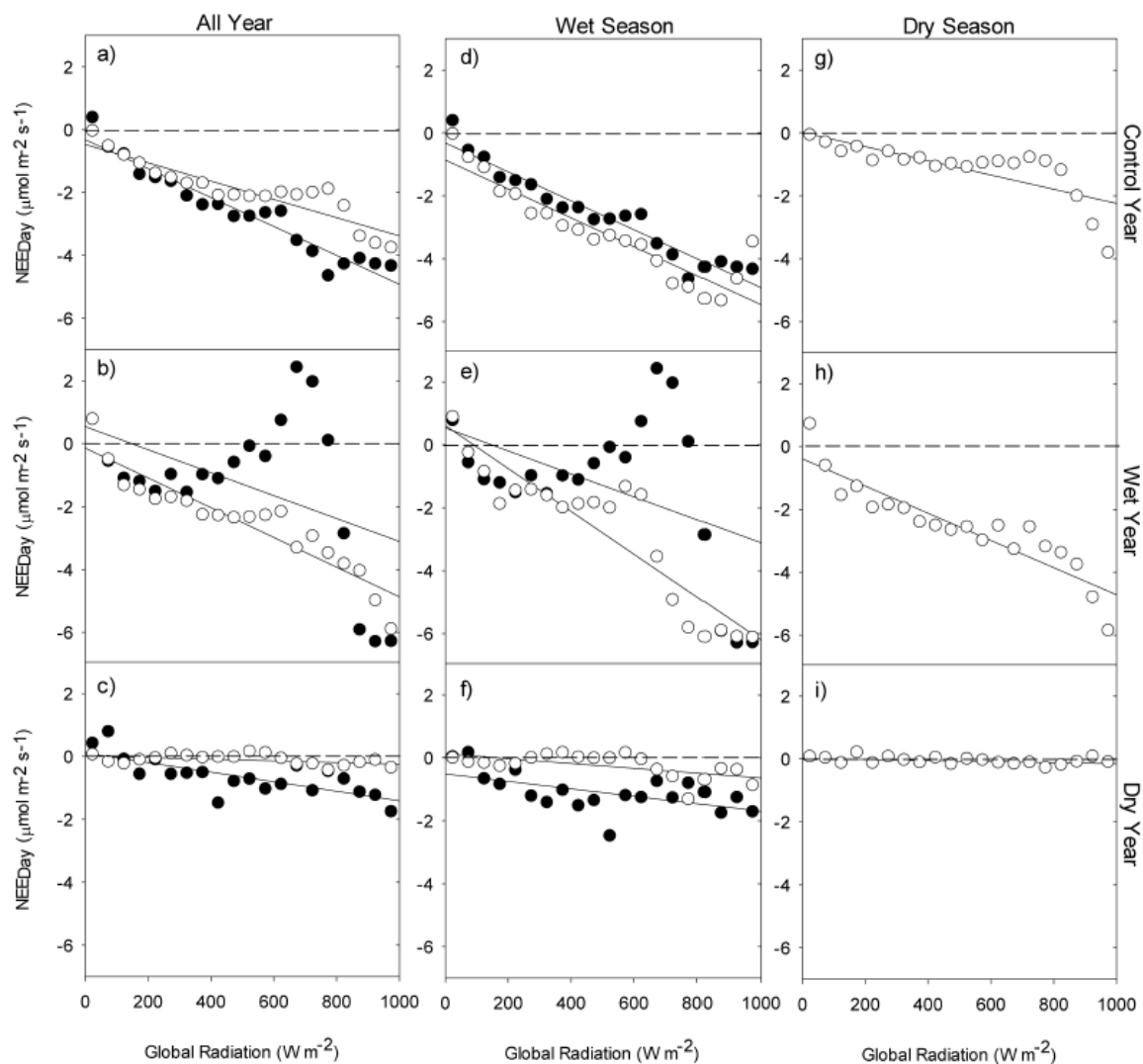


Figure 6. Relationship of daytime net ecosystem exchange and global radiation for: (a, b, c) all year, (d, e, f) wet season, and (g, h, i) dry season, for the control year (a, d, g), wet year (b, e, h), and dry year (c, f, i). Filled circles (\bullet) represent data where soil water content $>0.1 \text{ m}^3 \text{ m}^{-3}$; open circles (\circ) represent data where soil water content $<0.1 \text{ m}^3 \text{ m}^{-3}$. Dashed lines represent $\text{NEE} = 0$.

We found generally good relationships of NEE_{Day} with global radiation (R_g ; Figure 6; Table 2) except in wetter soil in the wet year. These responses differed between the dry and wet seasons, as well as in different soil moisture conditions (Figure 6; Table 2). In the control year, we found that apparent quantum yield (AQY, the slope of the line) was higher in the wet season than in the dry season (Table 2), while SWC did not affect the AQYs responses during the wet season in the control year (Table 2). During the wet year, we found that the relationship of NEE_{Day} to R_g was not significant during the wet season in soil moisture conditions of $\text{SWC} > 0.1 \text{ m}^3 \text{ m}^{-3}$ (Table 2). Moreover, we found that AQYs during the dry season of the wet year were higher in comparison with the control year (Table 2). Finally, in the dry year we found lower AQY values than in either the control or wet years, but generally lower at dry soil conditions (Table 2) than

while $SWC > 0.1 \text{ m}^3 \text{ m}^{-3}$ (Table 2). The NEE_{Day} -to- R_g relationship was not significant during the dry season of the dry year (Table 2).

Table 2. Values of the parameters of the relationship of daytime net ecosystem exchange with global radiation under different seasons and soil moisture conditions. Bold text represent significant ($P < 0.05$) relationship.

	Treatment	AQY ($\times 10^{-3}$)	R_d	R^2	P-value
All year					
Control Year	SWC > 0.1	-4.6 (-5.2, -3.9)	-0.32 (-0.68, 0.04)	0.93	<0.001
	SWC < 0.1	-2.9 (-3.5, -2.2)	-0.47 (-0.84, -0.10)	0.84	<0.001
Wet Year	SWC > 0.1	-3.5 (-7.3, 0.005)	-0.54 (-1.57, 2.64)	0.20	0.05
	SWC < 0.1	-4.73 (-5.6, -3.8)	-0.14 (-0.67, 0.38)	0.87	<0.001
Dry Year	SWC > 0.1	-1.5 (-2.2, -0.84)	0.11 (-0.28, 0.50)	0.55	<0.001
	SWC < 0.1	-0.26 (-0.5, -0.03)	0.02 (-0.12, 0.15)	0.23	0.03
Wet Season					
Control Year	SWC > 0.1	-4.6 (-5.2, -4.0)	-0.32 (-0.67, 0.04)	0.93	<0.001
	SWC < 0.1	-4.6 (-5.6, -3.6)	-0.86 (-1.44, -0.28)	0.84	<0.001
Wet Year	SWC > 0.1	-3.6 (-7.3, 0.004)	0.54 (-1.57, 2.64)	0.20	0.05
	SWC < 0.1	-6.8 (-8.4, -5.2)	0.61 (-0.28, 1.50)	0.83	<0.001
Dry Year	SWC > 0.1	-1.2 (-2.0, -0.3)	-0.51 (-0.99, -0.03)	0.33	<0.01
	SWC < 0.1	-0.8 (-1.3, -0.3)	0.13 (-0.17, 0.42)	0.36	<0.01
Dry Season					
Control Year	SWC < 0.1	-2.3 (-3.2, -1.3)	0.02 (-0.53, 0.57)	0.58	<0.001
Wet Year	SWC < 0.1	-4.3 (-5.3, -3.3)	-0.39 (-0.95, 0.17)	0.83	<0.001
Dry Year	SWC < 0.1	-0.2 (-0.3, 0.01)	0.02 (-0.07, 0.12)	0.18	0.06

2.4 Discussion

We presented 7 data-years of net ecosystem exchange and meteorological variables in a semiarid shrubland (2008-2014), including two years of anomalous total precipitation, with 226% and 16% of the long-term mean of 281 mm. Our results do not support our H1, because we observed large differences in the strength and duration of the ecosystem being a carbon sink/source during the dry season, when water availability is progressively diminished and always limiting. The results also do not support H2: we found differences in the responses to other physical controls of the net ecosystem exchange during the wet season, when water was not a limiting factor.

We found that our study site acted as a carbon sink 69% of the time in average years. However, this level could change if unexpected water availability or deficit occurs. The length of the net carbon uptake period increased during the wet year by only 4%, but there was a stronger effect during the dry year with a decrease of 21%. Although the wet year had little effect on the duration of net uptake, it showed substantially higher NEE during the dry season, driven by greater-than-normal SWC (Scott et al., 2004).

The anomalously wet winter also had a period of high net emission and was not exceptional in uptake. Thus, during abnormally wet years there could be an extended growing season (Heisler-White et al., 2008) although the excess of water availability also implies an increase in respiratory processes (Kim et al., 2012) such that an appreciable part of the growing season could have net emission of CO₂. For the wet season, the duration of net carbon uptake was similar in the wet and dry years (57% and 54%), but longer in the control (77%). Again, during the wet season of the wet year, a stronger net emission was seen (Figure 4B) in comparison with the control and dry years. There may be various causes of this net efflux. The excess of water availability could influence the rates of decomposition by microorganisms in the soil, increasing the soil CO₂ efflux. Also this excess of water could have promoted decomposition of organic matter deeper within the soil profile than in other years, or an extended decomposition period may have affected more recalcitrant organic matter (Kuzyakov, 2010). These may be common in arid and semiarid ecosystems where water availability is the main constrain on metabolic rates (Xu et al., 2004).

On the other hand, during the wet season of the dry year, the carbon uptake period was potentially shortened by the lack of water availability, constraining vegetation to photosynthesize, as previous studies had reported (Scott et al., 2015). Moreover, it is acknowledged that the amount and intensity of precipitation events could promote different ecosystem processes. For instance, Huxman et al. (2004) suggested that small and infrequent precipitation events could promote higher heterotrophic respiration, rather than photosynthesis which needs a moderate accumulation of precipitation to be activated.

Clearly, there is a need to enhance our knowledge on how abnormally wet conditions can influence respiratory process both above and below ground, and how these interact with photosynthesis. This is particularly important to ecosystem carbon budgets because it would improve flux partitioning algorithms based in nighttime or daytime data (Lasslop et al., 2010; Reichstein et al., 2005) by integrating ecosystem processes that have not been taken into account previously (Heskel et al., 2013). For example, our results showed that daytime net ecosystem exchange had an unstable relationship with global radiation during the wet year, particularly in the wet season. This could have been due to enhanced decomposition rates during daytime. Moreover, during the dry season of the dry year this relationship was lost, probably due to an inhibition of photosynthesis due to water stress. Thus, incorporating information about decomposition rates (Phillips et al., 2016) and the effect of drought (Vargas et al., 2013a) in empirical- and process-based models should improve carbon budgets estimates. Whether the dynamic of NEE or respiration are affected by photodegradation in dry conditions (Austin and Vivanco, 2006) is beyond the scope of this study.

In contrast, during the dry season, we noted a longer net uptake period in the wet year (85% of the season), and a shortened carbon uptake period for the dry year (42 % of the season), in comparison with the control year (60 % of the dry season). The strength of the carbon sink also was higher in the dry season of the wet year than for the control year. The extended net uptake period during the dry season of the wet year was probably due to the water availability within the soil profile, raised to a high-than-normal level during the wet season. The depth of water storage and withdrawal probably varies according to precipitation total and pattern, and may leave water available beyond the end of a wet year, for transpiration or deeper drainage (Del Toro-Guerrero et al., 2014).

Furthermore, we noted that the apparent quantum yield (AQY) changed between seasons and among the study years. This is important for remote sensing applications for the estimation of gross primary production (GPP). For example, AQY can be used as analogous of light use efficiency (LUE) (Knox et al., 2017), since is the relationship of carbon uptake and solar irradiance. The Moderate Resolution Imaging Spectroradiometer (MODIS) GPP product (MOD17A2/A3) uses fixed values of LUE for specific ecosystem types. Then, during droughts or higher than expected water availability potential biases could be expected. Thus, during drought overestimations of GPP could occur, since the LUE decreases under limiting water conditions, and during excess of water availability underestimations could occur, due to an increase of the LUE. Then, incorporate the effects of the changes in water availability across ecosystems would increase the accuracy of global scale estimations of GPP.

2.5 Conclusion

This research explored the effects on net ecosystem exchange and its relation to physical factors, of contrasting extremes of annual climate in terms of precipitation. We found that during the wet year our semiarid ecosystem was not constrained by water availability, presenting a period of net carbon uptake extended across most of the year, although excess of water also could enhance decomposition rates during daytime, affecting the relationship of daytime net ecosystem exchange to radiation and pushing the system to be a CO₂ source. This is important when flux partitioning algorithms are used, in particular when using light-response curves to estimate gross primary productivity, because there could be ecosystem processes not taken into account, leading to potential biases in its estimations. Although soil moisture variation (or precipitation) organized most of the NEE dynamic, the variable of first importance in the wet season of control, wet and dry years was photosynthetically active radiation, and the first in the dry season for all years was vapor pressure deficit.

Chapter 3. Gross primary productivity in a dryland ecosystem: models with greenness, meteorological factors and a proxy of foliage senescence

3.1 Introduction

It has been demonstrated that water-limited ecosystems may have an important contribution to the inter-annual variability of the terrestrial carbon cycle (Ahlström et al., 2015; Poulter et al., 2014). However, water-limited ecosystems are poorly represented among sites that monitor short-term carbon fluxes, since these areas are generally remote and mostly found in low-developed countries, and it is unlikely that eddy covariance (EC) stations will proliferate widely in such ecosystems; thus, alternative methods are clearly needed.

The EC technique (Baldocchi, 2003; Baldocchi, 2014), coupled with flux-partitioning algorithms (Lasslop et al., 2010; Reichstein et al., 2005), has provided unique information about the major fluxes of carbon between ecosystems and the atmosphere at the ecosystem scale. The EC methods are promoted as the method most integrative of processes (e.g., ecosystem productivity and respiration) and detailed in time and least disruptive of its sample area (Baldocchi, 2014). However, it is acknowledged that regional and global networks of EC stations do not have a good spatial representation of water-limited ecosystems (Biederman et al., 2017; Hargrove et al., 2003; Kumar et al., 2016; Yang et al., 2008). Moreover, recent global-scale studies (Beer et al., 2010; Tramontana et al., 2016; Yuan et al., 2014) highlighted that empirical- and process-based models, including MOD17 from MODIS, have a lower performance in approximating EC-derived gross primary production (GPP) in water-limited ecosystems and under drought conditions than in mesic-temperate sites, probably due to the generalization of its algorithms across terrestrial ecosystems.

In the last two decades, automated digital time-lapse cameras or “phenocams”, digital cameras programmed to take photographs in a continuous fixed interval of time, has been used as a near-surface remote sensing technique, gaining popularity to monitor vegetation phenology across regional and global networks (Brown et al., 2016). Time-lapse photography has been demonstrated to be a powerful tool for detecting important temporal changes in local vegetation status (Keenan et al., 2014), mainly in forested ecosystems, with a few examples in water-limited ecosystems. For instance, in a semiarid creosote shrubland in Arizona, an index derived from phenocam data tracked the green-up of the evergreen vegetation, having a good agreement with net ecosystem exchange of CO₂ (Kurc and Benton, 2010). In a

C3-dominated prairie in Wyoming, Zelikova et al. (2015) found a good agreement between their phenocam-derived greenness index and total biomass across different treatments in a temperature and CO₂ enrichment experiment. In a savanna in the Northern Territory of Australia, phenocam data were used to evaluate the correlation of GPP between the understory (grasses) and overstory (trees) (Moore et al., 2017). Thus, time-lapse digital photography can provide spectral as well as panchromatic data, mainly in the visible light region, to evaluate aspects of vegetation phenology in water-limited ecosystems.

Recently, phenocam data have been coupled with meteorological indices to model gross primary productivity of terrestrial ecosystems, including grasslands (Migliavacca et al., 2011), wetlands (Knox et al., 2017; Westergaard-Nielsen et al., 2013), savannas (Moore et al., 2017), and agro-ecosystems (Sakamoto et al., 2012; Zhou et al., 2013). Those studies use a light use efficiency model (Monteith, 1972), such as the GPP model from the MODIS satellite platform (Running et al., 2004), which relate vegetation carbon uptake to the amount of radiation absorbed by vegetation. However, it is acknowledged that empirical- and process-based models to predict GPP need a better representation of vegetation phenology (Richardson et al., 2012).

A current challenge, aside the proper estimation of the start, end, and length of the growing season (Liu et al., 2016), is how to incorporate the influence of senescence or ageing of leaves of vegetation in the estimation of GPP. Leaves have higher photosynthetic rates when new than at the end of the growing season, as had been noted in studies at the ecosystem (Shi et al., 2014; Turner et al., 2003; Yuan et al., 2014) and leaf scale (Chabot and Hicks, 1982; Niinemets, 2016; Niinemets et al., 2005; Sobrado, 1994). Thus, it seems likely that the omission of foliage senescence could bias the estimation of GPP from vegetation indices, especially after the foliage has passed its maximum photosynthetic rates. Furthermore, most of the efforts to improve the understanding of vegetation phenology have come from forested ecosystems, and there is a lack of knowledge of how phenology influences GPP in water-limited ecosystems.

Our main goal was to develop a semi-empirical model of GPP dynamics for a semiarid shrubland, adjusted to GPP derived from eddy covariance, using phenocam and meteorological data. We addressed the following research questions: i) Can a vegetation index, obtained from phenocam imagery, represent the canopy seasonal dynamics of a sclerophyllous semiarid shrubland? ii) Which meteorological variables contribute to adjusting a simple light-use vegetation-index model to GPP as obtained from EC flux methods? iii) Can a meteorological proxy for canopy aging or senescence improve GPP estimates? These

research questions were explored using one year of data from a water-limited shrubland in northwestern Mexico.

3.2 Methodology

3.2.1 Study site

We carried out our experiment from January to December 2016 at Rancho El Mogor, Valle de Guadalupe, Baja California, México (c. 32.0302 N, 116.6042 W, 406 m). The vegetation was dominated by a mixture of chaparral and sclerophyllous shrubs, and was last burned in 1988. The region has a Mediterranean-type climate with warm and dry summers, and cool and moist winters. The mean annual temperature was 17°C and mean annual precipitation was 281 mm, with most rain from November to March. Soils at El Mogor were a shallow sandy loam, developed from intrusive igneous rock (Franco-Vizcaíno and Sosa-Ramírez, 1997; León et al., 2014; Villarreal et al., 2016).

3.2.2 Time-lapse repeated photography

To monitor plant greenness, we used a similar methodology to that of Kurc and Benton (2010). Briefly, we used three wildlife cameras (M-550, Moultrie, Birmingham, AL, USA) with an image resolution of 2304x1728 pixels. The cameras were located within the footprint of the EC tower, each facing a representative patch of vegetation, with a depth of field from 6 to 10 m. The cameras were static, oriented in parallel with the soil surface, facing north, at ~1.5m aboveground. Photographs were taken at 30 minute intervals between 4:00 and 19:30, but to minimize shadows and restrict the variation of light intensity, this study includes only photographs taken between 11:00 and 15:00. About 10,000 images were analyzed, corresponding to a time range of 365 days; gaps in the records were caused by battery failure.

3.2.3 Image analysis

We defined a single polygon or region of interest (ROI) in the view of each camera, limited to include only vegetation. Each of the ROIs was invariant across the duration of the study. From each pixel within the ROIs, the digital signatures of the intensity of red, green and blue were extracted and averaged on a per-day frequency (Supplementary Figure S3) using the Matlab-based PhenoCam GUI software, available from the PhenoCam Network (<https://phenocam.sr.unh.edu/webcam/tools/>). With these data we estimated a daily greenness index (Ig) following (Richardson et al., 2007):

$$Ig = (2 \times green) - (red + blue) \quad \text{Equation 2}$$

3.2.4 Eddy covariance and meteorological data

We established an eddy covariance tower equipped with an infrared gas analyzer (LI7500, LI-COR, Lincoln, NE, USA), an ultrasonic tridimensional anemometer (WindMaster, Gill Instruments, Hampshire, UK), connected to a datalogger (LI7550A, LI-COR, Lincoln, NE, USA) with a recording frequency of 20 Hz. Meteorological measurements consisted in air temperature and relative humidity (HMP155, Vaisala, Helsinki, Finland), precipitation (TR-525M, Texas Electronics, TX, USA), global radiation (LI-200R, LI-COR, Lincoln, NE, USA), photosynthetic active radiation (LI-190R, LI-COR, Lincoln, NE, USA), soil moisture and temperature (Hydra Probe II, Stevens, Portland, OR, USA), net radiation (NR Lite2, Kipp & Zonen), and soil heat flux (HFPO1, Hukseflux, Delf, The Netherlands). All meteorological data was collected on a datalogger (XLite 9210B, Sutron, Sterling, VA, USA).

Data derived from the eddy covariance tower were processed to 30 min averages, using EddyPro (V6.0.0, LI-COR, Lincoln, Nebraska, USA; available at <https://www.licor.com/>). Corrections to flux measurements included the WPL correction (Webb et al., 1980), as well as the planar fit correction (Wilczak et al., 2001), discard of fluxes under low turbulence ($u^* < 0.1 \text{ m s}^{-1}$), removal of extreme and improbable values outside the average ± 3 standard deviations using first the year-round dataset and then 5-day running window (Papale et al., 2006). Gap-filling of missing values were performed according to Falge et al. (2001) and Reichstein et al. (2005). We estimated gross primary productivity (GPP) based on the relationship of nighttime net ecosystem exchange (NEE) with air temperature to estimate ecosystem respiration (Reco), following Reichstein et al. (2005), thus $GPP = NEE - Reco$. Both gap-filling and flux-partitioning were

performed in the online tool of the Max Planck Institute, available at: <https://www.bgc-jena.mpg.de/bgi/index.php/Services/REddyProcWeb>.

3.2.5 Growing season index

We used a modification of the growing season index (GSI) developed by Jolly et al. (2005). The GSI is a bioclimatic index used to model canopy development that considers three climatic explanatory variables: daily minimum temperature, daily day-length or photoperiod, and daily daytime vapor pressure deficit. Each of those variables is assumed to limit biochemical processes in vegetation and account for the variation of terrestrial vegetation phenology (Jolly et al., 2005). The effect of each variable is expressed as a unit-less scalar (0 to 1). Each variable has two thresholds which define an intermediate range in which the scalar has a linear relation to the variable, and two ranges outside the thresholds with scalar values of 0 (process stopped) or 1 (unconstrained). This type of double-threshold linear-constraint model (ramp function) has a long history and broad current use (Running et al., 2004; Zhao and Running, 2010).

We modified the original GSI formulation, using four distinct variables: 1) We used daily maximum temperature (T_{max}), rather than daily minimum temperature, due to the virtual lack of subzero temperatures and because T_{max} is a limiting factor in the hot-dry summer in the Mediterranean-climate regions (Reichstein et al., 2002); 2) We used the daily average vapor pressure deficit (VPD) due to its controls on stomatal conductance that can be linked to carbon uptake and photosynthesis (Katul et al., 2009; Medlyn et al., 2017); 3) We used daily day-length or photoperiod (P_p) which may be important for leaf flush and leaf senescence (Bauerle et al., 2012; Stoy et al., 2013); 4) We included daily averages of soil water content (SWC) in the GSI formulation due to the water-limited nature of our study region (León et al., 2014) and its importance in gas exchange processes during non-rainy periods, as well as for being a good predictor of canopy conductance and ecosystem carbon uptake (Reichstein et al., 2002). Thus, our formulation of GSI was

$$GSI = f(T_{max}) \times f(P_p) \times f(VPD) \times f(SWC) \quad \text{Equation 3}$$

Regarding the thresholds, we considered that $T_{max} \leq 15$ °C does not constrain photosynthesis, while $T_{max} \geq 35$ °C restricts photosynthesis in C3 plants (Tenhunen et al., 1987), as has been seen previously in semiarid ecosystems (Jia et al., 2014). VPD values were treated in a way similar to Jolly et al. (2005), assuming that

VPD \leq 0.9 kPa does not constrain photosynthesis and VPD \geq 4.1 kPa constrains it. For Photoperiod (Pp) values, in contrast to Jolly et al. (2005), we consider that, contrary to the inhibition of photosynthesis due to reduced length days in boreal environments, it is an excess of light can inhibit photosynthesis in subtropical arid and semiarid ecosystems. Thus, we considered that Pp \geq 12 h stopped photosynthesis but Pp \leq 10 h was not constraining. Pp was determined from thresholds of global radiation (Rg): thus, Rg $>$ 20 W m⁻² was considered as daytime and Rg $<$ 20 W m⁻² as nighttime. Finally, we specified that photosynthesis stopped with SWC \leq 0.05 m³ m⁻³ but was unconstrained with SWC \geq 0.15 m³ m⁻³ (Bell et al., 2012).

3.2.6 GPP derived from a light use efficiency model and GSI

Light use efficiency (LUE) is a metric that summarizes the amount of photosynthesis in relation to the amount of solar irradiance (Monteith, 1972). The LUE model assumes that GPP follows a linear relationship with the absorbed photosynthetically active radiation (APAR). APAR can be represented by a spectral vegetation index (Gamon et al., 1997), such as the greenness index (I_g) derived from time-lapse photography (Zhou et al., 2013). Thus, modeled GPP (GPP_{mod}; $\mu\text{mol CO}_2 \text{ m}^{-2} \text{ s}^{-1}$) can be estimated as:

$$GPP_{mod} = LUE_{max} \times I_g \times GSI \times PAR \quad \text{Equation 4}$$

where LUE_{max} is the maximum LUE ($0.012 \mu\text{mol CO}_2 \text{ m}^{-2} \text{ s}^{-1} / \mu\text{mol Photon m}^{-2} \text{ s}^{-1}$) in the entire year of study, estimated as in Gilmanov et al. (2010), using the ratio between GPP_{EC} and total incoming photosynthetically active radiation, I_g is the normalized greenness index (dimensionless), GSI is the growing season index (dimensionless), and PAR is the photosynthetically active radiation ($\mu\text{mol Photon m}^{-2} \text{ s}^{-1}$).

It is acknowledged that one of the challenges in modeling GPP is to account for foliage senescence, especially in LUE-based models because one of their main assumptions is a constant LUE_{max} (Ruimy et al., 1999; Schwalm et al., 2006). Moreover, there is a substantial lack of knowledge about the factors influencing leaf senescence (Keenan and Richardson, 2015). In northern forest ecosystems, a combination of accumulated cold degree-days and photoperiod has been used to predict leaf coloring and senescence (Delpierre et al., 2009; Keenan and Richardson, 2015). Here we use heat degree days (HDD) as a parameter to represent leaf senescence as a progressive loss of photosynthetic capacity due to accumulated heat exposure. Thus, daily HDDs was calculated as:

$$HDD(d) = \begin{cases} (T_b - T_d) & \text{if } T_d > T_b \\ 0 & \text{if } T_d \leq T_b \end{cases} \quad \text{Equation 5}$$

Where $HDD(d)$ is the heat degree-day for day d , T_b is the base temperature below which there is no adverse effect, set at the annual mean daily temperature as suggested in Idso et al. (1978), and T_d is the mean air temperature for the day d . Then, accumulated HDD (aHDD) was calculated as:

$$aHDD(d) = aHDD(d - 1) + HDD(d) \quad \text{Equation 6}$$

To initiate the accumulation of cold or heat degree-days, a certain day length is often used (e.g., Delpierre et al., 2009), but for the present study site we initiated aHDD on January 1 because January has the lowest mean temperature and is also coincident with the initiation of the moist season. We normalized aHDD and took the reciprocal as the index of senescence (iHDD), with a range between 1 (new leaves, high photosynthetic capacity) and 0 (very old leaves, no photosynthetic capacity):

$$iHDD = 1 - \frac{aHDD - aHDD_{min}}{aHDD_{max} - aHDD_{min}} \quad \text{Equation 7}$$

The full model of GPP was thus:

$$GPP_{mod} = LUE_{max} \times (I_g \times iHDD) \times GSI \times PAR \quad \text{Equation 8}$$

3.2.7 Evaluation of model performance

In order to evaluate how the GSI constraining factors and the iHDD influence the estimation of GPP_{mod} , we used 10 different formulations of its parameters (Table 3), in order to note the influence of the different environmental variables in GPP_{mod} . We use linear regressions to compare GPP_{mod} with GPP_{EC} regardless of date and different models using R^2 , root mean square error (RMSE), the Akaike Information Criterion (AIC), and the Lin's ρ concordance correlation coefficient for reproducibility.

Table 3. Representation of the different formulations used to test the growing season index (GSI), as described in Sections 2.5 and 2.6. Shaded areas represents the parameters used.

	Model formulation	$f(T_{max})$	$f(VPD)$	$f(Pp)$	$f(SWCs)$	lg_{+s}
Senescence not included						
	GSI _{T+V+P+W}					
	GSI _{V+P+W}					
	GSI _{T+P+W}					
	GSI _{T+V+W}					
	GSI _{T+V+P}					
Senescence included						
	GSI _{T+V+P+W}					
	GSI _{V+P+W}					
	GSI _{T+P+W}					
	GSI _{T+V+W}					
	GSI _{T+V+P}					

GSI=growing season index; T=maximum air temperature (Tmax within the text); V= vapor pressure deficit (VPD within the text); P=photoperiod (Pp within the text); W= soil volumetric water content (SWC within the text).

3.3 Results

3.3.1 Meteorology

For the study period, mean air temperature was 18.4°C, and the accumulated precipitation was 282 mm (Figure 7). Anomalous features of precipitation were the extreme excess in January and scarcity in February, and a moderate if highly anomalous event in September (remnants of Hurricane Paine). The minimum maximum temperature (Tmax) was 10.9 °C, and the maximum Tmax was 42.2 °C. Vapor pressure deficit (VPD) varied between 0.13 kPa and 4.7 kPa across the study period. Photoperiod (Pp) ranged between 8 h during wintertime, reaching maximums of 13 h during summertime. Measured soil volumetric water content varied between 0.01 and 0.2 m³ m⁻³.

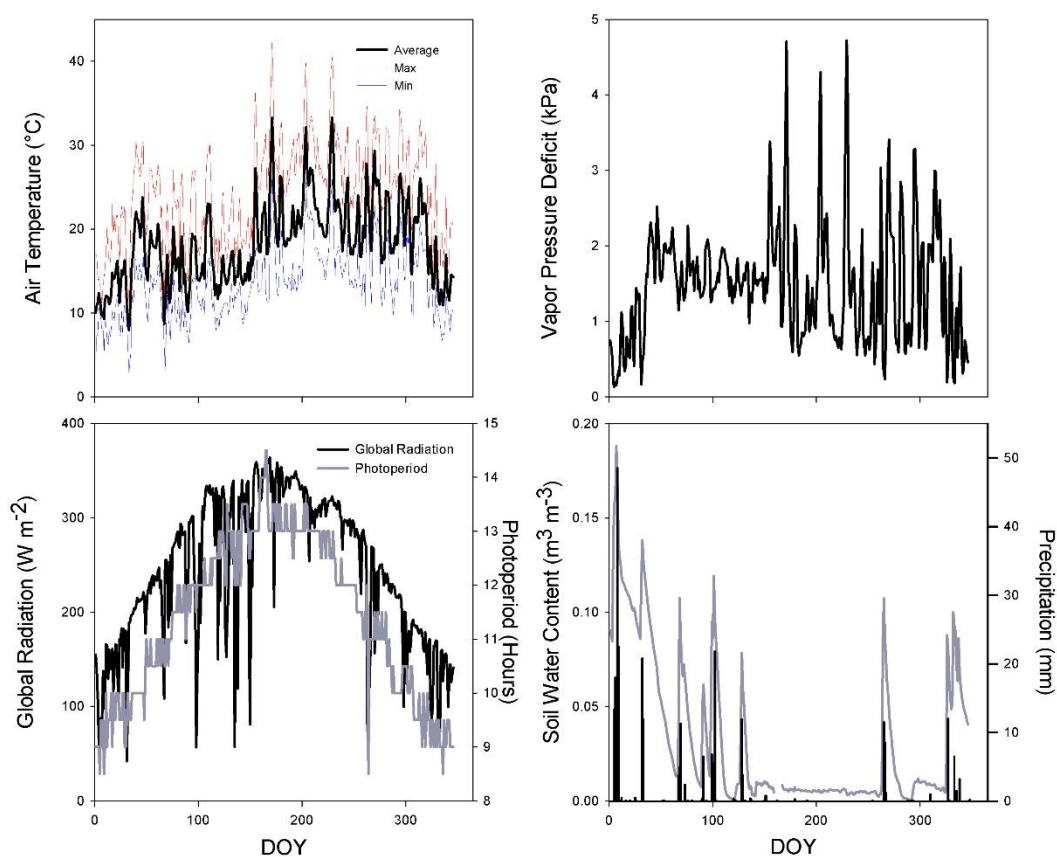


Figure 7. Daily averages of air temperature, vapor pressure deficit, global radiation, soil water content, and daily sum of precipitation, in our study sites during 2016.

3.3.2 Repeated photography and greenness index

The greenness index (I_g) showed a clear pattern of a broad annual pulse (Figure 8B), with I_g increasing from January (and perhaps before) until about 20 April followed by a persistent decline to about 31 August, with most of the values between 0.30 and 0.36 (dimensionless; Figure 8B). The abrupt increase of I_g in late September was clearly a response to the anomalous rainfall, and amounted to about 30% of the January-to-April increase. Due to a gap in the record, it is uncertain whether that level was maintained to the end of the year, or lost and then again recovered with rains in November.

When we compared the I_g index with the GPP_{EC} , using a simple linear regression, we found a good agreement ($R^2=0.63$, $P<0.01$; Figure 8C). However, the stepped increases in GPP_{EC} between January and March were not apparent in I_g , and the sudden green-up of the vegetation in late September, and moderate values of I_g through December, were not reflected in GPP_{EC} . Both records showed a brief, strong abyss in early April due to cloudy days and precipitation events in our study site (Figure 8).

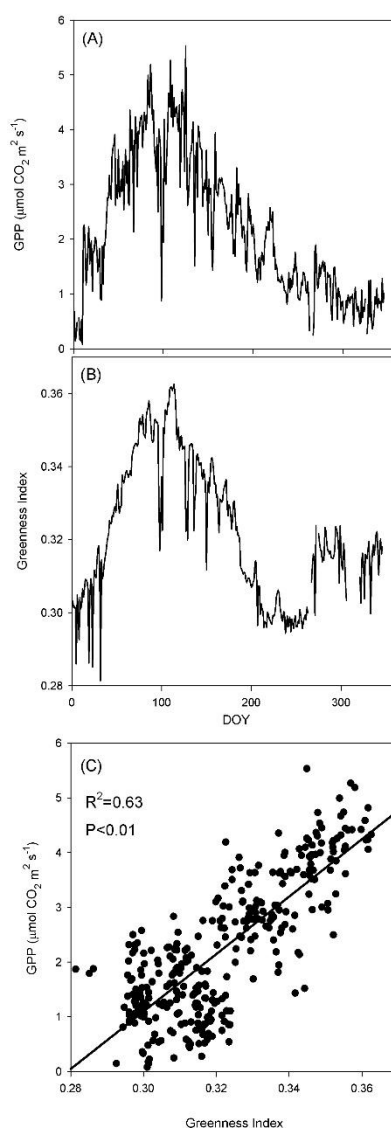


Figure 8. Time series of (A) daily averaged gross primary production derived from eddy covariance measurements (GPPEC), (B) the average of the greenness index (Ig) derived from our three phenocams located in our study site, and (C) the linear relationship of GPPEC and Ig.

3.3.3 Gross primary production from flux measurements

Daily averages of GPP_{EC} (Figure 8A) varied between 0.08 and $5.53 \mu\text{mol CO}_2 \text{ m}^{-2} \text{ s}^{-1}$, with a single broad pulse and maximum between late March and late April (Figure 8A). In the first quarter of 2016 there were sudden increases in GPP_{EC} due to precipitation events. The May to October decrease in GPP_{EC} included variations around the trend, some lasting more than 10 days, and abrupt decreases which were also marked in the Ig record. The low trough of GPP_{EC} may (or not) show a small and transitory effect of the

September rains and increased little before year end. However, from the end of October through December, GPP_{EC} remained at about twice the level of the previous January.

3.3.4 Comparison between GPP_{EC} and GPP_{mod}

The association between GPP_{EC} and GPP_{mod} improved when including the senescence parameter (GPP_{mod} without senescence $R^2=0.53$; GPP_{mod} with senescence $R^2=0.74$; Equation 3, Table 4; Figure 9B). For the growing season months (DOY 1 to DOY 180) GPP_{mod} with GPP_{EC} , we found similar results from the linear regression (i.e., similar y-intercept and regression slope) between GPP_{mod} estimated with and without the senescence parameter, however, in general, model-evaluation statistics improved slightly for the model that included the senescence parameter (Table 5; Figure 9B). For the months of decreasing GPP_{EC} (DOY 181 to DOY 365), including the senescence parameter notably improved the performance of GPP_{mod} , increasing the R^2 values from 0.45 to 0.63, decreasing RMSE values from ~ 0.5 to ~ 0.3 , decreasing AIC values from >300 to ~ 225 , and increasing Lin's ρ from ~ 0.3 to ~ 0.7 (Table 6; Figure 3B).

Table 4. Fitting statistics of linear regressions for the gross primary production (GPP_{mod}) estimated with the different formulations for the Growing Season Index described in Table 3, during all the study period, compared to the gross primary production from eddy covariance estimations (GPP_{EC}).

	Model formulation	$B0 \pm CI^*$	$m \pm CI^*$	R^2	RMSE	AIC	ρ
Senescence not included							
	$GSI_{T+V+P+W}$	1.07 ± 0.20	0.75 ± 0.08	0.53	0.77	923.1	0.67
	GSI_{V+P+W}	1.21 ± 0.22	0.84 ± 0.09	0.53	0.96	898.2	0.60
	GSI_{T+P+W}	1.11 ± 0.20	0.77 ± 0.08	0.53	0.80	840.5	0.66
	GSI_{T+V+W}	1.11 ± 0.21	0.79 ± 0.08	0.53	0.84	854.2	0.65
	GSI_{T+V+P}	1.91 ± 0.28	1.03 ± 0.11	0.53	1.50	1040.3	0.37
Senescence included							
	$GSI_{T+V+P+W}$	-0.15 ± 0.16	0.96 ± 0.06	0.74	0.49	687.2	0.84
	GSI_{V+P+W}	-0.16 ± 0.18	1.07 ± 0.07	0.74	0.62	759.1	0.84
	GSI_{T+P+W}	-0.15 ± 0.16	0.98 ± 0.06	0.74	0.52	701.9	0.85
	GSI_{T+V+W}	-0.15 ± 0.16	0.997 ± 0.06	0.74	0.53	711.7	0.85
	GSI_{T+V+P}	-0.22 ± 0.24	1.43 ± 0.09	0.74	1.10	942.3	0.70

GSI=growing season index; T=maximum air temperature (Tmax within the text); V= vapor pressure deficit (VPD within the text); P=photoperiod (Pp within the text); W= soil volumetric water content (SWC within the text); B0=linear regression intercept; m= slope of the linear regression; CI= 95% confidence interval; R^2 = coefficient of determination; RMSE=root mean square error; AIC= Akaike information criterion; ρ = Lin's concordance correlation coefficient for reproducibility; *All parameter of the linear regression models was statistically significant at $P < 0.05$.

Table 5. Fitting statistics of linear regressions for the different formulations for the Growing Season Index described in Table 3, during the growing season, compared to the gross primary production from eddy covariance estimations (GPP_{EC}).

	Model formulation	B0±CI*	m±CI*	R²	RMSE	AIC	ρ
Senescence not included							
	GSI _{T+V+P+W}	0.63±0.40	0.85±0.12	0.51	0.93	482.4	0.70
	GSI _{V+P+W}	0.71±0.45	0.95±0.14	0.51	1.17	521.2	0.63
	GSI _{T+P+W}	0.65±0.41	0.87±0.13	0.51	0.98	490.3	0.69
	GSI _{T+V+W}	0.66±0.42	0.89±0.13	0.51	1.01	495.6	0.68
	GSI _{T+V+P}	0.95±0.60	1.27±0.19	0.51	2.08	620.0	0.40
Senescence included							
	GSI _{T+V+P+W}	0.60±0.32	0.76±0.10	0.57	0.60	406.8	0.75
	GSI _{V+P+W}	0.67±0.36	0.85±0.11	0.57	0.75	445.6	0.73
	GSI _{T+P+W}	0.61±0.33	0.78±0.10	0.57	0.63	414.7	0.75
	GSI _{T+V+W}	0.62±0.33	0.79±0.10	0.57	0.65	420.0	0.75
	GSI _{T+V+P}	0.89±0.48	1.13±0.15	0.57	1.34	544.4	0.51

GSI=growing season index; T=maximum air temperature (T_{max} within the text); V= vapor pressure deficit (VPD within the text); P=photoperiod (P_p within the text); W= soil volumetric water content (SWC within the text); B0=linear regression intercept; m= slope of the linear regression; CI= 95% confidence interval; R²= coefficient of determination; RMSE=root mean square error; AIC= Akaike information criterion; ρ= Lin's concordance correlation coefficient for reproducibility; *All parameter of the linear regression models was statistically significant at P<0.05.

Table 6. Fitting statistics of linear regressions for the different formulations for the Growing Season Index described in Table 3, during the non-growing season, compared to the gross primary production from eddy covariance estimations (GPP_{EC}).

	Model formulation	B0±CI*	m±CI*	R²	RMSE	AIC	ρ
Senescence not included							
	GSI _{T+V+P+W}	0.86±0.28	1.03±0.19	0.45	0.49	317.0	0.37
	GSI _{V+P+W}	0.98±0.31	1.14±0.21	0.45	0.59	346.9	0.30
	GSI _{T+P+W}	0.90±0.28	1.05±0.19	0.45	0.50	319.9	0.36
	GSI _{T+V+W}	0.88±0.29	1.08±0.19	0.45	0.53	330.6	0.35
	GSI _{T+V+P}	1.96±0.30	1.20±0.20	0.49	0.57	340.1	0.14
Senescence included							
	GSI _{T+V+P+W}	-0.47±0.20	1.07±0.13	0.63	0.25	216.8	0.67
	GSI _{V+P+W}	-0.52±0.22	1.19±0.15	0.63	0.31	249.9	0.70
	GSI _{T+P+W}	-0.48±0.20	1.09±0.14	0.63	0.26	223.5	0.68
	GSI _{T+V+W}	-0.49±0.21	1.11±0.14	0.63	0.27	228.1	0.68
	GSI _{T+V+P}	-0.70±0.30	1.59±0.20	0.63	0.55	334.3	0.63

GSI=growing season index; T=maximum air temperature (T_{max} within the text); V= vapor pressure deficit (VPD within the text); P=photoperiod (P_p within the text); W= soil volumetric water content (SWC within the text); B0=linear regression intercept; m= slope of the linear regression; CI= 95% confidence interval; R²= coefficient of determination; RMSE=root mean square error; AIC= Akaike information criterion; ρ= Lin's concordance correlation coefficient for reproducibility; *All parameter of the linear regression models was statistically significant at P<0.05.

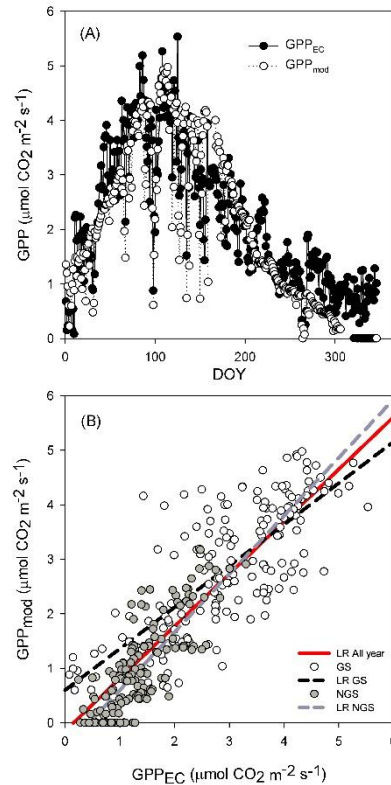


Figure 9. (A) Time series of daily averaged gross primary production derived from eddy covariance measurements (black dots; GPP_{EC}) and daily estimations of gross primary production (white dots; GPP_{mod}), from the $\text{GSI}_{\text{T+V+P+W}}$ formulation including the senescence parameter. The red line represents the linear regression for the entire study year, while the dashed black line is for the growing season, and the dashed grey line is for the non-growing season. DOY= Day of the year.

3.4 Discussion

Our results suggested that the greenness index (I_g), derived from time-lapse photography, can be used to represent the intra-annual variability of GPP in a warm, summer-dry, mostly-evergreen shrubland, because we found a good agreement between the I_g and the gross primary production derived from eddy covariance flux estimates (GPP_{EC}). Furthermore, it has been possible to develop a useful model of variability of GPP, closely related to GPP_{EC} ($R^2 = 0.74$), using light use efficiency modified by vegetation greenness and meteorological variables.

3.4.1 Digital repeated photography

We found a good agreement between the I_g and GPP_{EC} (Figure 8C), supporting the trend to apply a vegetation index from RGB intensities of time-lapse digital images as a proxy to monitor the timing and level of primary production in a semiarid Mediterranean-climate ecosystem. This proxy has been tested in various North temperate ecosystems, but there are few examples of this application of phenocams in water-limited ecosystems (Kurc and Benton, 2010; Moore et al., 2017; Zelikova et al., 2015).

In our study site the I_g index was well-suited to monitoring vegetation phenology regarding productivity. One of the main challenges to monitoring water-limited ecosystems with sclerophyllous vegetation is that leaves are present throughout the year. Across the year leaves could have different photosynthetic levels (Tenhunen et al., 1990), with or without perceptible shifts in coloration (Kurc and Benton, 2010), important shifts in concentrations of nutrients and pigments, as well as other characteristics that may not be apparent in a panchromatic view. However, despite of those temporal changes in within leaves, the I_g index in our sclerophyllous shrubland showed changes corresponding to changes in vegetation function (Figure 8B). The time series of I_g showed appreciable day-to-day variability which could be the product of changes in the quality of solar radiance (Richardson et al., 2009) due to the presence of clouds and aerosols (Kurc and Benton, 2010), or in the presence of mist, fog or dew (Sakamoto et al., 2012). Regarding this variability (Richardson et al., 2009), limitations of the cameras used in this study is that they could not be programmed to have a fixed white balance (e.g., auto-adjust of colors), do not have an infrared sensor or could be connected to internet access. However, in a comparative study by Sonnentag et al. (2012), it was shown that a model (Moultrie Game Spy I-60) similar to that used in the present study yielded results similar to cameras with a fixed white balance. Thus, our experience demonstrates that inexpensive (<\$100 dlls) consumer-grade digital cameras could serve to complement regional to international networks interested in monitoring vegetation phenology.

Despite of their usefulness, greenness indices (I_g) have not been derived from a calibrated scientific instruments although some guidelines, protocols, and recommendations have been proposed (Alberton et al., 2017; Mizunuma et al., 2014; Richardson et al., 2009; Sonnentag et al., 2012). As yet there is no basis for an absolute scale (e.g., to compare I_g from arid and mesic sites), in contrast with common remote sensing products such as NDVI. However, the PhenoCam Network (Richardson et al., 2013) has specific guidelines and protocols that may help in standardizing how vegetation phenology is monitored with consumer-grade cameras. Comparative laboratory tests (Mizunuma et al., 2014) may improve standardization.

In September 2016, when the vegetation had been stressed by months of heat and drought, there was 23 mm of rainfall at our site, from the highly anomalous remnant of a hurricane. Soon after, *Ig* showed greener vegetation but the eddy covariance system did not register an increase in GPP. The lack of functional response may have been due to the post-mature or senescent state of the foliage, perhaps with some rehydration from the rains but without substantial recovery in photosynthetic capacity. Another, non-exclusive, explanation could be that there was an abrupt increase in respiration as well as productivity. It has been reported elsewhere in warm and seasonally dry ecosystems (Verduzco et al., 2015), and observed by us at El Mogor, that the first substantial rain after a long dry season promotes a short-lived pulse of higher decomposition. Thus, while the *Ig* index was potentially showing the vegetation response to the precipitation events, the flux partitioning algorithm could have been underestimating the GPP response.

3.4.2 Modeled gross primary productivity

When we compared GPP_{mod} with GPP_{EC} we found that the best model formulation was the one that included the senescence parameter, as well as air temperature, vapor pressure deficit, photoperiod, and soil water content (Table 4, 5, and 6). The different estimates could provide insights on potential biases depending on the variable excluded. The notable example here was when our GSI index did not include SWC, formulations including and not including the senescence parameter showed the highest overestimations by GPP_{mod} (Table 4, 5, and 6). This suggests that LUE models used in water-limited ecosystems should account for constraints due to water availability. The scant effects of the exclusion of other variables suggests the GSI could be simplified.

The estimation of the light use efficiency parameter remains a crucial issue for the scientific community, with divergent practices (Gitelson and Gamon, 2015). For example, three common definitions of the light component of LUE are total incident radiation (as in the present study), total absorbed light (as in Sakamoto et al., 2012), and photosynthetically active radiation absorbed by vegetation. Use efficiency also has heterogeneous methods, with more recent innovation as the uses of vegetation-level measurements become more common and diverse (e.g., Knox et al., 2017). Clearly, the lack of a common operational definition of the LUE parameter implies a widespread lack of comparability among estimations of GPP and among the evaluation of process models (Gitelson and Gamon, 2015).

3.4.3 Foliage senescence

We have noted that the senescence parameter improved all model formulations, suggesting that decline in photosynthetic capacity is an important process that needs broader study (Niinemets, 2016) and application. While vegetation indices derived from time-lapse photography indicate the “greenness”, they do not account for photosynthetic activity, especially change in leaf function with maturation and senescence (Niinemets et al., 2005). Richardson et al. (2012) compared different process-based models and noted that they generally did not have a good representation of autumn senescence. For temperate broadleaf forest, Delpierre et al. (2009) and Keenan and Richardson (2015) provided a framework for the prediction of autumn senescence based on cold-degree days. Here, we had demonstrated that using heat-degree days in a water-limited ecosystem can improve GPP estimates derived from a LUE model.

Senescence is expected to occur from leaf budburst until the leaf drop, and leaves changes in leaf characteristics (e.g., photosynthetic capacity, nutrient content) are expected to occur from initial leaf expansion until abscission (Chabot and Hicks, 1982; Niinemets, 2016) and decline in function or senescence may be prolonged nearly throughout leaf life span. Thus, incorporating foliage senescence in empirical- and process-based models potentially could improve GPP estimates. Our results bring attention to the challenge of including vegetation senescence in models to predict GPP, and how the effect of longer growing seasons, especially due to extended periods in autumn, possibly for changes in the precipitation patterns (e.g., early or late precipitations events) and how to account for it.

The concept and application of degree-days (Wang, 1960) remain largely empirical and dependent on the biological and environmental subjects of interest, lacking a structure for comparisons among natural systems. For example, the criteria for designating the base temperatures across natural ecosystems are not standardized (Fisher et al., 2007). Also, there is a need to define when the accumulation of cold- or heat- degree days should begin. The definition of both parameters will have profound impacts on the timing, duration and degree of estimated senescence and, as a consequence, under- or over-estimations of GPP.

Thus, we suggest that if foliage senescence is not taken into account, GPP could be overestimated not only late in the year, but also in summer and spring in Mediterranean-climate shrublands (Figure 10). Clearly, more inter-seasonal study of photosynthetic capacity itself and its environmental determinants are needed. We suggest that including foliage senescence, as represented by iHDD, constrains carbon uptake in the extended duration of post-prime foliage, and should also constrain potential overestimations of GPP

during the spring and summer in relation to sporadic periods of relatively extreme heat waves. Moreover, the quality of estimates of GPP affects the evaluation of other important ecosystem properties, such as water use efficiency.

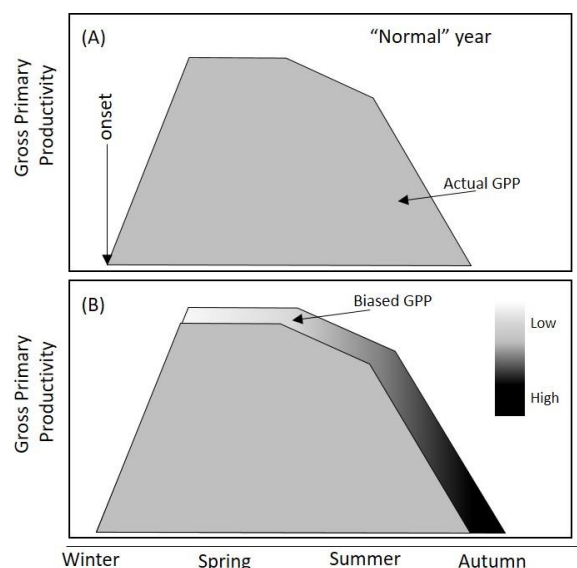


Figure 10. Schematic representation of the role of excluding the senescence parameter in models to predict gross primary productivity. In the upper panel, a “normal” year is exemplified for a Mediterranean-type ecosystem, where the physiological activity (i.e., GPP) increases during winter, have a plateau in early spring, level off in late spring and early summer, and decrease into late summer and fall. In bottom panel, the grey area represents the “ideal” model that predicts timely the phenological stages of vegetation, and the gradient area represents the potential overestimation of gross primary productivity due to the absence of limiting vegetation senescence. The omission of incorporating vegetation senescence will lead to an extended carbon uptake period, as well as a wider amplitude of the magnitude of physiological activity, with an apparent increase in gross primary productivity magnitude. This draw is based in those of Richardson et al. (2010).

3.5 Conclusion

Our study shows that daily gross primary productivity (GPP) can be modeled, with very good fidelity to the results of GPP derived from the EC technique, on seasonal and annual bases from phenocam and meteorological data in a water-limited ecosystem. This extends the validation of a low-cost method to monitor vegetation productivity and significantly change the parameters of models from mesic temperate sites. The application to water-limited systems is important because these play an important role in the inter-annual variability of the global terrestrial carbon cycle. This effort can be replicated in order to monitor warm water-limited regions which under-represented in international monitoring networks using the eddy covariance technique, and thus provide a new data stream for data-fusion modelling efforts.

We show that GPP derived from a widely-used light use efficiency model is improved if foliage senescence is included in its formulation, via a meteorological proxy. It is widely recognized that foliage senescence is not well represented in current process-oriented models. Recent methods to predict senescence in mesic temperate ecosystems using cold-degree days, need to be adapted to other terrestrial ecosystems, as we have done using heat-degree days for a semiarid site.

Chapter 4. On the spatial variability of soil respiration: does timing of measurements matter?

4.1 Introduction

Soil CO₂ efflux (or soil respiration; Rs) is considered the second largest carbon flux between terrestrial ecosystems and the atmosphere, and this flux exceeds by an order of magnitude the contribution of CO₂ due to the combustion of fossil fuels (Bond-Lamberty and Thomson, 2010; Reichstein and Beer, 2008). Temporal variability of Rs has been increasingly explored in the last two decades due to the incorporation of automated Rs measurements (Vargas et al., 2011). Nonetheless, there are still technical challenges as well as scientific tradeoffs between measuring through time or across space in ecosystems (Carbone and Vargas, 2008; Savage and Davidson, 2003). Furthermore, there is an increasing interest in understanding the spatial variability of Rs in order to integrate this knowledge into Earth System Models (Phillips et al., 2016)

Automated measurements of Rs provide unique information about temporal patterns at scales from minutes to years (Vargas et al., 2011). High-frequency measurements are capable of capturing the influence of abrupt water pulses or thawing events that result in fast metabolic changes in the soil, referred as *hot moments* of Rs (Jenerette et al., 2008; Kim et al., 2012; Kuzyakov and Blagodatskaya, 2015; León et al., 2014). However, automated measurements of Rs usually come at the expense of understanding spatial variability because of their high installation and maintenance costs.

Manual measurements performed with portable systems can provide unique information on the spatial variability of Rs, but with limited temporal resolution due to the movement of sample points (Savage and Davidson, 2003). These manual measurements have provided most of the information that is available on Rs around the world (Bond-Lamberty and Thomson, 2010), and will continue to provide results from field/laboratory experiments, and spatial surveys across ecosystems. Recently, manual measurements have revealed the importance of spatially defined areas that show disproportionately high Rs relative to the surrounding area (*hot spots*; León et al., 2014). Therefore, there is a need to quantify the factors controlling “cold”-to-“hot” Rs and the persistence of hot spots within ecosystems, to better understand the spatial variability of Rs and contribute to broader-scale models.

In a recent review, Phillips et al. (2016) noted the importance, and difficulties, of accounting for spatial variability in order to reconcile Rs with ecosystem respiration (Reco) estimates from eddy covariance

towers. It has been reported occasionally that $R_s > R_{eco}$ (Lavigne et al., 1997; Speckman et al., 2015), which is conceptually impossible, and the scientific community has been gaining interest in finding the causes of this mismatch.

To capture the spatial variability of R_s it is common that one or few instruments are used, moving from point 1 to point N . This type of survey is ideally performed within a few hours to minimize the influence of changes in soil moisture, soil temperature, and metabolic activity of heterotrophs and autotrophs throughout a day. Several biophysical factors that are considered drivers of R_s change during the day, mainly controlled by solar radiation, which influences vapor pressure deficit, soil moisture, and temperature. But spatial measurements of R_s are not independent of time because they are sequential and typically in the same sequence on every sample occasion. Among the many studies using space-time sequences of measurements, the temporal window goes from hours (León et al., 2014) to days (Søe and Buchmann, 2005). However, potentially important questions unaddressed: are the mean and variance of R_s , or the evaluation of its drivers, affected by the exact sequence of measurements?

This study tested the influence of temporal discrepancy of R_s measurements on the quantification of R_s , its drivers and its spatial dependency, in a Mediterranean shrubland across seasons. We used a gridded sampling design with two identical manual systems to measure R_s in opposite sequences but starting at the same time. The specific objectives of this study were: a) to identify differences between measurement sequences in overall means, temporal trends, and spatial dependency; and b) to determine variation in the relationships between R_s and its biophysical controls (soil temperature, soil moisture, leaf area index) associated with the timing of sampling on a range of minutes to months. The null hypothesis was that different sequences of measurement would not show significant differences in the mean value, temporal trends, and physical and spatial dependence of R_s . Our overall aim is to raise discussion on the representation of the spatial variability of R_s , on the importance of identifying hotspots of R_s throughout time, and on the effect of spatial-temporal variability in the interpretation of the biophysical determinants of R_s .

4.2 Methodology

4.2.1 Study site

The study site, El Mogor, is located in the Valle de Guadalupe, Baja California, México (32.03017 N, 116.60422 W, 406 m asl). The climate at El Mogor was semiarid Mediterranean, with warm- dry summers and cool- moist winters. Mean annual temperature was 17 °C and mean annual precipitation was 281 mm (Figure 11A). Most of the rainfall has occurred during winter (89%), with mean monthly temperatures of 11-14 °C, while in summer mean monthly temperature was 16-21 °C. Soils at the study site were shallow (~30 cm depth), and developed from intrusive igneous rock. Soil texture was sandy loam (75% sand, 14% silt, and 11% clay) with a bulk density of 0.93 g cm³ and pH between 6.6 and 7.0, with 5% of soil carbon, 0.9% of soil nitrogen (Franco-Vizcaíno and Sosa-Ramírez, 1997); fine root biomass was estimated at 0.5 kg m² (León et al., 2014). Vegetation at El Mogor was characterized by a mixture of chaparral and less sclerophyllous species. The species with the greatest ground cover at our study site were *Ornithostaphylos oppositifolia*, *Eriogonum fasciculatum*, *Adenostoma fasciculatum*, *Xylococcus bicolor* and *Malosma laurina*. The site was severely burned in 1988 and has been grazed occasionally since.

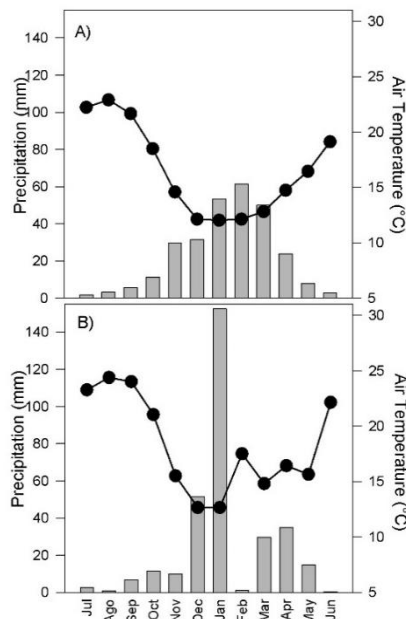


Figure 11. Mean monthly precipitation (bars, mm) and mean monthly temperature (dots, °C) during the period of 1954-2012 (A) and during the study period (July 2015-June 2016; B) at El Mogor, Baja California, Mexico.

4.2.3 Measurements and experimental design

Soil respiration (R_s) was measured using two identical LI-8100 (LI-COR, Lincoln, NE, USA) and 10 cm survey chambers (model 8100-102). Both LI-8100 infrared gas analyzers were calibrated based on factory specifications. Each sampling point had a collar of PVC of 10 cm diameter that had been inserted into the soil. The protocols of the soil respiration systems were identical and set to 30 s of pre-purge of the air within the system, 2 min and 15 s to monitor the changes in CO_2 concentration within the system to calculate soil CO_2 efflux rates, and 15 s of post purge of air within the system. Additional measurements of soil temperature and volumetric water content (Theta Probe, ML2x) were done at ≈ 10 cm depth, coupled to the LI-8100 systems.

Leaf area index (LAI) was measured at each R_s sampling point with a LAI-2200 (LI-COR, Lincoln, NE, USA). LAI measurements were carried out under diffuse light conditions using a 90° view cap to avoid the appearance of the operator on the sensor and to block direct light. The operator stood between the sensor and the rising sun at all times following protocols for Mediterranean ecosystems with open canopy (León et al., 2014; Ryu et al., 2010). Measurements were done between 6:00 and 7:00 am.

Our sampling design consisted of 25 locations across a plot of 0.5 ha distributed in a grid with 5x10 m spacing (1Figure 12). Based on Figure 12, “*forward*” measurements started at sampling point 1 continuing in order to finish at point 25, and “*backward*” measurements started sampling point 25, continuing in descending order to finish at point 1. All measurements were made between 9 am and 12 noon and both measurement sequences started and finished at the same time.

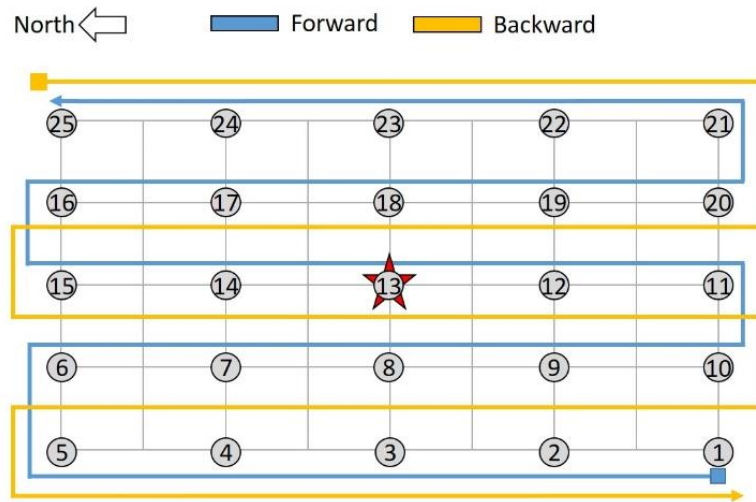


Figure 12. Schematic representation of the study plot and how was measured. The eddy covariance tower is located at the center (star). The plot extent is ~0.5 ha (approximately 50x100 m). Forward measurements (blue line) starts in the sampling point 1 in ascending order and finish in the sampling point 25, and backward measurements starts in the sampling point 25 in descendent order and finish in the sampling point 1 (yellow line).

Measurements of R_s , soil moisture, soil temperature, and leaf area index (LAI) were conducted on a monthly basis from July 2015 to June 2016. During the months of August and November of 2015 and January and April of 2016, we performed the “forward” and “backward” measurements of R_s , soil moisture and soil temperature using the LI-8100s. August is characterized by being the middle of the dry season, when the vegetation is still green but there has been no rain for months. November is usually the beginning of the wet season, and measurements were made two days after a small precipitation event (<5mm; 9.8mm in the month, Figure 11B). January is in the middle of the wet season and some precipitation events had been present (153mm in the month, Figure 11B). In April the vegetation is very active (Cueva et al., unpub.) and there were a few small precipitation events (35mm in the month, Figure 11B). The selection of those months to measure R_s was to reflect two dominant seasons, dry and wet, and the transitional periods for this water-limited ecosystem (Del Toro-Guerrero and Kretzschmar, 2016; Villarreal et al., 2016).

4.2.2 Ecosystem respiration

Micrometeorological measurements were taken from an eddy covariance tower located at our study site (MexFlux site MX-Emg, Vargas et al., 2013b). The instrumentation, data acquisition and pre-processing are described in Section 3.2.4.

We estimated ecosystem respiration (Reco) derived from nighttime measurements of net ecosystem exchange (NEE), based on the relationship of nighttime respiration and temperature following Reichstein et al. (2005). Gap-filling procedures were performed accordingly to Falge et al. (2001). The gap-filling and flux-partitioning were performed in an online tool, available at <http://www.bgc-jena.mpg.de/~MDIwork/eddyproc/index.php>.

4.2.5 Spatial analysis

To explore the spatial variability of Rs, soil moisture and soil temperature, as well as leaf area index, we used geostatistical techniques by fitting empirical semivariograms according to:

$$\gamma(h) = \frac{1}{2N_h} \sum_{i=1}^{N_h} [Y(x_{i+h}) - Y(x_i)]^2 \quad \text{Equation 9}$$

where $\gamma(h)$ is the semivariance at separation distance h , N is the number of pairs separated by h distance, $Y(x_i)$ is the value of variable Y (e.g., Rs, LAI) at point x_i , and $Y(x_i+h)$ is the value of variable Y at point x_i+h . After that, we fit different models (linear, spherical, Gaussian) to estimate the semivariogram and semivariogram parameters (nugget (τ), sill (σ), range (φ)). The choice of the semivariogram model was based on the residual sum of squares and the coefficient of determination (R^2). Estimates of variables throughout non-sampled areas were performed by ordinary kriging using the adjusted models. The weights (λ_i) for each neighboring point were determined based on the adjusted semivariogram model so that the variance of the estimates was minimized, leading to a linear system of equations according to:

$$\hat{Z}(x_0) = \lambda_i Z(x_i), \text{ with } \sum_{i=1}^{N(h)} = 1 \quad \text{Equation 10}$$

where $\hat{Z}(x_0)$ is the estimated value of the property at a non-sampled site, N is the number of values used for prediction, λ_i is the weighting associated with each value, and $Z(x_i)$ is the observed value at the i th point. All the geostatistical analyses were done using GS+ (Gamma Design Software, Plainwell, Michigan). As a measure of spatial heterogeneity, we estimated a spatial coefficient of variability according to Loescher et al. (2014):

$$CV_{\sigma} = \frac{\sqrt{2 \times \sigma}}{\mu_i}$$

Equation 11

where CV_{σ} is the coefficient of variability in relation to the sill (σ) derived from Eq. 2, and μ_i is the mean value of the measurement sequence (i.e., *forward* or *backward*). This estimate of spatial heterogeneity was shown to be more robust in comparison with the traditional coefficient of variability, because CV does not take into account the spatial correlation of data (Loescher et al., 2014).

4.2.6 Statistical analysis

Differences between means of the two measurement systems of Rs were evaluated using a two-tailed student t-test. Due to the lack of fit to a normal or Gaussian distribution for Rs, soil moisture and soil temperature, differences between measurement systems were also tested using the inverse of Bayes factors (BF; a value of $BF > 1$ indicates that data are n times better supported by the alternative hypothesis than by the null hypothesis) for student t-test and correlation analysis using JASP (V0.8.0.0; available at <https://jasp-stats.org/>).

We analyzed the correlation of Rs with soil moisture, soil temperature and LAI using empirical stepwise linear regressions, where the model selection was based on the Akaike Information Criterion, using the R package *MASS* (Venables and Ripley, 2002). When two or more variables were selected from the stepwise regression, we used a redundancy analysis ordination to partition the variability explained among the variables selected in the model, using the *vegan* package in R (Oksanen et al., 2016). We described the temporal variability of Rs, soil moisture, soil temperature, greenness index, and LAI using their monthly averages across the study period.

4.3 Results

4.3.1 Temporal variability

During the study period mean temperature was 17.8 °C and accumulated precipitation was 315.8 mm (Figure 11B). Monthly mean leaf area index (LAI) varied between 0.88 and 1.24. We noted a sharp decrease in LAI in May. Monthly means of soil respiration (Rs) varied between 0.13 and 1.65 $\mu\text{mol CO}_2 \text{ m}^2 \text{ s}^{-1}$, while ecosystem respiration (Reco) varied between 0.46 and 2.38 $\mu\text{mol CO}_2 \text{ m}^2 \text{ s}^{-1}$ (Figure 13). Rs and Reco followed a similar temporal pattern (Figure 13), and the 95% confidence intervals of Rs and Reco overlapped, showing no statistical differences.

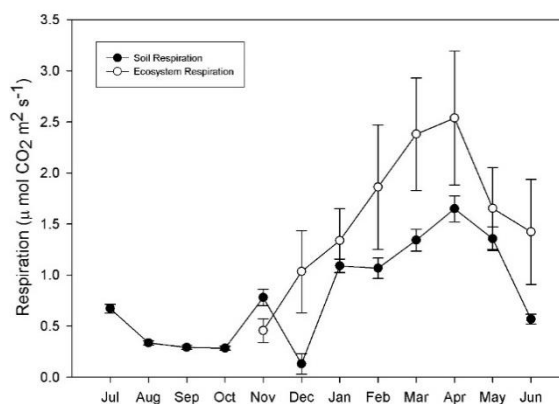


Figure 13. Temporal variability of ecosystem respiration (Reco; open circles) and soil respiration (Rs; filled circles) during the study period. For Rs each point represents the average value of 25 sampling points measured on a monthly basis across the study period. For Reco each point represents the monthly average value from half hourly estimations. Error bars represent the standard deviation.

4.3.2 Spatial variability

There was a spatial dependence for Rs (Figure 14; Table 7), soil moisture (Figure 15; Table 9), soil temperature (Figure 16; Table 8), and LAI (Figure 16; Table 10). The spatial dependence of Rs, soil temperature, and soil moisture changed across sampling months (i.e., August, November, January, and April), as well as with the sequence of measurements (i.e., *forward* and *backward*). In some instances, we found that there was no spatial dependence for Rs (August and November; Figure 14), soil moisture (November and April; Figure 15) or soil temperature (January and April; Figure 16) for one or the other of the measurement sequences. Furthermore, the variance explained by the fitted model of the semivariogram varied between measurement sequences (Table 7). The difference between the two measuring sequences was characterized by an east-to-west gradient, the differences being higher on the

west side in August and April (Figure 14C and 14L), higher on the east side during November (Figure 14F), but in January the differences were close to zero across the plot (Figure 14I).

Table 7. Semivariogram estimated parameters and models for soil respiration (Rs) during the campaigns of simultaneous measurements.

	Dir	Nugget	Sill	Range	Proportion	CV _σ	R ²	Residual SS	Model
Aug	F	0.00001	0.008	9.3	0.99	0.39	0.002	1.94x10 ⁻⁶	Exponential
	B	0.008	0.019	94.57	0.58	0.57	0.80	4.76 x10 ⁻⁶	Gaussian
	D	0.002	0.022	127.8	0.89	--	0.96	1.11x10 ⁻⁶	Gaussian
Nov	F	0.21	0.68	325.5	0.70	1.46	0.73	3.13x10 ⁻³	Exponential
	B	0.021	0.19	14.0	0.88	0.78	0	4.87x10 ⁻³	Spherical
	D	0.38	1.14	283.2	0.67	--	0.75	9.16x10 ⁻³	Exponential
Jan	F	0.0057	0.11	26.0	0.95	0.43	0.84	1.37x10 ⁻⁴	Spherical
	B	0.10	0.21	86.5	0.50	0.57	0.93	1.52x10 ⁻⁴	Spherical
	D	0.014	0.037	50.23	0.62	--	0.47	2.2x10 ⁻⁴	Gaussian
Apr	F	0.028	0.42	30.9	0.93	0.56	0.34	9.71x10 ⁻³	Exponential
	B	0.34	0.82	131.6	0.59	0.75	0.75	6.8x10 ⁻³	Spherical
	D	0.047	0.19	103.58	0.75	--	0.95	1.35x10 ⁻⁴	Gaussian

Aug: August; Nov: November; Jan: January; Apr: April; Dir: Direction of measurement; F: Forward; B: Backward; D: Difference (i.e., *forward* minus *backward*); CV_σ: Coefficient of variability in relation to the sill (it was not estimated for D, since in Eq. 4 $\mu_i \rightarrow 0$, producing unreliable results); Residual SS: Residual sum of squares.

Table 8. Semivariogram estimated parameters and models for soil temperature in the sampling months.

	Dir	Nugget	Sill	Range	Proportion	R ²	Residual SS	Model
Aug	F	4.54	12.21	31.9	0.63	0.18	24.9	Spherical
	B	4.03	13.07	122.28	0.69	0.5	6.99	Gaussian
	D	5.71	30.42	93.18	0.81	0.75	34.1	Gaussian
Nov	F	0.01	5.72	30.14	0.99	0.88	0.95	Gaussian
	B	6.87	27.6	152.77	0.75	0.80	4.05	Gaussian
	D	0.24	11.1	22.2	0.98	0.45	1.6	Exponential
Jan	F	0.001	0.81	24.1	0.99	0.54	0.032	Spherical
	B	0.001	1.01	14.0	0.99	0	0.26	Spherical
	D	1.02	2.3	214.5	0.554	0.20	0.455	Exponential
Apr	F	0.66	7.89	14.0	0.92	0	3.61	Spherical
	B	0.22	10.76	19.0	0.98	0.08	8.97	Spherical
	D	2.53	22.13	28.2	0.89	0.92	1.10	Exponential

Aug: August; Nov: November; Jan: January; Apr: April; Dir: Direction of measurement; F: Forward; B: Backward; D: Difference (i.e., *forward* minus *backward*); Residual SS: Residual sum of squares.

Table 9. Semivariogram estimated parameters and models for soil moisture in the sampling months.

	Dir	Nugget	Sill	Range	Proportion	R ²	Residual SS	Model
Aug	F	0.00007	0.00007	49.46	0	0.82	6.3 -10	Linear
	B	0.000008	0.00006	38.1	0.86	0.43	1.78 -10	Exponential
	D	0	0.00008	24.9	0.99	0.68	3.26 -10	Spherical
Nov	F	0.0002	0.0005	171.6	0.59	0.60	5.8 -9	Exponential
	B	0.00002	0.0003	3.98	0.91	0	5.6 -9	Gaussian
	D	0.000001	0.0005	14.0	0.99	0	1.47 -8	Spherical
Jan	F	0.00005	0.001	21.4	0.96	0.11	1.75 -7	Spherical
	B	0.00003	0.0007	21.3	0.96	0.07	1.34 -7	Spherical
	D	0.00001	0.001	23.2	0.90	0.40	6.52 -8	Spherical
Apr	F	0.000005	0.00008	14.0	0.94	0	8.69 -10	Spherical
	B	0.0004	0.0004	49.46	0	0.60	2.13 -8	Linear
	D	0.0007	0.0007	49.46	0	0.29	1.49 -7	Linear

Aug: August; Nov: November; Jan: January; Apr: April; Dir: Direction of measurement; F: Forward; B: Backward; D: Difference (i.e., *forward* minus *backward*); Residual SS: Residual sum of squares.

Table 10. Semivariogram estimated parameters and models for leaf area index (LAI) in the sampling months.

	Nugget	Sill	Range	Proportion	R ²	Residual SS	Model
LAI	0.037	0.82	26.1	0.95	0.30	0.03	Exponential

LAI: Leaf area index; Residual SS: Residual sum of squares

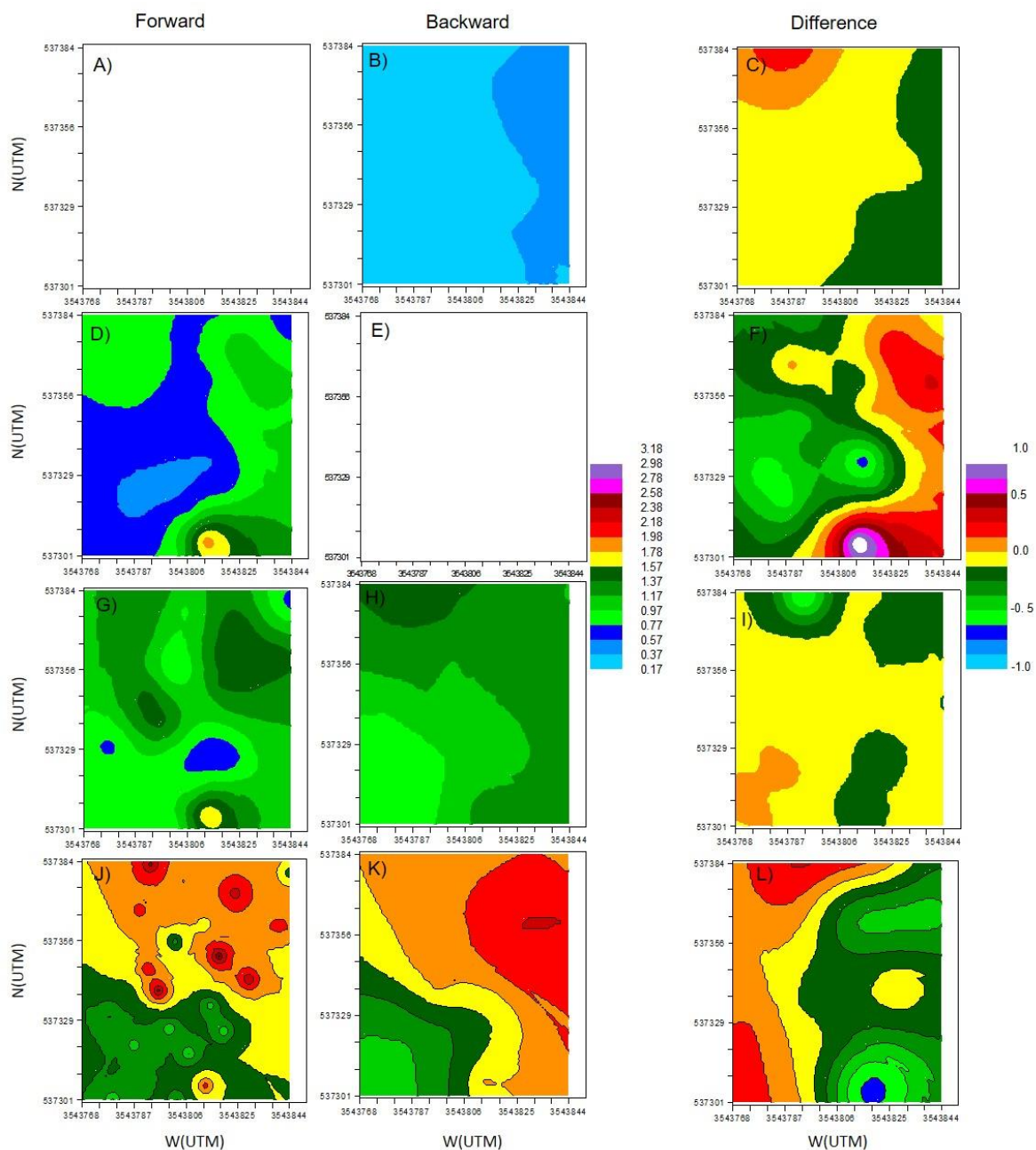


Figure 14. Spatial patterns of soil respiration (Rs) derived from ordinary kriging. Left column (A, D, G, and J) represents forward measurements, middle column (B, E, H, and K) represents backwards measurements. Right column (C, F, I, and L) represents the difference between forward minus backwards measurements. Panels A, B and C are the measurements made in August; panels D, E, and F are the measurements made in November; panels G, H, and I are the measurements made in January; panels J, K, and L are the measurements made in April.

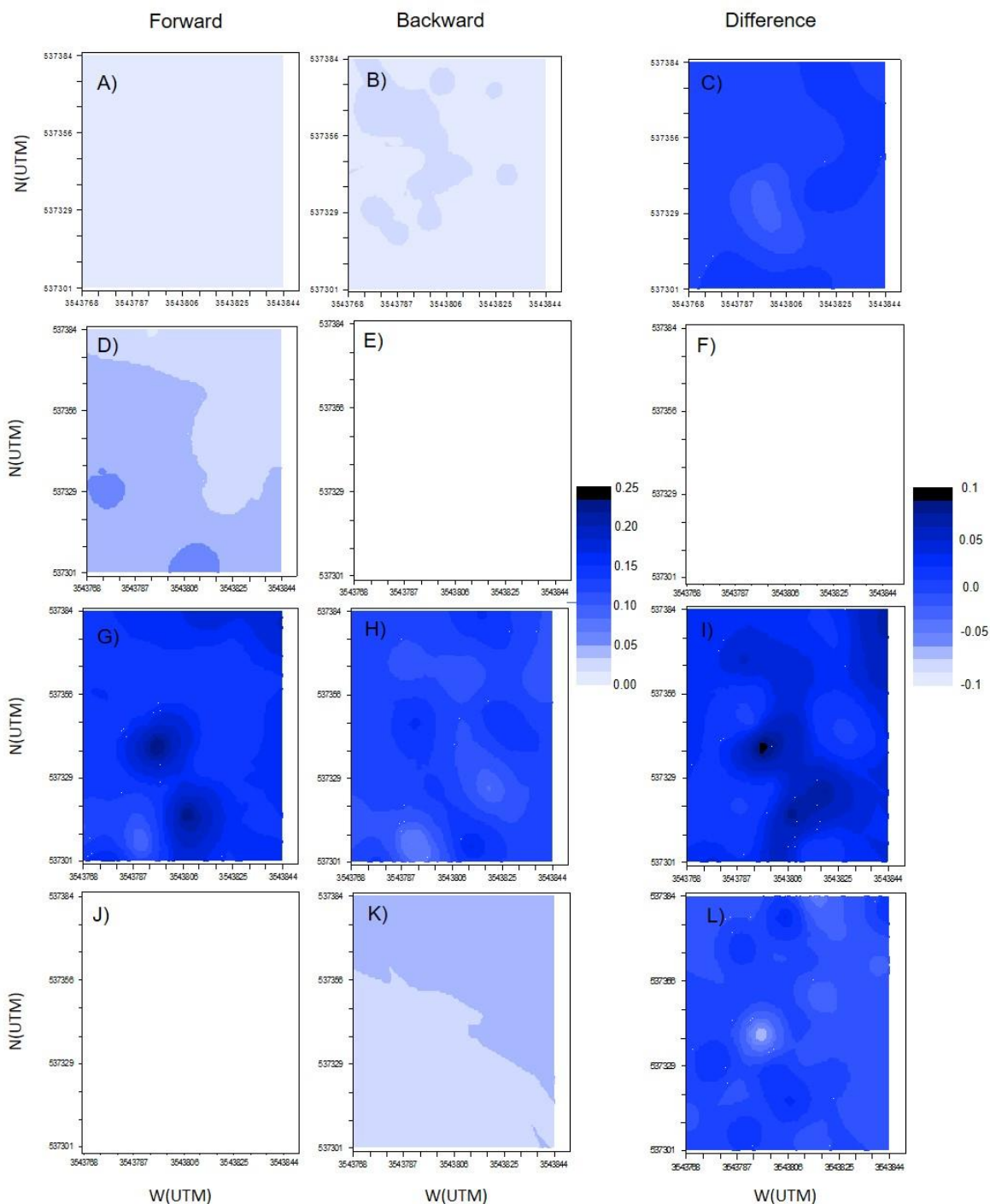


Figure 15. Spatial patterns of soil moisture (SWC) derived from ordinary kriging. Left column (A, D, G, and J) represents forward measurements, middle column (B, E, H, and K) represents backwards measurements. Right column (C, F, I, and L) represents the difference between forward minus backwards measurements. Panels A, B and C are the measurements made in August; panels D, E, and F are the measurements made in November; panels G, H, and I are the measurements made in January; panels J, K, and L are the measurements made in April.

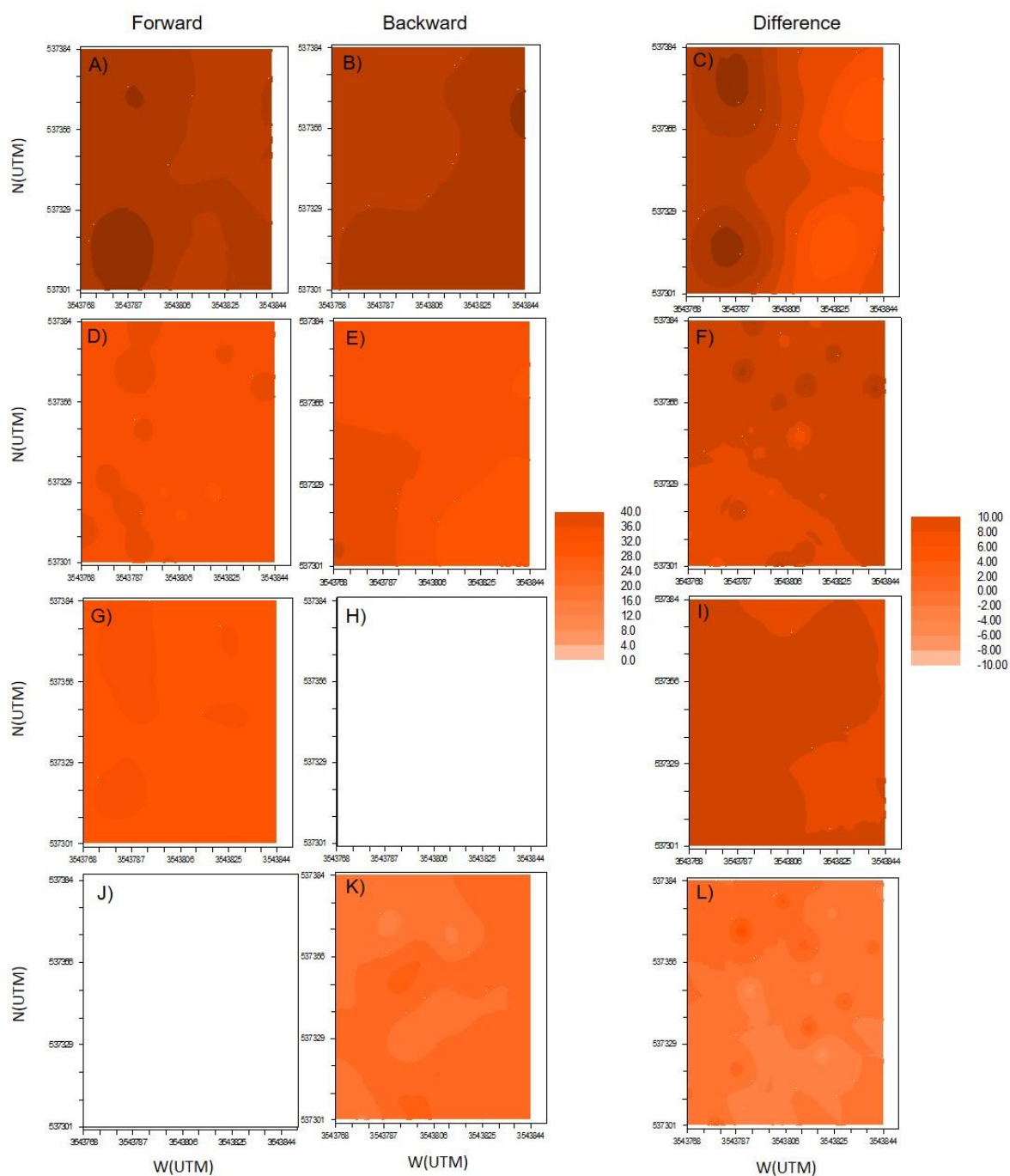


Figure 16. Spatial patterns of soil temperature (T_s) derived from ordinary kriging. Left column (A, D, G, and J) represents forward measurements, middle column (B, E, H, and K) represents backward measurements. Right column (C, F, I, and L) represents the difference between forward minus backward measurements. Panels A, B and C are the measurements made in August; panels D, E, and F are the measurements made in November; panels G, H, and I are the measurements made in January; panels J, K, and L are the measurements made in April.

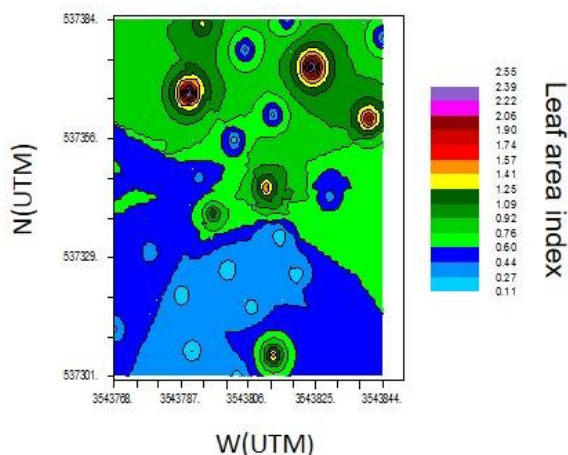


Figure 17. General spatial patterns of leaf area index (LAI) derived from ordinary kriging. LAI data represents the average value of each measurement point from September 2011 until June 2016.

The stepwise linear regression revealed that R_s consistently depended on LAI, and in lesser degree on soil moisture and soil temperature (Table 11), showing a good agreement between predicted and observed R_s (R^2 values from 0.26 to 0.64; Table 11). The redundancy analysis ordination revealed that LAI could explain from 5 to 40% of the spatial variability of R_s (inferred from the R^2), soil moisture from 5 to 14%, and soil temperature from 14 to 37% (Table 11). The predictive factors differed between the measurement sequences on any given day. It is noteworthy that during November within the *backward* sequence, neither a spatial dependence (i.e., semivariogram; Table 7) nor environmental predictors (LAI, soil moisture, soil temperature; Table 11) were found.

Table 11. Model parameters from the stepwise multiple regression and variation partitioning for the campaigns of simultaneous measurements.

Month	D	Equation	R^2				P-value
			Ts	SWC	LAI	Total	
Aug	F	$R_s = 0.29 + (0.028 * LAI)$			0.26	0.26	<0.001
	B	$R_s = -0.57 + (0.03 * Ts) + (0.02 * LAI)$	0.37		0.05	0.48	<0.001
Nov	F	$R_s = 0.28 + (8.29 * SWC) + (0.52 * LAI)$		0.05	0.21	0.29	0.02
	B	NS	NS	NS	NS	NS	NS
Jan	F	$R_s = 0.95 + (0.12 * LAI)$			0.37	0.37	<0.01
	B	$R_s = -1.41 + (0.16 * Ts) + (5.4 * SWC) + (0.12 * LAI)$	0.14	0.09	0.19	0.64	<0.001
Apr	F	$R_s = 1.40 + (0.19 * LAI)$			0.40	0.40	<0.001
	B	$R_s = 0.96 + (17.79 * SWC) + (0.12 * LAI)$		0.14	0.07	0.52	<0.001

Aug= August; Nov = November; Jan = January; Apr = April; D =Direction of measurements; F = Forward; B = Backward; Ts = soil temperature; SWC = soil water content; LAI = leaf area index; R_s = soil respiration; NS = Not Significant.

4.3.2. Comparison between measurement sequences

When we compared the measurements from the two sequences using the T-test, we did not find significant differences in Rs or soil temperature ($P>0.05$; $BF<1$; Table 12, Figure 18), but we did find differences in soil moisture during November and January ($P<0.05$; $BF\gg 1$; Table 12, Figure 18). The correlation test for Rs showed that during August, January and April the *forward* and *backward* sequences presented an approximately 1:1 agreement (Pearson correlation values (r) between 0.66 and 0.91; P -values <0.05 ; $BFs>100$; Table 13), however, during November there was no correlation between sequences (P -value=0.54; $BF<1$; Table 13).

Table 12. Descriptive statistics for soil respiration (Rs), soil temperature (Ts), and soil moisture (SWC) (mean values \pm standard deviation) during the campaigns of simultaneous measurements

	Direction	Rs ($\mu\text{mol m}^{-2} \text{s}^{-1}$)	BF	Ts ($^{\circ}\text{C}$)	BF	SWC ($\text{m}^3 \text{m}^{-3}$)	BF
August	Forward	0.32 \pm 0.10	0.293	29.3 \pm 3.43	0.36	0.009 \pm 0.009	0.235
	Backward	0.34 \pm 0.11		28.47 \pm 2.41		0.010 \pm 0.008	
November	Forward	0.80 \pm 0.58	0.224	15.15 \pm 2.25	0.252	0.04 \pm 0.02*	243,828.2
	Backward	0.79 \pm 0.41		14.53 \pm 3.22		0.08 \pm 0.01*	
January	Forward	1.09 \pm 0.33	0.484	11.51 \pm 0.90	1.06	0.16 \pm 0.03*	3250.2
	Backward	1.14 \pm 0.43		11.02 \pm 1.08		0.12 \pm 0.02*	
April	Forward	1.64 \pm 0.63	0.329	19.67 \pm 2.69	0.284	0.03 \pm 0.01	0.287
	Backward	1.71 \pm 0.73		20.39 \pm 3.25		0.03 \pm 0.02	

*Differences ($P<0.05$) using the T-test; BF: Bayes factor (Values of $BF>1$ indicates that data are n times better supported by the alternative hypothesis than by the null hypothesis).

Table 13. Correlation analysis between forward and backward measurements for soil respiration measurements.

	Intercept	Slope	r	R ²	P-value	BF
August	0.13 (0.03, 0.29)	0.57 (0.29, 0.85)	0.66	0.43	<0.001	103.7
November	0.94 (0.4, 1.48)	-0.18 (-0.78, 0.42)	-0.13	0.02	0.54	0.3
January	0.3 (0.12, 0.48)	0.69 (0.55, 0.83)	0.90	0.81	<0.001	1.2 $\times 10^7$
April	0.3 (0.01, 0.59)	0.79 (0.63, 0.94)	0.91	0.83	<0.001	3.4 $\times 10^7$

r: Pearson correlation coefficient; BF: Bayes Factor (Values of $BF>1$ indicates that data are n times better supported by the alternative hypothesis than by the null hypothesis).

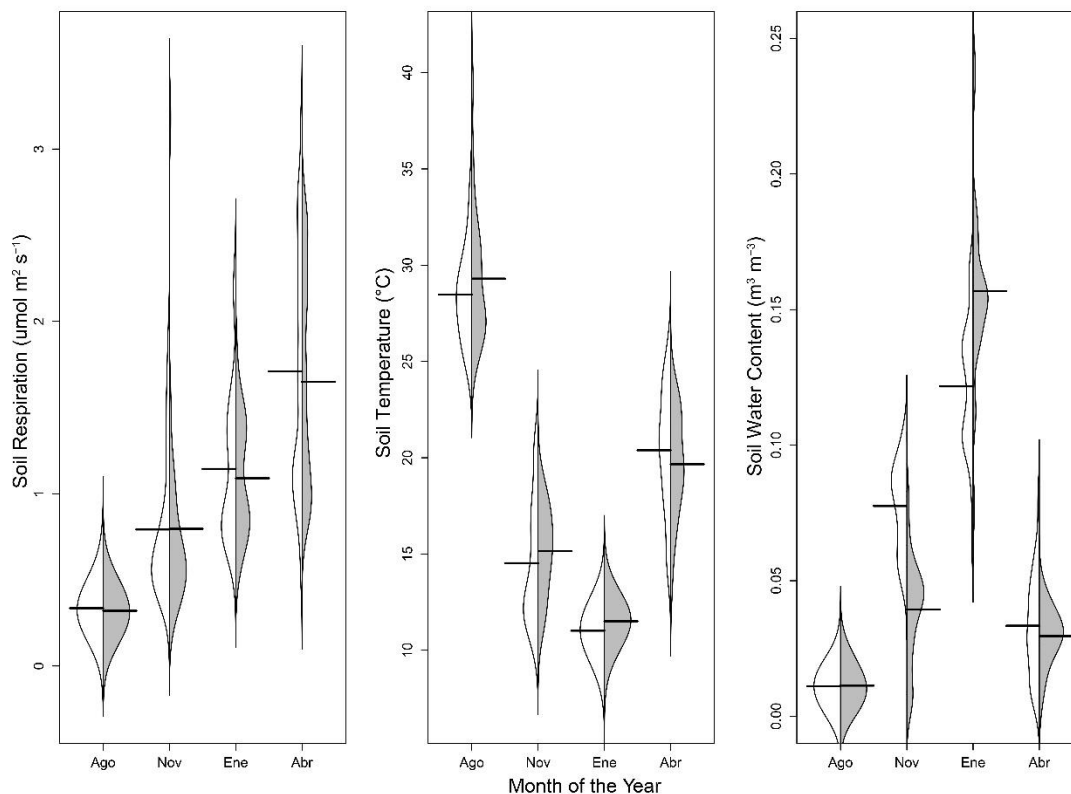


Figure 18. Bean plots of soil respiration (left), soil temperature (middle), and soil moisture (right) showing the distribution of forward (white) and backward (grey) measurements. The black line within the distributions represents the average value for the measurement direction.

4.4. Discussion

The results partially support our null hypothesis (i.e., the measurement sequence has no effect on the mean value of R_s), since we did not find statistical differences between mean plot-scale R_s from the *forward* and *backward* sequences. Nonetheless, when we explored the relationships of R_s with its environmental drivers across space (soil temperature, soil moisture, leaf area index) we found differences between measurement sequences. Moreover, we found that on two occasions (August and November) R_s did not present spatial dependence in one or the other of the measurement sequences. Lastly, we found that R_s and ecosystem respiration (R_{eco}) followed a similar temporal pattern; although in November the mean of R_s was higher than the mean of R_{eco} , they were not statistically different. Here we discuss the implications of these results (Table 14).

Table 14. Summary table of the main results of this study.

	Aug	Nov	Jan	Apr
Mean values				
Rs	↑	↑	↑	↑
Temp	↑	↑	↑	↑
θ	↑	↑*	↑*	↑
LAI	↑	↑	↑	↑
Spatial relationships				
Forward	LAI	θ+LAI	LAI	LAI
Backward	LAI+T	--	T+θ+LAI	θ+LAI
Spatial Representation				
Heterogeneity				
Forward	↑	↑	↑	↑
Backward	↑	↑	↑	↑

Rs: Soil respiration; (T)emp: Soil temperature; θ: soil moisture; LAI: Leaf area index. Arrow size represents schematically the proportional mean value of the variable. For example, the smallest arrow represents the smallest value (e.g., 1) and the biggest arrow represent the highest value (e.g., 4). Asterisks represents statistical differences in the mean value.

We demonstrated that measuring Rs in the same short sampling interval but measured in opposite sequences within a plot does not influence the plot-scale Rs average value. This provides support for temporal representation of Rs based on plot-scale measurements. However, we found that during the rewetting event in November, although we did not find statistical differences in the mean values between *forward* and *backward* sequences, their correlation was not statistically significant (i.e., 1:1 correlation). This might suggest that *hotspots* and *hot moments* could be active and potentially captured by one of the measurement sequences.

During November, the monthly average value of R_s was higher than the average value of Reco, which is theoretically impossible, but this discrepancy has been reported in other ecosystems (Phillips et al., 2016; Speckman et al., 2015) and across the scientific literature since almost 20 years ago (Lavigne et al., 1997). There could be several reasons for this discrepancy. We sampled R_s two days after a rain event which could have reactivated microbial metabolism as well as root respiration, leading to high R_s (e.g., due to a priming effect; Kuzyakov, 2010), influencing the month's mean of R_s , while Reco was averaged across the entire month from half-hour data. These high R_s fluxes (i.e., hot moments) during the beginning of the rainy season are common in Mediterranean ecosystems (León et al., 2014), but we recognize that extrapolating temporally limited R_s data to daily/monthly means could lead in overestimations of R_s across the extrapolated period (Kopittke et al., 2013).

Furthermore, R_s and Reco followed a similar temporal trend (Figure 13). This was expected since Reco and R_s depend not only on temperature and soil moisture, but also on vegetation metabolism. Other studies have noted that to improve the temporal representation of Reco, semi-empirical models need to relate temperature dependence with phenological parameters (e.g., gross primary production, NDVI, Ig, LAI) (Migliavacca et al., 2011), or include temporal lags between temperature and R_s to account for the influence of ecosystem metabolic activity on the temperature dependence of R_s (Vargas et al., 2010).

When the measurement of R_s is directed at understanding its spatial dependence, there could be confounding effects that influence its interpretation depending on measurement sequence. This is because R_s and the forcing variables are not necessarily independent of time. For example, there could be a small but significant temperature discrepancy between sampling sequences (and ultimately a temperature gradient) across the sampling period that could influence spatial dependency of R_s .

Our results show spatial and biophysical differences when analyzing the spatial dependence of R_s (Tables 7 and 11). For example, we found that the sampling error (inferred from the nugget values of the fitted semivariograms) varied between *forward* and *backward* sequences, coupled to different spatial heterogeneity, inferred from the coefficient of variability in relation to the sill (CV_o). In agreement with León et al. (2014) and Stoyan et al. (2000), we found larger spatial heterogeneity in April with higher R_s compared with August with low R_s . During January, the wettest month in our study period, the difference between sequences was close to zero (Figure 14I), and spatial heterogeneity inferred from the nugget and the CV_o was relatively low compared with November and April (Table 7), but higher than in August. This suggests that there could be *steady-state moments* of R_s , when the variability of metabolic activity is evenly distributed across space and time. Thus, sampling design (Rodeghiero and Cescatti, 2008), as well

as the number of sampling points (Adachi et al., 2005; Yim et al., 2003) have to be taken into account to improve the estimation of varying R_s (He et al., 2016), especially when high metabolic rates are expected, such as in rewetting or thawing events (Kim et al., 2012).

The stepwise linear regression showed that biophysical factors controlling R_s can change between measurement sequences as well as among sample months (Table 11). The different relationships found within each sequence indicate that soil temperature and soil moisture influenced R_s , especially in the *backward* direction (Table 11). The *backward* direction constantly presented a relationship with soil temperature and soil moisture, while the *forward* direction only presented relationships with LAI. This could be due to slight differences in morning solar radiation across the east-west axis of the plot affecting trends in soil temperature and moisture. This suggests that the spatial dependence of R_s could change within short periods of time, and could be influenced by the measurement sequence. *Hotspots* are areas of high metabolic activity in the space but are intermittent in time; consequently, they could influence the short-term relationships of R_s with biophysical factors. For instance, León et al. (2014) found a clear relationship of R_s with soil moisture in our study site, nonetheless, a hot moment influenced this relationship during November, a period of transition from dry to wet conditions. Our results bring attention to the complex spatial dynamics of R_s , and suggest that the spatial variability of R_s could change within hours or shorter time periods, not only between days (Kuzyakov and Blagodatskaya, 2015) or seasons (León et al., 2014).

4.5. Conclusion

There is an increasing interest in understanding the spatial dependence of R_s and other fluxes of soil greenhouse gases. Portable manual chambers are used to assess the spatial or environmental dependence of R_s . However, moving among sampling locations creates a temporal dependency among samples, which may entail significant changes in the apparent biophysical controls of R_s . Our main findings (Table 5) were that: 1) the measuring sequence did not affect the temporal representation of plot-level R_s , suggesting that when interest is in understanding the temporal variability of R_s , using a spatial array of samples, the average value is not affected. However, 2) the measuring sequence affected the spatial dependence of R_s and changed the significance of biophysical factors in determining R_s (soil temperature and moisture, leaf area index), altering R_s spatially. Thus, this study represents a step towards a better spatial understanding and representation of R_s in order to improve upscaling of plot-based R_s measurements to the ecosystem scale (Phillips et al., 2016).

Chapter 5. Potential bias of daily soil CO₂ efflux estimates due to sampling time¹

5.1 Introduction

Soil respiration (R_s) represents the second largest flux within the terrestrial carbon cycle, being surpassed only by gross primary productivity (Raich and Potter, 1995). This flux is estimated to be an order of magnitude greater than the CO₂ input to the atmosphere from anthropogenic fossil fuel combustion (Reichstein and Beer, 2008). R_s represents a net loss of carbon derived from root respiration and from microbial metabolism of soil carbon (Hanson et al., 2000; Ryan and Law, 2005), the largest carbon pool globally (Lal, 2004). R_s has complex spatio-temporal biophysical controls that vary on different scales (Vargas et al., 2011) as a consequence of changes in biotic (e.g., photosynthesis; Bahn et al., 2009; Kuzyakov and Gavrichkova, 2010; Mencuccini and Holtta, 2010; Vargas et al., 2010), microbial community (Nannipieri et al., 2003) and abiotic (e.g., soil temperature; Davidson and Janssens, 2006; Lloyd and Taylor, 1994), soil moisture (Kim et al., 2012; Vicca et al., 2014), soil texture (Cable et al., 2008) factors. It is important to recognize that a small change within this pool could represent a significant feedback to the earth system (Reichstein et al., 2003). Thus, sampling schemes and measurement strategies should be discussed to improve reports of R_s at the site level and across the world.

R_s is a composite of two main sources, heterotrophic (e.g., microbial metabolism) and autotrophic (root and mycorrhizae respiration) (Hanson et al., 2000). Partitioning of those sources is commonly done using trenching experiments (Bond-Lamberty et al., 2011), where roots are excised and excluded from small plots so that microbial metabolism can be assumed to be the only source of R_s . Understanding the contributions of autotrophic and heterotrophic respiration is important because they may respond differently to temperature, with different temporal correlations on a variety of time scales (Bond-Lamberty et al., 2004).

R_s has been measured for almost 90 years (Lundegårdh, 1927) and commonly has been measured using non-steady-state, manually-initiated portable chambers. Manual measurements have been popular around the world because of their portability, low implementation costs, and fewer power and security issues. Measurements using manual chambers are rapid (samples obtained within minutes), object-

¹Alejandro Cueva, Stephen H. Bullock, Eulogio López-Reyes, Rodrigo Vargas. 2017. Potential bias of daily soil CO₂ efflux estimates due to sampling time. *Scientific Reports*, 7 (11925). doi: 10.1038/s41598-017-11849-y

oriented (looking for differences between treatments without limits to their distribution), and involve visual assessment of the sample unit for every measurement. Results from these manual measurements have relatively good information on spatial variability (due to easy implementation) and are usually integrated to estimate longer-period emissions (Barton et al., 2015). These temporal integrations include annual fluxes, although this derives from a record with temporal gaps (Gomez-Casanovas et al., 2013) due to the low frequency of sampling typical of manual chambers (Figure 19). Furthermore, measurement campaigns are commonly done in daylight hours, and assume that measurements made at a specific time interval (e.g., 9 to 11 am) represent the mean daily value. Locally, that assumption could cause systematic under- or over-estimation and contribute to bias or error in annual estimates from local to global scales (see Barton et al. (2015) for an example of N₂O fluxes and Vargas and Allen (2008b) for CO₂ fluxes).

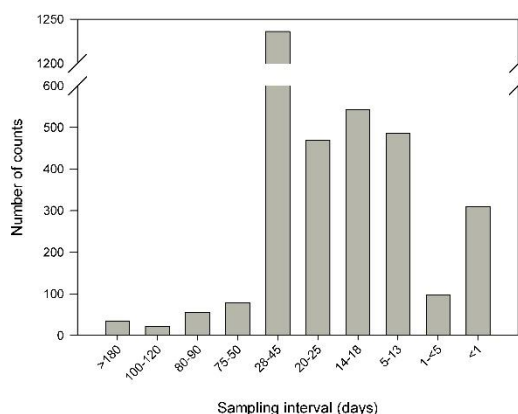


Figure 19. Histogram of a number of entries sorted by sampling interval reported in the Soil Respiration Database (SRDB V3.0). Note that the most common sampling interval is from 28-45 days (e.g., monthly, n=1236), followed by 14-18 (e.g., biweekly, n= 542). Also note that, despite the sampling interval, the annual coverage could be less than 365 days. The total number of entries in the SRDB V3.0 is 5174, but only 3332 reported a sampling interval. The SRDB V3.0 has data from 1961 to 2011.

Individual efforts to monitor Rs at the local scale are commonly performed in order to understand the temporal and spatial biophysical controls of Rs, as well as to estimate seasonal to annual carbon budgets. Those local results may be collected and input to databases of Rs for estimating global carbon budgets. However, any error in the measurements of Rs at the local scale could be propagated to the global estimation. Thus, it is important to obtain the best possible estimates at the local scale, in order to decrease uncertainties for upscaling purposes. For instance, the Global Soil Respiration Database (Bond-Lamberty and Thomson, 2010) has been constructed mostly from manual measurements of Rs. Remarkably, despite the long history of Rs measurements, little attention has been paid to how the sampling time during 24hr influences the estimation of Rs, while other shortcomings and pitfalls of

sampling have been addressed (e.g., systematic; Davidson et al., 2002; Pumpanen et al., 2004) and random (Cueva et al., 2015; Savage et al., 2008) errors in instrument measurements, sample size and strategy (He et al., 2016; Rodeghiero and Cescatti, 2008; Yim et al., 2003)).

The present work addresses the need to determine the effect of sampling time on R_s measurements. We based our analysis on the temporal stability concept (Vachaud et al., 1985; Xia et al., 2014). R_s for each hour has a relative difference (RD) with the 24hr site-level mean R_s . In turn, these values of RD may be relatively stable across hours for some months (e.g., seasonally) and can be represented by their mean (MRD). Then, MRD values close to zero indicate sampling times that are optimum, being closest to the 24hr mean; the concept can also be applied using the standard deviation or another moment. We performed our analysis on 24hr R_s data from two treatments intended to separate heterotrophic and autotrophic respiration in a Mediterranean-climate shrubland. Our purpose was to determine the time at which R_s measurements are most representative of the daily mean value and how the estimate of annual R_s could be affected by this artifact. Here we also introduce a correction factor to address the possibility of adjusting R_s measurements that are less representative due to sampling time.

5.2 Methodology

5.2.1 Estimation of the most representative time interval

Here we present a method to determine the most representative time interval to measure R_s , based on the temporal stability concept (Vachaud et al., 1985). For a collection of sample positions where R_s is measured at nearly the same times over 24hr, there is a stable relationship of the mean (or another statistic) at any time to the mean of the collection over all the times. This relationship may differ among the sample times and may also show seasonal changes. Then, the relative difference between an hourly mean of R_s and the daily mean R_s will have a range of values, and the closest to zero indicates the optimal time for sampling. This method could easily be applied regardless of site characteristics and to any periodic measurements, including other soil greenhouse gases.

The relative difference (RD) of R_s with respect to its expected value is given by:

$$RD_j = \frac{x_{ij} - \frac{\sum_{i=1}^n x_{ij}}{n}}{\frac{\sum_{i=1}^n x_{ij}}{n}}, \quad \text{Equation 12}$$

where j represents the treatment (e.g., trench), x represents the Rs measurement at the i th time interval (e.g., 9:00 am), and n represents the number of intervals (e.g., $n = 24$ (hours) in a day). The RD values are specific for each 24hr period. Thus, in order to determine a robust estimate of the most representative time interval, various 24hr periods should be taken into account. Then, to integrate the RD of different 24hr periods, the mean relative difference (MRD) is estimated as:

$$MRD_i = \frac{\sum_N^{Nmax} RD_i}{N}, \quad \text{Equation 13}$$

where N is the number of campaigns; we note that if $N=1$ then $MRD=RD$. Thus, MRD values should range between -1 and 1, or may be multiplied by 100 to be expressed as percentage. The standard deviation of the MRD (SDMRD) is defined by:

$$SDMRD_i = \sqrt{\frac{\sum_N^{Nmax} (RD_i - MRD_i)^2}{n-1}}. \quad \text{Equation 14}$$

The most representative sample interval should be that with MRD closest to zero (e.g., the minimum difference in relation with its daily mean value) and lowest SDMRD (e.g., the minimum variability in relation with its mean value; Ran et al., 2016). Thus, MRD quantifies the systematic bias of Rs at each sampling time, while SDMRD quantifies the precision of the bias. Finally, ranks are assigned in ascendant order to each MRD value (i.e., 1 is the lowest negative MRD and 24 is the highest positive MRD). Thus, we propose that the “ideal” time interval to measure Rs would be that with the middle ranking (12 or 13 for 24 hourly samples).

In order to adjust for sampling in “non-ideal” time intervals, a correction factor can be used (Xia et al., 2014):

$$\widehat{RS}_j = \frac{RS_i}{1+MRD_i'} \quad \text{Equation 15}$$

where \widehat{RS}_j is the RS_i measurement at time i th corrected by the offset derived from the MRD_i for time i th.

5.2.2 Study site

El Mogor is a MexFlux (Vargas et al., 2013b) site (MX-EMg) located within the Valle de Guadalupe, Baja California, México (32.02982 N, 116.60449 W, 409 m asl). The climate at El Mogor is semiarid Mediterranean, with warm-dry summers and cool-moist winters. Vegetation is a mixture of chaparral and sclerophyllous species. The site was severely burned in 1988 and has recovered to ~50% shrub cover. For further information about El Mogor see previous publications (Franco-Vizcaíno and Sosa-Ramírez, 1997; León et al., 2014; Villarreal et al., 2016).

5.2.3 Sampling design and measurements

In August 2011 we established three 1x1 m trenched plots, within the chaparral but lacking shrubs; we installed three PVC collars of 10 cm diameter within each plot. A trench of ~20 cm width and ~50 cm depth was excavated around each plot, lined with plastic sheeting (~1mm thick) and backfilled. The excavation depth was decided on the basis of previous studies of the depth distribution of chaparral roots, which showed >85% of the roots were in the upper 40cm of the soil profile (Kummerow et al., 1977; Stenberg et al., 1996). Herbaceous plants were removed as necessary during the study period. In areas surrounding the trenched plots (<5m) we inserted three more collars, placed within 50cm of the main stem of a shrub. The total number of collars was 2 (treatments; herein *trench* and *shrub*) x 3 (plots) x 3 (collars) = 18. Measurements in the trench and shrub plots were initiated three months after trenching (November 2011), to minimize the influence of disturbance.

We performed eight 24hr campaigns during 2014 (March, April, June, October, and November), 2015 (November), and 2016 (January and April). Those sampling campaigns represented the growing (wet) and non-growing (dry) seasons, with 4 campaigns per season. Measurements of RS , soil moisture and soil

temperature were made hourly from 9:00 of day T to 8:00 of day T+1. Furthermore, we made monthly measurements of R_s , from 12:00 to 14:00 at 25 collars on a grid pattern across 0.125 ha, in order to estimate annual carbon loss via R_s .

Soil respiration was measured using a LI-8100 (LI-COR, Lincoln, NE, USA) and a 10 cm survey chamber (model 8100-102). Measurements of soil temperature and volumetric water content (Theta Probe, ML2x) were done at ~10 cm depth within 30 cm of the R_s chamber.

5.2.3 Statistical analysis

Differences between means were tested using the inverse of Bayes factors (a value of Bayes Factor >1 indicates that data are n times better supported by the alternative hypothesis than by the null hypothesis (Méndez-Alonzo et al., 2016)) for Student's t-test. Furthermore, we used Bayesian linear regressions in order to test if functional responses of R_s with its main drivers (soil temperature and soil moisture) were maintained or affected by Equation 4. All statistical analyses were made in JASP (V0.8.0.0; available at <https://jasp-stats.org/>).

5.3 Results and Discussion

Using the temporal stability framework, we found that mean relative difference (MRD) values showed biases from -13 to +17% in the shrub treatment, and from -29 to +40% in the trench treatment (Figure 20; Table 15). During daylight hours (e.g., from 8:00 to 19:00) measurements frequently over-estimated R_s in relation to the daily mean value of both trench and shrub treatments.

Table 15. Summary statistics for mean relative difference (MRD) values

Treatment/Season	$\tilde{\mu}$ (%)	σ (%)	Min (%)	Max (%)
Trench-All data	-0.08	22.1	-29.1	39.6
Shrub-All data	1.23	8.1	-12.9	16.8
Trench-Dry season	-11.99	21.2	-31.02	55.6
Shrub-Dry season	-3.14	15.4	-20.22	32.7
Trench-Wet season	-4.95	23.2	-28.9	44.9
Shrub-Wet season	-0.1	7.8	-9.5	16.6

$\tilde{\mu}$: median; σ : standard deviation; Min: minimum value; Max: maximum value

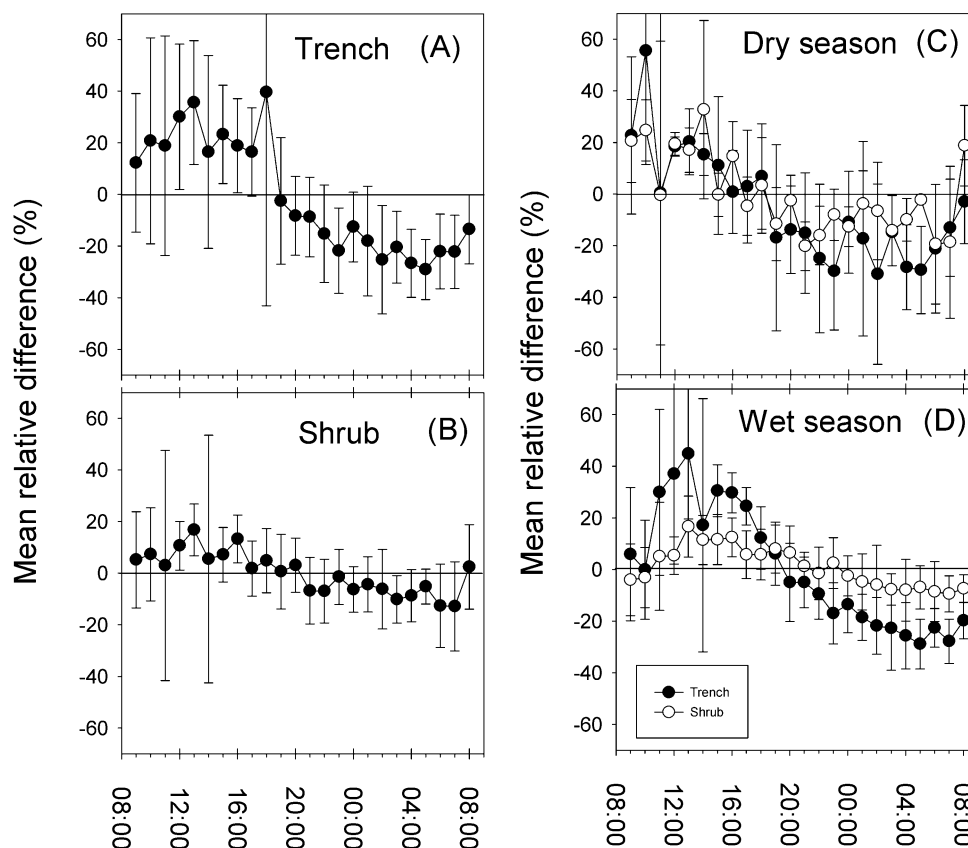


Figure 20. Mean relative difference (MRD) values \pm standard deviation for all the 24hr campaigns for the treatments (A) Trenched and (B) Shrub, and separated in (C) dry season and (D) wet season

In general, we found that MRD values in the trench treatment had higher variability ($-0.08 \pm 22.1\%$; median \pm standard deviation) than the shrub treatment ($1.23 \pm 8.1\%$; Fig. 20; Table 15). Furthermore, R_s in the trench treatment was often under-estimated: MRD median values were not close to zero because most hours were below the daily average (Table 1; Figure 20). There was usually a greater negative bias during the dry season (-12% for trench and -3.14% for shrub) than during the wet season (-4.95% for trench and -0.1% for shrub) (Table 15).

The most appropriate time intervals for measuring R_s at our study site were not in the customary morning hours but rather from 17:00 to 19:00 in the shrub treatment and 20:00 to 21:00 in the trench treatment (Figure 20). This could be due to R_s having a diurnal cycle, with its lowest values before sunrise, increasing through the morning and then decreasing more slowly sometime after noon and into the night. However, it has to be noted that the diurnal cycle of R_s did not follow a sinusoidal trajectory (as has been suggested for N_2O fluxes, Alves et al., 2012) in which case there would be two non-consecutive ideal hours that represent the mean daily value of R_s . Also, the hours with lowest MRD did not match those with the lowest

SDMRD. Thus, the “ideal” hour may present difficulties both in terms of concepts (accuracy of estimates of the annual budget) and logistics (sampling near noon or midnight); thus, other criteria for choosing the sampling hours may have to be taken into account. Furthermore, we found differences when we evaluated the most appropriate time intervals for the dry and wet seasons. For example, during the dry season, there was a more irregular pattern than during the wet season, such that appropriate hours for sampling R_s were dispersed across the 24hr (Figure 20). During the wet season, in contrast, the most appropriate hours to measure R_s were easily identifiable and consecutive (consecutive assigned ranks), ranging from 20:00 to 22:00 in the trench treatment and from 21:00 to 00:00 in the shrub treatment.

It is likely that optimal hours derived from the methodology we tested will vary among sites. For example, Davidson, et al. (2002) suggested that in a temperate mixed-hardwood forest the diel bias was $\pm 25\%$ of the daily mean, the most adequate hours to measure R_s being in the mid-morning. In a young poplar forest, Gana et al. (2016) found that the average of measurements made from 6:00 to 12:00 and 16:30 to 22:30 could represent the daily mean value of R_s , with potential biases of $\pm 20\%$. Moreover, in a temperate rainforest, Perez-Quezada et al. (2016) found that daytime measurements of R_s always overestimated the R_s mean daily value derived from 24h high-frequency measurements. Thus, the sampling times to obtain a representative daily R_s are likely to depend on the ecosystem or conditions studied, and should be determined for each site and season. Of course, study conditions include manipulations as in flux-partitioning experiments: our results showed that trenched plots had higher temporal bias and different optimal timing.

When we applied the constant offset (specific constant offsets for the dry and wet season) to our dataset, we found significant differences (Bayes Factor > 3) between corrected and uncorrected estimations of R_s at the annual scale, as well as during the dry and wet season (Table 16; Figure 21). When we compared the annual uncorrected values between the trench and the shrub treatments we did not find significant differences (Bayes Factor = 1.04; Table 17). However, the contrast of the annual corrected values of R_s between the shrub and the trench treatments was significant (Bayes Factor = 37.41; Table 17). Strong differences were always found during the wet season (Bayes Factor > 3 ; Table 17), but not during the dry season for either corrected or uncorrected values (Table 17). This suggests that during the season of low ecosystem metabolic activity, together with an irregular pattern of the most representative sampling hours, the sampling time was not substantially influencing the estimations of R_s . However, during the wet season, sampling time influenced the estimations of both trenched and shrub treatments. We found that our previous system of sampling around midday could be over-estimating R_s by approximately 11 to 25% at the annual scale and by 10 to 30% during the wet season (Table 2).

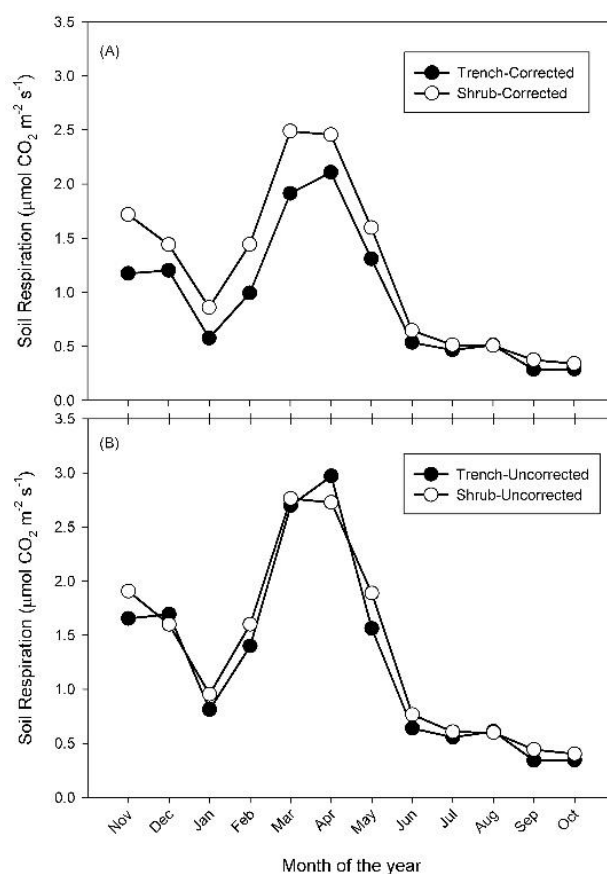


Figure 21. Corrected (A) and uncorrected (B) annual series of soil respiration. Note that we use a hydrological year (from November to October) instead of a calendar year (January to December).

Table 16. Bayesian paired samples Student's T-test of the time series of soil respiration data

T-test		Bayes Factor*
Shrub corrected – Shrub uncorrected	All year	582.1
Trench corrected – Trench uncorrected	All year	22.08
Shrub corrected – Trench corrected	All year	37.41
Shrub uncorrected – Trench uncorrected	All year	1.04
Shrub corrected – Shrub uncorrected	Dry season	4.41
Trench corrected – Trench uncorrected	Dry season	5.17
Shrub corrected – Trench corrected	Dry season	1.69
Shrub uncorrected – Trench uncorrected	Dry season	1.61
Shrub corrected – Shrub uncorrected	Wet season	36.03
Trench corrected – Trench uncorrected	Wet season	20.07
Shrub corrected – Trench corrected	Wet season	47.01
Shrub uncorrected – Trench uncorrected	Wet season	0.45

*Values of Bayes Factor >1 indicates that data are *n* times better supported by the alternative hypothesis than by the null hypothesis

Table 17. Annual and seasonal average (μ) \pm standard deviation (σ) of soil respiration from monthly mid-day measurements in trench and shrub treatments, corrected and uncorrected for temporal bias.

Treatment	Season	μ ($\mu\text{mol CO}_2 \text{ m}^{-2} \text{ s}^{-1}$)	σ ($\mu\text{mol CO}_2 \text{ m}^{-2} \text{ s}^{-1}$)	Difference (%)	Bayes Factor*
Shrub–corrected	All year	1.20	0.77	-11.1	582.1
Shrub–uncorrected	All year	1.35	0.85		
Trench–corrected	All year	0.95	0.61	-25.2	22.08
Trench–uncorrected	All year	1.27	0.89		
Shrub–corrected	Dry season	0.66	0.47	-15.4	4.41
Shrub–uncorrected	Dry season	0.78	0.56		
Trench–corrected	Dry season	0.57	0.38	-14.9	5.17
Trench–uncorrected	Dry season	0.67	0.45		
Shrub–corrected	Wet season	1.73	0.64	-9.9	36.03
Shrub–uncorrected	Wet season	1.92	0.71		
Trench–corrected	Wet season	1.32	0.58	-29.4	20.07
Trench–uncorrected	Wet season	1.87	0.81		

*Values of Bayes Factor >1 indicates that data are n times better supported by the alternative hypothesis than by the null hypothesis.

When we compared the relationships of R_s with its main drivers (i.e., soil temperature and soil moisture), we did not find significant differences between corrected and uncorrected values of R_s at seasonal or annual scales (95% confidence intervals; Table 18). Also, the variance explained remained similar between corrected and uncorrected values (Table 18). Thus, functional relationships of R_s were not affected by correcting suboptimal estimates of mean R_s by a constant offset, although there were important effects on the estimates of seasonal and annual R_s .

Table 18. Bayesian linear relationships of soil respiration with soil temperature (Temp) and soil moisture (SWC).

Treatment	Season	Temp	BF	R ²	SWC	BF*	R ²
Shrub-corrected	All-year	-0.05 (-0.1, 0.003)	1.58	0.3	6.54 (2.04, 11.05)	5.65	0.51
Shrub-uncorrected	All-year	-0.05 (-0.1, 0.006)	1.42	0.28	7.06 (2.0, 12.1)	4.88	0.49
Trench-corrected	All-year	-0.025 (-0.06, 0.01)	0.89	0.188	4.75 (0.98, 8.5)	3.44	0.44
Trench-uncorrected	All-year	-0.04 (-0.09, 0.01)	1.09	0.23	7.24 (2.04, 12.4)	4.83	0.49
Shrub-corrected	Dry season	-0.005 (-0.12, 0.11)	0.57	0.004	6.24 (-54.1, 66.7)	0.58	0.02
Shrub-uncorrected	Dry season	-0.006 (-0.15, 0.14)	0.57	0.004	7.4 (-64.0, 78.8)	0.58	0.02
Trench-corrected	Dry season	0.005 (-0.06, 0.07)	0.57	0.01	-9.87 (-68.5, 48.8)	0.6	0.05
Trench-uncorrected	Dry season	0.006 (-0.07, 0.09)	0.57	0.01	-11.8 (-81.8, 58.2)	0.6	0.05
Shrub-corrected	Wet season	0.19 (0.003, 0.37)	2.04	0.66	3.67 (-5.1, 12.5)	0.79	0.25
Shrub-uncorrected	Wet season	0.21 (0.003, 0.41)	2.04	0.67	4.1 (-5.7, 13.8)	0.79	0.25
Trench-corrected	Wet season	0.18 (0.04, 0.31)	3.15	0.77	3.05 (-5.03, 11.1)	0.75	0.22
Trench-uncorrected	Wet season	0.25 (0.06, 0.44)	3.13	0.77	4.3 (-7.1, 15.7)	0.75	0.22

*Values of Bayes Factor (BF) >1 indicates that data are *n* times better supported by the alternative hypothesis than by the null hypothesis

5.4. Conclusion

Our findings show that measurement of Rs in the customary morning to midday hours may not be appropriate for integrating temporal variability of Rs. At our study site, Rs measurements in daylight hours tend to overestimate the mean daily value of Rs, especially in the growing season. Repeated 24hr campaigns can define sampling times that yield measurements most representative of the daily mean for

each season. Such intensive but limited campaigns can also yield appropriate corrections for non-optimal timing of sampling in monitoring programs. It is noteworthy that the implications of this research may be geographically broad, and also may apply to other GHG emissions from soil (e.g., N_2O , CH_4), especially in treatment-effect experiments. For studies with manual systems, with one measurement per sampling position per sampling date, there should be baseline work on the 24hr cycle, preferably per season, because convenient sampling could lead to over- or under- estimation of the annual R_s flux. It is important to combine locally appropriate timing of measurements with accurate spatial representation because these site-specific measurements provide information to databases that are used to estimate regional-to-global R_s .

Chapter 6. General conclusions

6.1. Conclusion

Although arid and semi-arid ecosystems cover over 40% of the Earth and contribute significantly to the interannual variability of the global carbon balance, they are under-represented in global networks for vegetation dynamics of carbon fluxes. Thus, further research is needed on the environmental factors that control the function of arid and semiarid ecosystems, to understand when they act as carbon sinks/sources, and how they feedback the global climate. This thesis attempted to propose new methodologies to explore the effects of contrasting extremes of annual precipitation on NEE and GPP, by using eddy covariance, repeated photography and soil respiration devices. My main results were that during very wet years, when water availability is not a constrain, the growing season extends through the entire year; this excess of water also enhances decomposition rates during daytime, affecting the relationship of daytime net ecosystem exchange to radiation. This is important when light-response curves are used to estimate gross primary productivity: some ecosystem processes may not be taken into account, leading to biased in estimations of fluxes. We also found that the relation of daytime net ecosystem exchange to radiation was affected by drought in the dry year. Our results call attention to the need to incorporate the effects of decomposition and the inhibition of photosynthesis in empirical- and process-based models.

It is recognized that empirical- and process-oriented models do not have a good representation of vegetation phenology, especially of foliage senescence, and are sensitive to drought conditions, two main characteristics of water-limited ecosystems. We built a framework to estimate daily gross primary production (GPP) using vegetation indices to quantify phenology changes derived from time-lapse photography with consumer-grade cameras and meteorological variables in a water-limited ecosystem with Mediterranean climate. It was found that the cumulative sum of heat degrees, as a proxy of leaf senescence, was a critical parameter to reduce seasonal bias of GPP, in relation to estimates from eddy covariance. The heat sum is interpreted as a driver or proxy of progressive change in rates capacity, i.e. leaf senescence. We demonstrated that not including leaf senescence in the model formulation yield an overestimation of total annual GPP_{mod} between 24 and 90%, while including the senescence parameter reduced the biases between -10 and 34% compared with.

There is a growing interest in understanding the spatial variability of soil respiration (R_s) to identify spatial dependency and hot-spots of soil emissions within ecosystems. Spatial variation of R_s is measured using

manual portable chambers, but moving among sampling locations introduces a temporal effect because it is not possible to measure all locations at the same time. Most studies minimize the temporal effect by collecting all spatial measurements during a short window of time (e.g., 2-hours), assuming that changes in soil moisture, soil temperature, and metabolic activity of heterotrophic and autotrophic organisms are minimized. We tested the effect of the temporal discrepancy of measurements (i.e., measurements taken within a 2-hour window) on the spatial dependency of R_s . We used a gridded sampling design with two manual systems to measure R_s in opposite sequences but starting at the same time. Results showed that the overall plot mean value of R_s was not statistically different between measurement sequences. Geostatistical analyses revealed differences between the measurement sequences in spatial dependency and the presence of hot-spots. Leaf area index was important in explaining the overall spatial variability of R_s , but the relevance of soil temperature and soil moisture to R_s changed between measurement sequences. The measurements had similar temporal trends to ecosystem respiration estimated using the eddy covariance technique, but were consistently lower. We conclude that a small temporal discrepancy in R_s measurements does not affect the plot mean values or the seasonal trends, but sampling sequence influences the spatial dependency of R_s , identification of hot-spots, and the apparent relationships between R_s and other biophysical factors.

R_s has customarily been measured during daylight hours using manual chambers since almost 90 years. This approach assumes that measurements made during the typical time interval (9 to 11 am) represent the mean daily value; locally, this may not always be correct and could result in systematic bias of daily and annual R_s budgets. We proposed a simple method, based on the temporal stability concept, to determine the most appropriate time of the day for manual measurements to capture a representative mean daily R_s value. We introduce a correction factor to adjust for biases due to non-optimally timed sampling. It was found that optimum times to measure R_s were at night and biases at other times ranged from -29 to +40% in relation to the 24hr mean of R_s , especially in trenched plots. The degree of bias varied between treatments and seasons, having a greater influence during the wet season when efflux was high than during the dry season when efflux was low. This study proposed a framework for improving local R_s estimates that informs how to decrease temporal uncertainties, of great significance in upscaling to the annual total.

Further scientific efforts should be made to decrease uncertainties in carbon fluxes to and from terrestrial ecosystems, not only by having high frequency measurements, but also taking into account their spatial variability, among major global ecosystems in distinct environments and at the local scale where environments change rapidly in time and space. Moreover, it is clearly beneficial to have long-term

datasets because the range of growing conditions is increased. This could facilitate its upscaling with empirical- or process-based models to regional, and global and long-term.

In Mexico, research in the terrestrial carbon cycle is a nascent research field. Despite that research on carbon fluxes have a relatively long story (Lundegårdh, 1927), in Mexico the first experiments on the exchange of soil gases were on the early 90s, being until 2004 the first soil CO₂ effluxes reported in the peer reviewed literature (Cueva et al., 2016), and in 2005 the first ecosystem scale carbon fluxes (Hastings et al., 2005). Despite that research on the terrestrial carbon cycle in Mexico has been increasing in the last decade (Cueva et al., 2016; Vargas et al., 2013b), much work is still needed in order to enhance our understanding of the carbon dynamics in ecosystems across Mexico.

Literatura citada

- Ahlström, A. et al., 2015. The dominant role of semi-arid ecosystems in the trend and variability of the land CO₂ sink. *Science*, 348(6237): 895-899, 10.1126/science.aaa1668
- Alberton, B. et al., 2017. Introducing digital cameras to monitor plant phenology in the tropics: applications for conservation. *Perspectives in Ecology and Conservation*, 15(2): 82-90, 10.1016/j.pecon.2017.06.004.
- Alves, B.J.R. et al., 2012. Selection of the most suitable sampling time for static chambers for the estimation of daily mean N₂O flux from soils. *Soil Biology and Biochemistry*, 46: 129-135, 10.1016/j.soilbio.2011.11.022.
- Andela, N., van Dijk, A.I.J.M., de Jeu, R.A.M. and McVicar, T.R., 2013. Global changes in dryland vegetation dynamics (1988–2008) assessed by satellite remote sensing: comparing a new passive microwave vegetation density record with reflective greenness data *Biogeosciences*, 10: 6657-6676, 10.5194/bg-10-6657-2013.
- Austin, A.T. and Vivanco, L., 2006. Plant litter decomposition in a semi-arid ecosystem controlled by photodegradation. *Nature*, 442(7102): 555-558, 10.1038/nature05038.
- Austin, A.T. et al., 2004. Water pulses and biogeochemical cycles in arid and semiarid ecosystems. *Oecologia*, 141(2): 221-35, 10.1007/s00442-004-1519-1.
- Bahn, M., Schmitt, M., Siegwolf, R., Richter, A. and Bruggemann, N., 2009. Does photosynthesis affect grassland soil-respired CO₂ and its carbon isotope composition on a diurnal timescale? *New Phytologist*, 182(2): 451-60, 10.1111/j.1469-8137.2008.02755.x.
- Baldocchi, D.D., 2003. Assessing the eddy covariance technique for evaluating carbon dioxide exchange rates of ecosystems: past, present and future. *Global Change Biology*, 9: 479-492, 10.1046/j.1365-2486.2003.00629.x
- Baldocchi, D.D., 2014. Measuring fluxes of trace gases and energy between ecosystems and the atmosphere – the state and future of the eddy covariance method. *Global Change Biology*, 20(12): 3600-3609, 10.1111/gcb.12649.
- Baldocchi, D.D., Chu, H. and Reichstein, M., In Press. Inter-annual variability of net and gross ecosystem carbon fluxes: A review. *Agricultural and Forest Meteorology*, 10.1016/j.agrformet.2017.05.015
- Barton, L. et al., 2015. Sampling frequency affects estimates of annual nitrous oxide fluxes. *Scientific Reports*, 5: 15912, 10.1038/srep15912.
- Bauerle, W.L. et al., 2012. Photoperiodic regulation of the seasonal pattern of photosynthetic capacity and the implications for carbon cycling. *Proceedings of the National Academy of Sciences*, 109(22): 8612–8617, 10.1073/pnas.1119131109.
- Beer, C. et al., 2010. Terrestrial Gross Carbon Dioxide Uptake: Global Distribution and Covariation with Climate. *Science*, 329(5993): 834-838, 10.1126/science.1184984 .
- Bell, T.W., Menzer, O., Troyo-Diéquez, E. and Oechel, W., 2012. Carbon dioxide exchange over multiple temporal scales in an arid shrub ecosystem near La Paz, Baja California Sur, Mexico. *Global Change Biology*, 18(8): 2570–2582 10.1111/j.1365-2486.2012.02720.x.
- Berg, N. and Hall, A., 2015. Increased Interannual Precipitation Extremes over California under Climate Change. *Journal of Climate*, 28(16): 6324-6334, 10.1175/JCLI-D-14-00624.1.
- Biederman, J.A. et al., 2017. CO₂ exchange and evapotranspiration across dryland ecosystems of southwestern North America. *Global Change Biology*, 00: 1-18, 10.1111/gcb.13686.

- Biederman, J.A. et al., 2016. Terrestrial carbon balance in a drier world: the effects of water availability in southwestern North America. *Global Change Biology*, 22(5): 1867–1879, 10.1111/gcb.13222.
- Bond-Lamberty, B., Bronson, D., Bladyka, E. and Gower, S.T., 2011. A comparison of trenched plot techniques for partitioning soil respiration. *Soil Biology and Biochemistry*, 43(10): 2108-2114, 10.1016/j.soilbio.2011.06.011.
- Bond-Lamberty, B. and Thomson, A., 2010. A global database of soil respiration data. *Biogeosciences*, 7(6): 1915-1926, 10.5194/bg-7-1915-2010.
- Bond-Lamberty, B., Wang, C. and Gower, S.T., 2004. A global relationship between the heterotrophic and autotrophic components of soil respiration? *Global Change Biology*, 10(10): 1756-1766, 10.1111/j.1365-2486.2004.00816.x.
- Brown, T.B. et al., 2016. Using phenocams to monitor our changing Earth: toward a global phenocam network. *Frontiers in Ecology and the Environment*, 14(2): 84–93 10.1002/fee.1222.
- Cable, J.M., Ogle, K., Williams, D.G., Weltzin, J.F. and Huxman, T.E., 2008. Soil Texture Drives Responses of Soil Respiration to Precipitation Pulses in the Sonoran Desert: Implications for Climate Change. *Ecosystems*, 11(6): 961-979, 10.1007/s10021-008-9172-x.
- Castro, A. et al., 2017. A low-cost modular data-acquisition system for monitoring biometeorological variables. *Computers and Electronics in Agriculture*, 141: 357-371, 10.1016/j.compag.2017.08.010.
- Ciais, P. et al., 2005. Europe-wide reduction in primary productivity caused by the heat and drought in 2003. *Nature*, 437(7058): 529-33, 10.1038/nature03972.
- Cox, P.M., Betts, R.A., Jones, C.D., Spall, S.A. and Totterdell, I.J., 2000. Acceleration of global warming due to carbon-cycle feedbacks in a coupled climate model. *Nature*, 408: 184-187, 10.1038/35041539.
- Cueva, A., Bahn, M., Litvak, M., Pumpanen, J. and Vargas, R., 2015. A multisite analysis of temporal random errors in soil CO₂ efflux. *Journal of Geophysical Research: Biogeosciences*, 120(4): 737-751, 10.1002/2014jg002690.
- Cueva, A., Robles-Zazueta, C.A., Garatuza-Payan, J. and Yepez, E.A., 2016. Soil respiration in Mexico: Advances and future directions. *Terra Latinoamericana*, 34(3): 253-269.
- Chabot, B.F. and Hicks, D.J., 1982. The Ecology of Leaf Life Spans. *Annual Review of Ecology and Systematics* 13: 229-259, 10.1146/annurev.es.13.110182.001305.
- Chapin, F.S. et al., 2006. Reconciling Carbon-cycle Concepts, Terminology, and Methods. *Ecosystems*, 9(7): 1041-1050, 10.1007/s10021-005-0105-7.
- Davidson, E. and Janssens, I.A., 2006. Temperature sensitivity of soil carbon decomposition and feedbacks to climate change. *Nature*, 440(7081): 165-173, 10.1038/nature04514.
- Davidson, E.A., Savage, K., Verchot, L.V. and Navarro, R., 2002. Minimizing artifacts and biases in chamber-based measurements of soil respiration. *Agricultural and Forest Meteorology*, 113(1-4): 21-37, 10.1016/S0168-1923(02)00100-4.
- Del Toro-Guerrero, F.J. and Kretschmar, T., 2016. Identificación de periodos de sequía histórica en una región de clima tipo semiárido mediterráneo. *Revista Mexicana de Ciencias Agrícolas*, 7(6): 1311-1320 .
- Del Toro-Guerrero, F.J., Kretschmar, T. and Hinojosa-Corona, A., 2014. Estimación del balance hídrico en una cuenca semiárida, El Mogor, Baja California, México. *Tecnología y Ciencias del Agua*, 5(6): 69-81.

- Delpierre, N. et al., 2009. Modelling interannual and spatial variability of leaf senescence for three deciduous tree species in France. *Agricultural and Forest Meteorology*, 149(6-7): 938-948, 10.1016/j.agrformet.2008.11.014.
- Diffenbaugh, N.S., Giorgi, F. and Pal, J.S., 2008. Climate change hotspots in the United States. *Geophysical Research Letters*, 35(16), 10.1029/2008gl035075.
- Diffenbaugh, N.S., Swain, D.L. and Touma, D., 2015. Anthropogenic warming has increased drought risk in California. *Proceedings of the National Academy of Sciences*, 112(13): 3931–3936, 10.1073/pnas.1422385112.
- Dore, M.H., 2005. Climate change and changes in global precipitation patterns: what do we know? *Environment International*, 31(8): 1167-81, 10.1016/j.envint.2005.03.004.
- Falge, E. et al., 2001. Gap filling strategies for defensible annual sums of net ecosystem exchange. *Agricultural and Forest Meteorology*, 107(1): 43-69, 10.1016/S0168-1923(00)00225-2.
- Fatichi, S., Ivanov, V.Y. and Caporali, E., 2012. Investigating Interannual Variability of Precipitation at the Global Scale: Is There a Connection with Seasonality? . *Journal of Climate*, 25: 5512-5523, 10.1175/JCLI-D-11-00356.1.
- Fisher, J.I., Richardson, A.D. and Mustard, J.F., 2007. Phenology model from surface meteorology does not capture satellite-based greenup estimations. *Global Change Biology*, 13(3): 707-721, 10.1111/j.1365-2486.2006.01311.x.
- Franco-Vizcaíno, E. and Sosa-Ramírez, J., 1997. Soil properties and nutrient relations in burned and unburned Mediterranean-climate shrublands of Baja California, Mexico. *Acta Oecologica*, 18(4): 503-517, 10.1016/S1146-609X(97)80037-9.
- Friedlingstein, P. et al., 2006. Climate–Carbon Cycle Feedback Analysis: Results from the C4MIP Model Intercomparison. *Journal of Climate*, 19(14): 3337-3353, 10.1175/JCLI3800.1.
- Gamon, J.A., Serrano, L. and Surfus, J.S., 1997. The photochemical reflectance index: an optical indicator of photosynthetic radiation use efficiency across species, functional types, and nutrient levels. *Oecologia*, 112(4): 492–501, 10.1007/s004420050337.
- Gana, C., Nouvellon, Y., Marron, N., Stape, J.L. and Epron, D., 2016. Sampling and interpolation strategies derived from the analysis of continuous soil CO₂ flux. *Journal of Plant Nutrition and Soil Science*, 10.1002/jpln.201600133.
- Gilmanov, T.G. et al., 2010. Productivity, Respiration, and Light-Response Parameters of World Grassland and Agroecosystems Derived From Flux-Tower Measurements. *Rangeland Ecology & Management*, 63(1): 16-39, 10.2111/rem-d-09-00072.1.
- Gitelson, A.A. and Gamon, J.A., 2015. The need for a common basis for defining light-use efficiency: Implications for productivity estimation. *Remote Sensing of Environment*, 156: 196-201, 10.1016/j.rse.2014.09.017.
- Gomez-Casanovas, N., Anderson-Teixeira, K.J., Zeri, M., Bernacchi, C.J. and Delucia, E.H., 2013. Gap filling strategies and error in estimating annual soil respiration. *Global Change Biology*, 19(6): 1941–1952, 10.1111/gcb.12127.
- Griffin, D. and Anchukaitis, K.J., 2014. How unusual is the 2012–2014 California drought? *Geophysical Research Letters*, 41(24): 9017-9023, 10.1002/2014GL062433.
- Hagen, S.C. et al., 2006. Statistical uncertainty of eddy flux–based estimates of gross ecosystem carbon exchange at Howland Forest, Maine. *Journal of Geophysical Research*, 111(D08S03), 10.1029/2005jd006154.

- Hanson, P.J., Edwards, N.T., Garten, C.T. and Andrews, J.A., 2000. Separating root and soil microbial contributions to soil respiration: A review of methods and observations. *Biogeochemistry*, 48(1): 115–146, 10.1023/A:1006244819642.
- Hargrove, W.W., Hoffman, F.M. and Law, B.E., 2003. New analysis reveals representativeness of the AmeriFlux network. *Eos*, 84(48): 529–535, 10.1029/2003EO480001.
- Hastings, S.J., Oechel, W. and Muhlia-Melo, A., 2005. Diurnal, seasonal and annual variation in the net ecosystem CO₂ exchange of a desert shrub community (*Sarcocaulis*) in Baja California, Mexico. *Global Change Biology*, 11: 927–939, 10.1111/j.1365-2486.2005.00951.x.
- He, Y., Gibbons, J. and Rayment, M., 2016. A two-stage sampling strategy improves chamber-based estimates of greenhouse gas fluxes. *Agricultural and Forest Meteorology*, 228: 52–59, 10.1016/j.agrformet.2016.06.015.
- Heimann, M. and Reichstein, M., 2008. Terrestrial ecosystem carbon dynamics and climate feedbacks. *Nature*, 451(7176): 289–92, 10.1038/nature06591.
- Heisler-White, J.L., Knapp, A.K. and Kelly, E.F., 2008. Increasing precipitation event size increases aboveground net primary productivity in a semi-arid grassland. *Oecologia*, 158(1): 129–140,
- Heskel, M.A., Atkin, O.K., Turnbull, M.H. and Griffin, K.L., 2013. Bringing the Kok effect to light: A review on the integration of daytime respiration and net ecosystem exchange. *Ecosphere*, 4(8): 1–14, 10.1890/ES13-00120.1.
- Hollinger, D.Y. and Richardson, A.D., 2005. Uncertainty in eddy covariance measurements and its application to physiological models. *Tree Physiology*, 25: 873–885, 10.1093/treephys/25.7.873.
- Huxman, T.E. et al., 2004. Precipitation pulses and carbon fluxes in semiarid and arid ecosystems. *Oecologia*, 141(2): 254–68, 10.1007/s00442-004-1682-4.
- Idso, S.B., Jackson, R.D. and Reginato, R.J., 1978. Extending the "Degree Day" Concept of Plant Phenological Development to Include Water Stress Effects. *Ecology*, 59(3): 431–433, 10.2307/1936570
- Jägermeyr, J. et al., 2014. A high-resolution approach to estimating ecosystem respiration at continental scales using operational satellite data. *Global Change Biology*, 20: 1191–1210, 10.1111/gcb.12443.
- Jia, X. et al., 2014. Biophysical controls on net ecosystem CO₂ exchange over a semiarid shrubland in northwest China. *Biogeosciences*, 11(17): 4679–4693, 10.5194/bg-11-4679-2014.
- Jolly, W.M., Nemani, R. and Running, S., 2005. A generalized, bioclimatic index to predict foliar phenology in response to climate. *Global Change Biology*, 11(4): 619–632, 10.1111/j.1365-2486.2005.00930.x.
- Jung, M. et al., 2010. Recent decline in the global land evapotranspiration trend due to limited moisture supply. *Nature*, 467(7318): 951–4, 10.1038/nature09396.
- Katul, G.G., Palmroth, S. and Oren, R., 2009. Leaf stomatal responses to vapour pressure deficit under current and CO₂-enriched atmosphere explained by the economics of gas exchange. *Plant, Cell & Environment*, 32(8): 968–79, 10.1111/j.1365-3040.2009.01977.x.
- Keenan, T.F. et al., 2014. Tracking forest phenology and seasonal physiology using digital repeat photography: a critical assessment. *Ecological Applications*, 24(6): 1478–1489, 10.1890/13-0652.1.
- Keenan, T.F. and Richardson, A.D., 2015. The timing of autumn senescence is affected by the timing of spring phenology: implications for predictive models. *Global Change Biology*, 21(7): 2634–2641, 10.1111/gcb.12890.

- Kim, D.G., Vargas, R., Bond-Lamberty, B. and Turetsky, M.R., 2012. Effects of soil rewetting and thawing on soil gas fluxes: a review of current literature and suggestions for future research. *Biogeosciences*, 9(7): 2459-2483, 10.5194/bg-9-2459-2012.
- Knox, S.H. et al., 2017. Using digital camera and Landsat imagery with eddy covariance data to model gross primary production in restored wetlands. *Agricultural and Forest Meteorology*, 237-238: 233-245, 10.1016/j.agrformet.2017.02.020.
- Kumar, J., Hoffman, F.M., Hargrove, W.W. and Collier, N., 2016. Understanding the representativeness of FLUXNET for upscaling carbon flux from eddy covariance measurements. *Earth System Science Data Discuss*, 10.5194/essd-2016-36, 2016.
- Kummerow, J., Krause, D. and Jow, W., 1977. Root systems of chaparral shrubs. *Oecologia*, 29: 163-177, 10.1016/0016-7061(96)00019-5.
- Kurc, S.A. and Benton, L.M., 2010. Digital image-derived greenness links deep soil moisture to carbon uptake in a creosotebush-dominated shrubland. *Journal of Arid Environments*, 74(5): 585-594, 10.1016/j.jaridenv.2009.10.003.
- Kuzyakov, Y., 2010. Priming effects: Interactions between living and dead organic matter. *Soil Biology and Biochemistry*, 42(9): 1363-1371, 10.1016/j.soilbio.2010.04.003.
- Kuzyakov, Y. and Gavrichkova, O., 2010. REVIEW: Time lag between photosynthesis and carbon dioxide efflux from soil: a review of mechanisms and controls. *Global Change Biology*, 16(12): 3386-3406, 10.1111/j.1365-2486.2010.02179.x.
- Lal, R., 2004. Soil carbon sequestration to mitigate climate change. *Geoderma*, 123(1-2): 1-22, 10.1016/j.geoderma.2004.01.032.
- Lasslop, G. et al., 2010. Separation of net ecosystem exchange into assimilation and respiration using a light response curve approach: critical issues and global evaluation. *Global Change Biology*, 16(1): 187-208, 10.1111/j.1365-2486.2009.02041.x.
- Lavigne, M.B. et al., 1997. Comparing nocturnal eddy covariance measurements to estimates of ecosystem respiration made by scaling chamber measurements at six coniferous boreal sites. *Journal of Geophysical Research: Atmospheres*, 102(D24): 28977-28985 10.1029/97JD01173.
- León, E. et al., 2014. Hot spots, hot moments, and spatio-temporal controls on soil CO₂ efflux in a water-limited ecosystem. *Soil Biology and Biochemistry*, 77: 12-21, 10.1016/j.soilbio.2014.05.029.
- Li, J. et al., 2007. Impacts of Hurricane Frances on Florida scrub-oak ecosystem processes: defoliation, net CO₂ exchange and interactions with elevated CO₂. *Global Change Biology*, 13(6): 1101-1113, 10.1111/j.1365-2486.2007.01358.x.
- Liu, Q. et al., 2016. Delayed autumn phenology in the Northern Hemisphere is related to change in both climate and spring phenology. *Global Change Biology*, 22(11): 3702-3711, 10.1111/gcb.13311.
- Lundegårdh, H., 1927. Carbon dioxide evolution of soil and crop growth. *Soil Science*, 23: 417-453, 10.1097/00010694-192706000-00001.
- Lloyd, J. and Taylor, J.A., 1994. On the temperature dependence of soil respiration. *Functional Ecology*, 8(3): 315-323 10.2307/2389824
- Medlyn, B.E. et al., 2017. How do leaf and ecosystem measures of water-use efficiency compare? *New Phytologist*, 10.1111/nph.14626.
- Mencuccini, M. and Holtta, T., 2010. The significance of phloem transport for the speed with which canopy photosynthesis and belowground respiration are linked. *New Phytologist*, 185(1): 189-203, 10.1111/j.1469-8137.2009.03050.x.

- Méndez-Alonzo, R., López-Portillo, J., Moctezuma, C., Bartlett, M.K. and Sack, L., 2016. Osmotic and hydraulic adjustment of mangrove saplings to extreme salinity. *Tree Physiology*, 36 (12): 1562-1572, 10.1093/treephys/tpw073.
- Migliavacca, M. et al., 2011. Using digital repeat photography and eddy covariance data to model grassland phenology and photosynthetic CO₂ uptake. *Agricultural and Forest Meteorology*, 151(10): 1325-1337, 10.1016/j.agrformet.2011.05.012.
- Mizunuma, T. et al., 2014. Sensitivity of colour indices for discriminating leaf colours from digital photographs. *Methods in Ecology and Evolution*, 5(10): 1078-1085, 10.1111/2041-210x.12260.
- Monteith, J.L., 1972. Solar Radiation and Productivity in Tropical Ecosystems *Journal of Applied Ecology*, 9(3): 747-766, 10.2307/2401901
- Moore, C.E., Beringer, J., Evans, B., Hutley, L.B. and Tapper, N.J., 2017. Tree–grass phenology information improves light use efficiency modelling of gross primary productivity for an Australian tropical savanna *Biogeosciences*, 14: 111-129, 10.5194/bg-14-111-2017.
- Nannipieri, P. et al., 2003. Microbial diversity and soil functions. *European Journal of Soil Science*, 54: 655-670, 10.1046/j.1365-2389.2003.00556.x.
- Niinemets, Ü., 2016. Leaf age dependent changes in within-canopy variation in leaf functional traits: a meta-analysis. *Journal of Plant Research*, 129(3): 313–338, 10.1007/s10265-016-0815-2.
- Niinemets, Ü., Cescatti, A., Rodeghiero, M. and Tosens, T., 2005. Leaf internal diffusion conductance limits photosynthesis more strongly in older leaves of Mediterranean evergreen broad-leaved species. *Plant, Cell and Environment*, 28(12): 1552-1566, 10.1111/j.1365-3040.2005.01392.x.
- Papale, D. et al., 2006. Towards a standardized processing of Net Ecosystem Exchange measured with eddy covariance technique: algorithms and uncertainty estimation. *Biogeosciences*, 3: 571-583, 10.5194/bg-3-571-2006.
- Perez-Quezada, J.F. et al., 2016. How many measurements are needed to estimate accurate daily and annual soil respiration fluxes? Analysis using data from a temperate rainforest. *Biogeosciences*, 13: 6599-6609, 10.5194/bg-13-6599-2016, 2016.
- Phillips, C.L. et al., 2016. The value of soil respiration measurements for interpreting and modeling terrestrial carbon cycling. *Plant and Soil*, 413 (1-2):1-25, 10.1007/s11104-016-3084-x
- Potts, D.L., Huxman, T.E., Enquist, B.J., Weltzin, J.F. and Williams, D.G., 2006. Resilience and resistance of ecosystem functional response to a precipitation pulse in a semi-arid grassland. *Journal of Ecology*, 94(1): 23-30, 10.1111/j.1365-2745.2005.01060.x.
- Potts, D.L., Scott, R.L., Cable, J.M., Huxman, T.E. and Williams, D.G., 2008. Sensitivity of Mesquite Shrubland CO₂ Exchange to Precipitation in Contrasting Landscape Settings. *Ecology*, 89(10): 2900-2910, 10.1890/07-1177.1.
- Poulter, B. et al., 2014. Contribution of semi-arid ecosystems to interannual variability of the global carbon cycle. *Nature*, 509(7502): 600-3, 10.1038/nature13376.
- Poulter, B. et al., 2014. Contribution of semi-arid ecosystems to interannual variability of the global carbon cycle. *Nature*, 509: 600-603, 10.1038/nature13376.
- Pumpanen, J. et al., 2004. Comparison of different chamber techniques for measuring soil CO₂ efflux. *Agricultural and Forest Meteorology*, 123(3-4): 159-176, 10.1016/j.agrformet.2003.12.001.
- Raich, J.W. and Potter, C.S., 1995. Global patterns of carbon dioxide emissions from soils. *Global Biogeochemical Cycles*, 9(1): 23-36, 10.1029/94GB02723.

- Ran, Y. et al., 2016. Spatial representativeness and uncertainty of eddy covariance carbon flux measurements for upscaling net ecosystem productivity to the grid scale. *Agricultural and Forest Meteorology*, 230-231: 114-127, 10.1016/j.agrformet.2016.05.008.
- Reichstein, M. et al., 2013. Climate extremes and the carbon cycle. *Nature*, 500(7462): 287-95, 10.1038/nature12350.
- Reichstein, M. and Beer, C., 2008. Soil respiration across scales: The importance of a model–data integration framework for data interpretation. *Journal of Plant Nutrition and Soil Science*, 171(3): 344-354, 10.1002/jpln.200700075.
- Reichstein, M. et al., 2005. On the separation of net ecosystem exchange into assimilation and ecosystem respiration: review and improved algorithm. *Global Change Biology*, 11(9): 1424-1439, 10.1111/j.1365-2486.2005.001002.x.
- Reichstein, M. et al., 2003. Modeling temporal and large-scale spatial variability of soil respiration from soil water availability, temperature and vegetation productivity indices. *Global Biogeochemical Cycles*, 17(4): 1104, 10.1029/2003GB002035.
- Reichstein, M. et al., 2002. Severe drought effects on ecosystem CO₂ and H₂O fluxes at three Mediterranean evergreen sites: revision of current hypotheses? *Global Change Biology*, 8(10): 999–1017 10.1046/j.1365-2486.2002.00530.x.
- Reynolds, J.F. et al., 2007. Global desertification: building a science for dryland development. *Science*, 316(5826): 847-51, 10.1126/science.1131634.
- Richardson, A.D. et al., 2012. Terrestrial biosphere models need better representation of vegetation phenology: results from the North American Carbon Program Site Synthesis. *Global Change Biology*, 18(2): 566–584, 10.1111/j.1365-2486.2011.02562.x.
- Richardson, A.D. et al., 2010. Influence of spring and autumn phenological transitions on forest ecosystem productivity. *Philosophical transactions of the Royal Society of London. Series B, Biological sciences*, 365(1555): 3227-46, 10.1098/rstb.2010.0102.
- Richardson, A.D., Braswell, B.H., Hollinger, D.Y., Jenkins, J.P. and Ollinger, S.V., 2009. Near-surface remote sensing of spatial and temporal variation in canopy phenology. *Ecological Applications*, 19(6): 1417–1428, 10.1890/08-2022.1.
- Richardson, A.D. and Hollinger, D.Y., 2005. Statistical modeling of ecosystem respiration using eddy covariance data: Maximum likelihood parameter estimation, and Monte Carlo simulation of model and parameter uncertainty, applied to three simple models. *Agricultural and Forest Meteorology*, 131(3-4): 191-208, 10.1016/j.agrformet.2005.05.008.
- Richardson, A.D. et al., 2007. Use of digital webcam images to track spring green-up in a deciduous broadleaf forest. *Oecologia*, 152(2): 323-34, 10.1007/s00442-006-0657-z.
- Richardson, A.D. et al., 2013. Climate change, phenology, and phenological control of vegetation feedbacks to the climate system. *Agricultural and Forest Meteorology*, 169: 156-173, 10.1016/j.agrformet.2012.09.012.
- Rodeghiero, M. and Cescatti, A., 2008. Spatial variability and optimal sampling strategy of soil respiration. *Forest Ecology and Management*, 255(1): 106-112, 10.1016/j.foreco.2007.08.025.
- Ruimy, A., Kergoat, L. and Bondeau, A., 1999. Comparing global models of terrestrial net primary productivity (NPP): analysis of differences in light absorption and light-use efficiency. *Global Change Biology*, 5(S1): 56-94, 10.1046/j.1365-2486.1999.00007.x.

- Running, S.W. et al., 2004. A Continuous Satellite-Derived Measure of Global Terrestrial Primary Production. *BioScience*, 54(6): 547-560, 10.1641/0006-3568(2004)054[0547:ACSMOG]2.0.CO;2.
- Ryan, M.G. and Law, B.E., 2005. Interpreting, measuring, and modeling soil respiration. *Biogeochemistry*, 73(1): 3-27, 10.1007/s10533-004-5167-7.
- Sakamoto, T. et al., 2012. An alternative method using digital cameras for continuous monitoring of crop status. *Agricultural and Forest Meteorology*, 154-155: 113-126, 10.1016/j.agrformet.2011.10.014.
- Savage, K. and Davidson, E.A., 2003. A comparison of manual and automated systems for soil CO₂ flux measurements: trade-offs between spatial and temporal resolution. *Journal of Experimental Botany*, 54(384): 891-899, 10.1093/jxb/erg121.
- Savage, K., Davidson, E.A. and Richardson, A.D., 2008. A conceptual and practical approach to data quality and analysis procedures for high-frequency soil respiration measurements. *Functional Ecology*, 22(6): 1000-1007, 10.1111/j.1365-2435.2008.01414.x.
- Scott, R.L., Biederman, J.A., Hamerlynck, E.P. and Barron-Gafford, G.A., 2015. The carbon balance pivot point of southwestern U.S. semiarid ecosystems: Insights from the 21st century drought. *Journal of Geophysical Research: Biogeosciences*, 120(12): 2612–2624, 10.1002/2015JG003181.
- Scott, R.L. et al., 2004. Interannual and seasonal variation in fluxes of water and carbon dioxide from a riparian woodland ecosystem. *Agricultural and Forest Meteorology*, 122(1-2): 65-84, 10.1016/j.agrformet.2003.09.001.
- Scott, R.L., Jenerette, G.D., Potts, D.L. and Huxman, T.E., 2009. Effects of seasonal drought on net carbon dioxide exchange from a woody-plant-encroached semiarid grassland. *Journal of Geophysical Research*, 114(G4), 10.1029/2008jg000900.
- Schaefer, K. et al., 2012. A model-data comparison of gross primary productivity: Results from the North American Carbon Program site synthesis. *Journal of Geophysical Research: Biogeosciences*, 117(G3), 10.1029/2012jg001960.
- Scheiter, S., Langan, L. and Higgins, S.I., 2013. Next-generation dynamic global vegetation models: learning from community ecology. *New Phytologist*, 198(3): 957-69, 10.1111/nph.12210.
- Schwalm, C.R. et al., 2006. Photosynthetic light use efficiency of three biomes across an east–west continental-scale transect in Canada. *Agricultural and Forest Meteorology*, 140(1-4): 269–286, 10.1016/j.agrformet.2006.06.010.
- Schwalm, C.R. et al., 2010. Assimilation exceeds respiration sensitivity to drought: A FLUXNET synthesis. *Global Change Biology*, 16(2): 657-670, 10.1111/j.1365-2486.2009.01991.x.
- Schwinning, S. and Sala, O.E., 2004. Hierarchy of responses to resource pulses in arid and semi-arid ecosystems. *Oecologia*, 141(2): 211-20, 10.1007/s00442-004-1520-8.
- Seager, R. et al., 2015. Causes of the 2011–14 California Drought. *Journal of Climate*, 28(18): 6997-7024, 10.1175/JCLI-D-14-00860.1.
- Shi, H. et al., 2014. Intrinsic climate dependency of ecosystem light and water-use-efficiencies across Australian biomes. *Environmental Research Letters*, 9(10): 104002, 10.1088/1748-9326/9/10/104002.
- Sobrado, M.A., 1994. Leaf age effects on photosynthetic rate, transpiration rate and nitrogen content in a tropical dry forest. *Physiologia plantarum*, 90(1): 210-2015, 10.1111/j.1399-3054.1994.tb02213.x.

- Søe, A.R.B. and Buchmann, N., 2005. Spatial and temporal variations in soil respiration in relation to stand structure and soil parameters in an unmanaged beech forest. *Tree physiology*, 25(11): 1427–1436, 10.1093/treephys/25.11.1427.
- Sonnentag, O. et al., 2012. Digital repeat photography for phenological research in forest ecosystems. *Agricultural and Forest Meteorology*, 152: 159-177, 10.1016/j.agrformet.2011.09.009.
- Speckman, H.N. et al., 2015. Forest ecosystem respiration estimated from eddy covariance and chamber measurements under high turbulence and substantial tree mortality from bark beetles. *Global Change Biology*, 21(2): 708-21, 10.1111/gcb.12731.
- Stenberg, P.D., Anderson, M.A., Graham, R.C., Beyers, J.L. and Tice, K.R., 1996. Root distribution and seasonal water status in weathered granitic bedrock under chaparral. *Geoderma*, 72: 89-98, 10.1016/0016-7061(96)00019-5.
- Stoy, P., Trowbridge, A.M. and Bauerle, W.L., 2013. Controls on seasonal patterns of maximum ecosystem carbon uptake and canopy-scale photosynthetic light response: contributions from both temperature and photoperiod. *Photosynth Research*, 119(1): 49-64, 10.1007/s11120-013-9799-0.
- Tenhunen, J.D., Beyschlag, W., Lange, O.L. and Harley, P.C., 1987. Changes during summer drought in leaf CO₂ uptake rates of macchia shrubs growing in Portugal: Limitations due to photosynthetic capacity, carboxylation efficiency, and stomatal conductance. In: J.D. Tenhunen, F.M. Catarino, O.L. Lange and W. Oechel (Editors), *Plant Responses to Stress*. Springer-Verlag Berlin Heidelberg, pp. 305-327.
- Tramontana, G. et al., 2016. Predicting carbon dioxide and energy fluxes across global FLUXNET sites with regression algorithms. *Biogeosciences*, 13: 4291–4313, 10.5194/bg-13-4291-2016.
- Turner, D.P. et al., 2003. A cross-biome comparison of daily light use efficiency for gross primary production. *Global Change Biology*, 9(3): 383-395, 10.1046/j.1365-2486.2003.00573.x.
- Vachaud, G., Passerat de Silans, A., Balabanis, P. and Vauclin, M., 1985. Temporal Stability of Spatially Measured Soil Water Probability Density Function. *Soil Science of America Journal*, 49(4): 822-828, 10.2136/sssaj1985.03615995004900040006x.
- Valentini, R. et al., 2000. Respiration as the main determinant of carbon balance in European forests. *Nature*, 404: 861-865, 10.1038/35009084.
- Vargas, R., 2012. How a hurricane disturbance influences extreme CO₂ fluxes and variance in a tropical forest. *Environmental Research Letters*, 7(3): 035704, 10.1088/1748-9326/7/3/035704.
- Vargas, R. and Allen, M.F., 2008a. Diel patterns of soil respiration in a tropical forest after Hurricane Wilma. *Journal of Geophysical Research*, 113(G3), 10.1029/2007JG000620.
- Vargas, R. and Allen, M.F., 2008b. Environmental controls and the influence of vegetation type, fine roots and rhizomorphs on diel and seasonal variation in soil respiration. *New Phytologist*, 179(2): 460–471, 10.1111/j.1469-8137.2008.02481.x.
- Vargas, R. et al., 2010. Looking deeper into the soil: environmental controls and seasonal lags of soil CO₂ production and efflux across multiple vegetation types. *Ecological Applications*, 20(6): 1569-1582, 10.1890/09-0693.1
- Vargas, R., Carbone, M.S., Reichstein, M. and Baldocchi, D.D., 2011. Frontiers and challenges in soil respiration research: from measurements to model-data integration. *Biogeochemistry*, 102: 1-13, 10.1007/s10533-010-9462-1.

- Vargas, R. et al., 2013a. Drought Influences the Accuracy of Simulated Ecosystem Fluxes: A Model-Data Meta-analysis for Mediterranean Oak Woodlands. *Ecosystems*, 16(5): 749-764, 10.1007/s10021-013-9648-1.
- Vargas, R. et al., 2013b. Progress and opportunities for monitoring greenhouse gases fluxes in Mexican ecosystems: the MexFlux network. *Atmósfera*, 23(3): 325-336.
- Verduzco, V.S. et al., 2015. Variations of net ecosystem production due to seasonal precipitation differences in a tropical dry forest of northwest Mexico. *Journal of Geophysical Research: Biogeosciences*, 120(10): 2081-2094, 10.1002/2015JG003119.
- Vicca, S. et al., 2014. Can current moisture responses predict soil CO₂ efflux under altered precipitation regimes? A synthesis of manipulation experiments. *Biogeosciences*, 11(11): 2991-3013, 10.5194/bg-11-2991-2014.
- Villarreal, S. et al., 2016. Contrasting precipitation seasonality influences evapotranspiration dynamics in water-limited shrublands. *Journal of Geophysical Research - Biogeosciences*, 121(2): 494-508, 10.1002/2015JG003169.
- Waliser, D.E. et al., 2012. The “Year” of Tropical Convection (May 2008–April 2010): Climate Variability and Weather Highlights Bulletin of the American Meteorological Society, 93(8): 1189-1218, 10.1175/2011BAMS3095.1.
- Webb, E.K., Pearman, G.I. and Leuning, R., 1980. Correction of flux measurements for density effects due to heat and water vapour transfer. *Quarterly Journal of the Royal Meteorological Society*, 106(447): 85-100, 10.1002/qj.49710644707.
- Westergaard-Nielsen, A., Lund, M., Hansen, B. and Tamstorf, M.P., 2013. Camera derived vegetation greenness index as proxy for gross primary production in a low Arctic wetland area. *ISPRS Journal of Photogrammetry and Remote Sensing*, 89: 89-99, 10.1016/j.isprsjprs.2013.09.006.
- Wilczak, J.M., Oncley, S.P. and Stage, S.A., 2001. Sonic Anemometer Tilt Correction Algorithms. *Boundary-Layer Meteorology*, 99(1): 127–150, 10.1023/A:1018966204465.
- Wolf, S. et al., 2016. Warm spring reduced carbon cycle impact of the 2012 US summer drought. *Proceedings of the National Academy of Sciences*, 113(21): 5880–5885, 10.1073/pnas.1519620113.
- Xia, Y., She, D., Li, Y. and Yan, X., 2014. Impact of sampling time on chamber-based measurements of riverine nitrous oxide emissions using relative difference analysis. *Geoderma*, 214-215: 197-203, 10.1016/j.geoderma.2013.09.011.
- Xu, L., Baldocchi, D.D. and Tang, J., 2004. How soil moisture, rain pulses, and growth alter the response of ecosystem respiration to temperature. *Global Biogeochemical Cycles*, 18(4), 10.1029/2004gb002281.
- Yang, F. et al., 2008. Assessing the representativeness of the AmeriFlux network using MODIS and GOES data. *Journal of Geophysical Research: Biogeosciences*, 113(G4), 10.1029/2007JG000627.
- Yepez, E.A., Scott, R.L., Cable, W.L. and Williams, D.G., 2007. Intraseasonal Variation in Water and Carbon Dioxide Flux Components in a Semiarid Riparian Woodland. *Ecosystems*, 10(7): 1100-1115, 10.1007/s10021-007-9079-y.
- Yim, M.H., Joo, S.J., Shutou, K. and Nakane, K., 2003. Spatial variability of soil respiration in a larch plantation: estimation of the number of sampling points required. *Forest Ecology and Management*, 175(1-3): 585-588, 10.1016/S0378-1127(02)00222-0.

- Yuan, W. et al., 2014. Global comparison of light use efficiency models for simulating terrestrial vegetation gross primary production based on the LaThuile database. *Agricultural and Forest Meteorology*, 192-193: 108-120, 10.1016/j.agrformet.2014.03.007.
- Zelikova, T.J. et al., 2015. Seasonality of soil moisture mediates responses of ecosystem phenology to elevated CO₂ and warming in a semi-arid grassland. *Journal of Ecology*, 103(5): 1119-1130, 10.1111/1365-2745.12440.
- Zeng, H. et al., 2009. Impacts of tropical cyclones on U.S. forest tree mortality and carbon flux from 1851 to 2000. *Proceedings of the National Academy of Sciences*, 106(19): 7888-7892, 10.1073/pnas.0808914106.
- Zhao, M. and Running, S.W., 2010. Drought-induced reduction in global terrestrial net primary production from 2000 through 2009. *Science*, 329(5994): 940-3, 10.1126/science.1192666.
- Zhou, L. et al., 2013. Modeling winter wheat phenology and carbon dioxide fluxes at the ecosystem scale based on digital photography and eddy covariance data. *Ecological Informatics*, 18: 69-78, 10.1016/j.ecoinf.2013.05.003.